A STUDY ON THE TRANSPORT AND DISTRIBUTION OF ATMOSPHERIC AEROSOLS AND ITS INFLUENCE ON REGIONAL METEOROLOGICAL PARAMETERS OVER THE INDIAN SUBCONTINENT

Thesis submitted to the

Cochin University of Science and Technology

in partial fulfillment of the requirement for the Degree of

DOCTOR OF PHILOSOPHY
in
ATMOSPHERIC SCIENCE

BY

ABISH B

Department of Atmospheric Sciences
Cochin University of Science and Technology
Cochin - 682 016, India

APRIL 2011

Dedicated
To
My Parents

DECLARATION

I hereby declare that this thesis entitled **A Study on the Transport and Distribution of Atmospheric Aerosols and its Influence on Regional Meteorological Parameters over the Indian Subcontinent** is a genuine record of research work carried out by me and no part of this work has been submitted to any University or Institution for the award of any Degree or Diploma.

Cochin-682016 **Abish B**
April, 2011

Acknowledgments

I would like to express my sincere and deepest gratitude to my thesis supervisor Prof. Dr. K. Mohankumar, Professor, Department of Atmospheric Sciences and Dean, Faculty of Environmental Studies, for the overall guidance, supervision, encouragement, advice and care given to me since I joined with him. His incessant support, kindness and inspiration made this Ph.D. thesis a reality within three years time. I owe my indebtedness for his sincerity, patience, deep concern and wholehearted support for the fulfillment of this thesis.

My sincere thanks are due to Prof. Dr. H.S. Ram Mohan, Dean, Faculty of Marine Sciences, for his advice, motivation and encouragement. His valuable suggestions have helped me in different stages of this work.

I am thankful to Dr. Santhosh K.R., Head, Department of Atmospheric Sciences, for his helpful advice and for providing all the facilities to carry out the research work. Thanks are due to Dr. C.A. Babu, Former Head, Department of Atmospheric Sciences for providing computer facilities required for my research work. A word of thanks to Mr. Baby Chakrapany, Dr. G. Venu, Dr. V. Madhu for their comments and suggestions.

I express my deepest respect and regards to Dr. K. Krishnamoorthy, Director, Space Physics Laboratory (SPL), Thiruvananthapuram, who has introduced me to the branch of aerosol science during my M.Tech project at SPL. The knowledge imparted by Dr. S. Suresh Babu, Scientist, SPL on the subject has enabled me to develop a profound interest in aerosol science.

My heartfelt gratitude to Dr. Bijoy, Dr. Girish, Dr. Vineeth, Dr. Rupanand, Johny and Prem for their outstanding support and friendship which helped me to overcome many hardships. I am grateful to Dr. Marina, Dr. Susan, Veena, Ancy and Sudeena who helped me with fruitful discussions and for their valuable advices throughout my work.

I thankfully remember my friends Anand, Hareesh, Yashin, Rejoy, Jaison, Denny, Dipu, Susmitha, Dr. Vijayakumar and Naseema for their care and timely help.

I cannot forget my dearest colleagues and lab mates Johnson Zacharia, Anila, Asha, Resmi, Smitha. A, Krishnamohan, Lorna Nayagam, Nithin, Vani, Vijayakumar and Dr. Bindhu for their support and help I got during my research work. Their camaraderie and interaction made it a convivial place and presented lot of lighter moments that eased my strenuous research work.

I am grateful to CSIR for providing me a fellowship during my tenure as a research scholar. I specially acknowledge NASA Goddard Earth Sciences (GES) Data and Information Services Centre (DISC) team members for providing me with the data required for this work.

I record my sincere thanks to Dr. Sreedevi M.G., Mr. G. Yasodharan and office staff of Department of Atmospheric Sciences for the technical and administrative support I have received during my research tenure. I acknowledge the librarian and staff for providing me the relevant literature required for my thesis work.

Words are inadequate to express my love and affection to my family members for the unfeigned support and affection they have given me. I offer my special thanks to my brother Anish, sister-in-law Dr. Mini for taking keen interest in helping me with statistical analysis and to their little ones Akshadha and Adinath. The inspiration and blessing of my father right from the beginning of my career and all the way throughout till his last breath is emotionally remembered at this moment. I am sure that it is his blessing paved the way to achieve my goal within the prescribed time limit. I take this opportunity to pay homage to my dearest father. My mother, with her bountiful affection has always been a source of strength and motivation for me. I have no suitable words to describe her eternal love towards me. To my parents I dedicate this Ph.D. thesis.

Abish B

CONTENTS

Preface i

List of Tables v

List of Figures vi

1 An Overview of Atmospheric Aerosols

1.1. Introduction 1

1.2. Importance of aerosol study 2

1.3. Aerosol Production mechanism

1.3.1. Bulk to Particle Conversion 3

1.3.2. Gas to Particle Conversion 3

1.4. Sources of aerosols

1.4.1. Natural 4

1.4.2. Anthropogenic 10

1.4.3. Source Strength 13

1.5. Classification of Aerosols 14

1.6. Size Distribution

1.6.1. Junge Power Law 17

1.6.2. Log Normal Distribution 18

1.7. Aerosol size transformation processes 18

1.8. Residence time 20

1.9. Vertical distribution 21

1.10. Aerosol transport 22

1.11. Aerosol removal 22

1.12. Effects of aerosol

1.12.1. Optical Effects 24

1.12.2. Physiological Effects 30

1.12.3. Chemical Effects 30

1.12.4. Effect on cloud properties 31

1.13. Radiative forcing of aerosols

1.13.1. Direct Radiative forcing 33

1.13.2. Indirect Radiative forcing 34
1.14. Measurement Techniques 34
1.15. Objective of the Study 35

2 Data and Methodology

2.1. Introduction 40
2.2. The MODIS Sensor 41
2.3. Detection of Aerosols using Ultraviolet observation 50
2.3.1. The TOMS sensor 51
2.3.2. The OMI sensor 54
2.4. The Atmospheric Infrared Sounder 57
2.5. HYSPLIT model 60
2.6. Reanalysis Data 63
2.6.1. ERA-Interim 64
2.6.2. NCEP Reanalysis Data 65

3 Transport and Distribution of Atmospheric Aerosols as Inferred By Satellite Measurements

3.1. Introduction 68
3.2. Data and Analysis 70
3.3. Results and Discussion 72
3.3.1. Seasonal variation of Aerosol Index 72
3.3.2. Influence of wind speed on Aerosol Index 77
3.3.3. Back Trajectory Analysis 81
3.3.4. Effect of El-Nino and La-Nina 86
3.3.5. Conclusions 94

4 Biennial Variability of Atmospheric Aerosol and its Relation With QBO

4.1. Introduction 95
4.2. Data and Analysis 97
4.3. Results and Discussion 99

4.3.1. Meridional Circulations 101
4.3.2. Vertical Distribution of Aerosols 103
4.3.3. Tropopause Characteristics 104
4.4. Conclusions 107

5 Role of Fine Mode Aerosol Particles in Modulating Cloud Properties

5.1. Introduction 110
5.2. Data Description 112
5.3. Results and Discussion
5.3.1. Angstrom exponent and its relation to aerosol size 113
5.3.2. Aerosol Indirect Effect and its influence on precipitation 115
5.3.3. Relation between Aerosols and Cloud Cover 125
5.4. Conclusions 129

6 Time series Analysis and Forecasting using the Statistical Model ARIMA

6.1. Introduction 131
6.2. Methodology
6.2.1. Description of Box-Jenkins ARIMA model 132
6.2.2. Model Identification 134
6.2.3. Model parameter estimation 135
6.2.4. Seasonal ARIMA model (SARIMA) 136
6.2.5. Diagnostic Stage 137
6.3. Results and Discussion
6.3.1. ARIMA model forecasting for AOD 139
6.3.2. ARIMA model forecasting for CER 147
6.4. Conclusions 155

7 Summary and Conclusions 156

References 162

List of Publications 182

PREFACE

Atmospheric aerosols are particles of solid or liquid phase dispersed in the atmosphere. They have a size range of 0.001 to 100 μm in radius and exhibits large variations in space and time. Aerosols are generated by a variety of natural and anthropogenic mechanisms, both directly and indirectly; while they are removed mainly by sedimentation (dry deposition) and washout (wet removal). During their lifetime in the atmosphere, aerosols also undergo transformation in their physical and chemical properties with consequent impact on the climate.

Aerosol particles in the atmosphere scatter and absorb incoming solar radiation as well as emitted and reflected radiation from the earth, to different degrees, depending on their chemical and physical properties. Also, certain aerosol types interact with cloud droplets, modifying their microphysical properties, thereby influencing their radiative properties and precipitation processes. Aerosols modifies cloud properties when an increase in the concentration of cloud condensation nuclei (CCN) would lead to an increase in the concentration of cloud droplets in a given cloud; accompanied by a reduction in the average cloud drop diameter. A decrease in droplet size delays the onset of collision and coalescence in clouds, reducing precipitation thereby increasing the lifespan and the areal coverage of the cloud. This leads to an increase in the cloud reflectance and consequently the planetary albedo.

The Indian subcontinent which is very diverse in topography, population distribution, meteorology and emission sources, exhibits spatial and seasonal variability of aerosol properties. This heterogeneity arises due to the complex combination of anthropogenic factors mixed with the contribution from the natural sources which is prominant in the non-monsoon months.

This doctoral thesis addresses the growing concern about the significant changes in the climatic and weather patterns due to the aerosol loading that have taken place in the Indo Gangetic Plain (IGP) which includes most of the Northern Indian region. The study region comprises of major industrial cities in India (New Delhi, Kanpur, Allahabad, Jamshedpur and Kolkata). Northern and central parts of India are one of the most thickly populated areas in the world and have the most intensely farmed areas. Rapid increase in population and urbanization has resulted in an abrupt increase in aerosol concentrations in recent years. The IGP has a major source of coal; therefore most of the industries including numerous thermal power plants that run on coal are located around this region. They inject copious amount of aerosols into the atmosphere. Moreover, the transport of dust aerosols from arid locations is prevalent during the dry months which increase the aerosol loading in the atmosphere.

The topography of the place is also ideal for the congregation of aerosols. It is bounded by the Himalayas in the north, Thar Desert in the west, the Vindhyan range in the south and Brahmaputra ridge in the east. During the non-monsoon months (October to May) the weather in the location is dry with very little rainfall. Surface winds are weak during most of the time in this dry season. The aerosols that reach the location by means of long distance transport and from regional sources get accumulated under these favourable conditions.

The increase in aerosol concentration due to the complex combination of aerosol transport and anthropogenic factors mixed with the contribution from the natural sources alters the optical properties and the life time of clouds in the region. The associated perturbations in radiative balance have a significant impact on the meteorological parameters and this in turn determines the precipitation forming process. Therefore, any change in weather which disturbs the normal hydrological pattern is alarming in the socio-economic point of view. Hence, the main focus of this work is to determine the variation in transport and distribution of aerosols in the region and to understand the interaction of these aerosols with meteorological parameters and cloud properties.

The thesis consists of 7 chapters. Chapter 1 is an overview of atmospheric aerosols. A detailed description on the major types and sources of aerosols, aerosol production, transport and removal mechanisms, its effects and radiative forcing on the Earth-atmosphere system, its spatial distribution, methods used for measuring the aerosol properties and the physical characteristics and the importance of the study region is given. Remote sensing measurements from satellites are used to characterise the spatial and temporal heterogeneities of aerosol distribution. Chapter 2 gives the details of the retrieval of aerosol data from the satellite sensors and also gives an account on the supplementary datasets used in the analysis. The characteristics of each satellite sensors and their associated uncertainty limits are presented in this chapter.

In Chapter 3 the aerosol transport and distribution over the Indian region is presented. The observed seasonal variations as well as the annual variation of the Aerosol Index (AI) are presented. Datasets from TOMS and OMI sensors are used for this purpose. The role of prevailing winds in transporting atmospheric aerosols is examined in this chapter.

Biennial variability exhibited by the aerosols are analysed in Chapter 4. The biennial variations in aerosol optical depth (AOD) associated with QBO modulated tropopause characteristics are detailed in this chapter. The influence of stratospheric oscillations on concentration of aerosols which is predominantly a tropospheric constituent has been examined.

Chapter 5 brings out the modification of cloud properties as a result of aerosol accumulation in the study region. This chapter deals with the modification of cloud properties as a result of piling up of aerosols particularly in the non-monsoon months. The indirect effects of aerosols on cloud micro-physics have been examined. The analysis gives an input on how the cloud drop size varies with increasing aerosol content. The analysis also focuses on delaying of

monsoon onset in the study region due to the presence of aerosols in the pre-monsoon season.

In Chapter 6 an empirical study of model building, estimation and forecasting the time series data of cloud effective radius (CER) and AOD is done. Based on the features of data, the classes of seasonal ARIMA (autoregressive integrated moving average) models are considered to fit the data. The autocorrelation function and the partial autocorrelation function of the transformed series are estimated and the significant lags were used for finding out the order of the model. The residual analysis, *Akaike* information criterion was used to evaluate the goodness-of-fit of the model. The forecast accuracy for each model was evaluated via mean absolute percentage error (MAPE). The values thus obtained are found to have a reasonably well goodness of fit with the observed CER and AOD datasets. The forecasts are also carried out based on the selected model.

Major conclusions of the studies are presented in this Chapter 7 and an outline of future scope of research is also mentioned. References are given at the end of the thesis in alphabetical order.

List of Tables

Table No.	Title	Page No.
1.1.	Annual source strength for emissions of gas phase aerosol (Tg/yr)	14
1.2.	Classification of aerosols based on size	15
1.3.	Densities of different aerosol species	16
1.4.	Refractive indices of different aerosol species	17
1.5.	Residence time of aerosols in different altitudes	21
2.1.	Characteristics of MODIS channels used in aerosol retrieval	42
3.1.	Warm and cold phases of Oceanic Nino Index (ONI)	87
3.2.	Intensity of El-Nino and La-Nina phases	88
5.1.	Monsoon onset dates over Kerala and IGP	117
6.1.	Parameter Estimates for the ARIMA(1,0,2)x$(2,1,2)_{12}$	141
6.2.	ARIMA forecast summary	143
6.3.	Comparison of estimation parameters of different models fitted to the data	145
6.4.	Forecast for AOD	146
6.5.	ARIMA model summary for CER	149
6.6.	Parameter Estimates for CER - ARIMA(1,1,2)x$(1,1,2)_{12}$	149
6.7.	Comparison of estimation parameters of different models fitted	151
6.8.	Forecast Table for CER given by ARIMA(1,1,2) x $(1,1,2)_{12}$	154

List of Figures

Fig. No.	Caption	Page No.
1.1.	Tearing of wave crusts leading to sea salt production	5
1.2.	Transport of mineral aerosols during a dust storm	6
1.3.	A volcanic eruption emitting massive amount of gases and ash	7
1.4.	Biomass burning ejecting organic aerosols into the atmosphere	9
1.5.	Industrial emission of anthropogenic sulphates	11
1.6.	Intensity distribution pattern for Rayleigh and Mie scattering	25
1.7.	Schematic diagram showing the various radiative mechanisms associated with cloud effects that have been identified as significant in relation to aerosols.	32
1.8.	Map of India with area chosen for study	36
2.1.	A schematic diagram of the MODIS sensor	41
2.2.	Overview of MODIS sensing geometry	43
2.3.	Level-3 monthly product of cloud effective particle radius for liquid water clouds from MODIS Terra in April 2003	48
2.4.	The TOMS- Earth Probe space craft and its sensor	52
2.5.	The optical layout of the OMI sensor	56
2.6.	Schematic overview of the measurement principle of the instrument	57
2.7.	AIRS viewing geometry and coverage	59
3.1.(a)	Aerosol Index during the pre-monsoon season over the Indian subcontinent	72-73
3.1.(b)	Aerosol Index during the post-monsoon season over the Indian subcontinent	75-76
3.2.(a)	Prevailing winds at 700 hPa during pre-monsoon season for the years 2000 to 2009	78-79
3.2.(b)	Prevailing winds at 700 hPa during post-monsoon season for the years 2000 to 2009	80-81

3.3.(a)	Back trajectories of aerosol particles reaching the location during the pre-monsoon season.	82-83
3.3.(b)	Back trajectories of aerosol particles reaching the location during the post-monsoon season.	84-85
3.4.	Composite of prevailing winds at 700 hPa during El-Nino and La-Nina years respectively	89
3.5.	Height-longitude plot of the u wind and omega averaged over the latitude (7^0 N – 30^0 N)	90
3.6.	Aerosol Index composites for El-Nino years and La-Nina years over the Indian subcontinent	92
3.7.	Back trajectory analysis for El-Nino and La-Nina composites	93
4.1.	A comparison between monthly mean zonal winds at 50hPa and 30hPa ((50hPa + 30 hPa)/2) and monthly mean AOD.	100
4.2.	Schematic representation of the mean meridional circulation driven by the QBO	102
4.3.	Anomalies of tropical tropopause (a) pressure (b) height (c) temperature respectively for the years 2002 to 2009	105
5.1.	Monthly mean time series between AOD and angstrom exponent for the years 2000 to 2010	114
5.2.	Time series of monthly mean fine mode AOD and CER over the study region.	116
5.3.	Diagram showing the latitudinal variation of CER	118
5.4.	Scatter diagram between LWP and CER for (a) non-monsoon months and (b) monsoon months	120
5.5.	Scatter plots between COD and LWP for (a) dry months and (b) monsoon months	123
5.6.	Correlation between fine mode aerosols and cloud cover during the non-monsoon months for the years 2000 to 2010	126
5.7.	Scatter plot between fine mode AOD and surface temperature indicating a negative relation	128
6.1.	(a) Autocorrelation function (ACF) for AOD (b) Partial Autocorrelation function (PACF) for AOD	140
6.2.	Estimated autocorrelation function between residuals for fine mode AOD at various lags.	142
6.3.	Estimated partial autocorrelation between residuals for fine mode AOD at various lags	143

6.4.	Time series plot showing the actual and model output values. The forecast values till December 2011 is shown at 95% confidence level.	146
6.5.	(a) Autocorrelation function (ACF) for CER (b) Partial Autocorrelation function (PACF) for CER	147-148
6.6.	Estimated autocorrelation between residuals for CER at various lags.	152
6.7.	Estimated partial autocorrelation between residuals for CER at various lags.	153
6.8.	Time series plot showing the actual and model output values for CER. The forecast values till December 2011 is shown at 95% confidence level.	154

CHAPTER 1

AN OVERVIEW OF ATMOSPHERIC AEROSOLS

1.1. Introduction

Atmospheric aerosols are particles of solid or liquid phase dispersed in the atmosphere. They have a size range of 0.001 to 100 μm in radius. These aerosols are produced either by the mechanical disintegration processes occurring over land (e.g., lift up of dust) and ocean (e.g., sea-spray), volcanic debris, chemical reactions occurring in the atmosphere (e.g., conversion of sulphur dioxide to sulphuric acid droplets), biomass burning and industrial process (Junge, 1963; Prospero et al., 1983). Thus, aerosols are natural and anthropogenic in origin. On a global scale, the natural sources of aerosols are three to four times stronger than anthropogenic ones, but regionally anthropogenic emissions can be significant (Charlson et al., 1991;1992). After production from one location, aerosols are often carried to locations far away from their sources. Most of the aerosols sources are located near the Earth's surface and hence their concentration (mass per unit volume) is larger near the surface. Occasionally there may be layers aloft depending upon the atmospheric conditions and transport phenomena. Aerosols vary greatly in sources, production mechanisms, size, chemical composition, abundance and distribution in space and time.

Aerosols are mainly produced either by bulk to particle (e.g. mechanical disintegration such as wind blown dust, sea spray aerosols) or gas to particle conversion nucleation (condensation) of low volatile gases mainly produced as a result of industrial activities, forest fires etc. The natural sources of aerosols are marine aerosols (sea salt and non sea salt aerosols) mineral dust, volcanic, extra terrestrial (meteorites), biological particles (plant debris and pollen) and biomass burning. The anthropogenic sources are mainly emissions from industries and vehicles.

1.2. Importance of Aerosol Study

Aerosols can have significant influence on Earth's climate, although making up only one part in a billion of the mass of the atmosphere. Aerosols scatter and absorb solar and terrestrial radiation (termed as direct effect) depending on their physical and chemical characteristics. Consequently, aerosols act to modify the Earth's radiation budget and thus influence the warming/cooling of the planet (Charlson et al., 1992). Aerosols can also modify the properties of clouds, where absorbing aerosols present in the clouds evaporate the clouds (cloud burn off) termed as indirect effect (Twomey, 1974).

Aerosol particles can have an indirect effect on heterogeneous chemistry, which in turn can influence climate by modifying the concentration of climate-influencing constituents (such as greenhouse gases). An increase in aerosols enhances the cloud droplet concentration, reduces the mean droplet size, thereby increasing the cloud lifetime and thus inhibiting precipitation (Twomey, 1974). Consequently the albedo of clouds increases which prevents the radiation from reaching the Earth's surface and thus plays a significant role in determining the global energy balance. Moreover, aerosols affect the air quality, in which inhalable fine particles get into our respiratory system and are hazardous to health.

Black carbon (BC), which strongly absorbs solar radiation, plays a major role in the forcing by partially shielding the surface from the solar radiation. As the aerosols are more regionally concentrated with life times of the order of a week, regional climate may be strongly influenced by absorbing aerosols. Also absorbing aerosols may have a large impact on regional hydrological cycle. As the climatic effects of aerosols receive large attention there is a greater need to reduce the uncertainties in their impacts. For these extensive measurements of physical and chemical properties of aerosols are needed.

1.3. Aerosol Production Mechanism

Atmospheric aerosols are basically produced by two mechanisms (i) bulk particle conversion (ii) gas to particle conversion.

1.3.1. Bulk to Particle Conversion (mechanical disintegration)

The fine soil and sand particles become airborne by wind. Over a rough terrain, the presence of irregular soil and sand particles cause the turbulent air motion, that picks-up the loose particles from the surface and transport to distant locations. Wind speeds as low as 0.5 ms^{-1} are capable of picking up and keeping air borne soil particles as large as 2 μm in size. Another type of mechanical production of aerosols is from the ocean waves, which produce spray droplets at their crests during strong wind conditions (wind speed > 10 ms^{-1}) (Durkee et.al., 1991, Fitzgerald, 1991).

1.3.2. Gas to Particle Conversion

The particles in the atmosphere are also produced by nucleation (condensation) of low volatile gases as a result of industrial activities, forest fires etc. This process is called Gas to Particle Conversion (GPC). Gas to Particle Conversion can form by heterogeneous or homogeneous nucleation. In homogeneous nucleation the precursor gases directly condense to form new particle whereas in heterogeneous nucleation the precursor gases condense on the surface of the other pre-existing nuclei. Heterogeneous nucleation occurs on pre-existing aerosols with sufficient surface area. The pre-existing aerosols considerably reduce the amount of super saturation required to start condensation. Chemical reactions between various gaseous species also result in products, which are highly volatile in nature and then undergo nucleation or condensation and these are catalysed by ultraviolet (UV) radiation from the Sun and presence of water vapour or OH radical. Since the particles produced by GPC are hygroscopic in nature, they can act as cloud condensation nuclei (CCN). The major components

involved in the process of GPC are sulphur and nitrogen bearing gases (Kiehl and Briegleb, 1993).

1.4. Sources of Aerosols

On the basis of sources, aerosols are generally classified into two categories such as (i) primary and (ii) secondary. Primary aerosols are those injected into the atmosphere as particles from the surface of the earth (e.g. sea salt, volcanic dust, pollen grains). Whereas, secondary aerosols are those produced by precursor gases, condensation and other atmospheric processes (e.g. SO_2, NO_x). The sources of atmospheric aerosols can be both *natural* and *anthropogenic*. The source characteristics are significant in determining the chemical nature and hence the refractive index of aerosols. Chemical composition of aerosols determines their complex refractive index. On a global scale, natural sources are stronger in abundance compared to anthropogenic sources, but on a regional scale anthropogenic sources can be stronger especially near industrialized regions.

1.4.1. Natural

Natural sources include production from sea spray, dust produced from soil by winds, volcanic eruptions, extra terrestrial, biological and forest fires.

1.4.1.1. Marine aerosols

1.4.1.1.1. Sea –salt aerosols

Sea-salt particles are produced over the sea mainly by the processes associated with the bursting of bubbles (Hoppel et al., 1990; Fitzgerald, 1991). During strong winds (wind speed greater than10 ms^{-1}) direct sea-spray production takes place by the breaking of wave crests (Russel et al., 1994). At moderate wind speeds of 3-5 ms^{-1} white capping occurs as the ocean surface waves overturn. The air trapped by these waves produces a large number of air bubbles in the near sea surface. Bubbles of air reaching the air-sea interface burst and eject

liquid droplets into the marine atmosphere. These are called jet droplets. During bursting of bubbles the breakup of the bubble film produces a shower of very small particles called film droplets (Fig 1.1).

Fig 1.1. Tearing of wave crusts leading to sea salt production

After production the seawater droplet evaporate in order to maintain equilibrium with the ambient relative humidity (RH). Depending on the RH, the particle can exist either as solution droplet or crystalline matter. Extensive measurements of sea-salt aerosols revealed that the bubble production at the sea surface and hence the concentration of sea-salt particles depends strongly on wind speed at the sea surface. Sea salt particles cover a wide size range (about 0.05 to 10 μm diameter), and have a correspondingly wide range of atmospheric lifetimes. Thus, as for dust, it is necessary to analyse their emissions and atmospheric distribution in a size-resolved model.

1.4.1.1.2. Non-sea salt (oceanic) sulphate aerosols

The main source of non-sea-salt sulphate (NSS) aerosols is from the GPC of sulphur bearing gases. The sulphur compounds present over the remote oceans can be of continental origin. Almost all species of marine phytoplankton release Di Methyl Sulphide (DMS), which get oxidized by different radicals (like OH, in presence of solar UV radiation) to form SO_2 (Charlson et al., 1987; Clarke, 1993;

Russel et al., 1994). The NSS particles present in the marine boundary layer are hygroscopic and acts as CCN. An increase in the marine DMS emission increases the number density of sulphate aerosols over the marine atmosphere and consequently the number density of cloud droplets. These in turn increase the cloud albedo. This enhancement in cloud albedo reduces global temperature and lower temperature in turn reduces productivity and emission of marine DMS. Thus a negative feedback mechanism exists which control the production of NSS aerosols.

1.4.1.2. Mineral dust

Soil dust is a major contributor to aerosol loading and optical thickness, especially in sub-tropical and tropical regions. They are produced over arid and semi-arid regions by the action of surface winds. Dust is a mixture of quartz and clay minerals. Dust deflation occurs in a source region when the surface wind speed exceeds a threshold velocity, which is a function of surface roughness elements, grain size, and soil moisture. A typical dust storm is given in Fig 1.2.

Fig.1.2. Transport of mineral aerosols during a dust storm

The long range transport of mineral dust by the combined action of convection currents and general circulation systems make these particles a significant constituent seen at locations far from their sources (Covert et al., 1996). The atmospheric lifetime of dust depends on particle size; large particles are quickly removed from the atmosphere by gravitational settling, while sub-micron sized particles can have atmospheric lifetimes of several weeks. Since these particles are generated at the Earth's surface, they are mainly confined within the troposphere. Also, the composition of the soil varies locally; the mineral aerosols derived from soil exhibit high variability in their radiative effects.

1.4.1.3. Volcanic Aerosols

Two components of volcanic emissions are of most significance for aerosols: primary dust and gaseous sulphur. A photograph of the volcanic emission is shown in Fig 1.3.

Fig1.3. A volcanic eruption emitting massive amount of gases and ash

Volcanic eruptions of large magnitude can impact global climate, reducing the amount of solar radiation reaching the Earth's surface, lowering temperatures in the troposphere, and changing atmospheric circulation patterns. Large scale volcanic activity may last only a few days, but the massive outpouring of gases and ash can influence climate patterns for years. Sulphuric gases convert to sulphate aerosols, sub-micron droplets containing about 75 percent sulphuric acid.

Following eruptions, these aerosol particles can linger as long as three to four years in the stratosphere. Volcanic eruptions alter the Earth's radiative balance, mainly because volcanic aerosol clouds absorb terrestrial radiation and scatter a significant amount of the incoming solar radiation.

1.4.1.4. Extra terrestrial Aerosols

Perhaps the most fundamental natural background level for the atmospheric aerosol consists of extraterrestrial dust (Opik, 1958). The origin of this material is thought to be associated largely with debris from comets. These particles are considered to be the primary cause for the positive ion concentration in the upper atmosphere. The extraterrestrial component has its greatest influence in the high atmosphere, and may be best known through the explanation of the zodiacal light (the scattering of light by particles at high altitudes). The extraterrestrial materials make up a larger share of particles found above 30 to 40 km height. Extraterrestrial or interplanetary dust refers to the solid particles present in space ranging in size from tenths of micrometers to a few millimeters in diameter. The origin of this material is thought to be associated largely with debris from comets. These particles are considered to be the primary cause for the positive ion concentration in the upper atmosphere.

1.4.1.5. Biological Aerosols

Biological aerosol consists of plant debris (cuticular waxes, leaf fragments etc.), humic matter and microbial particles (bacteria, fungi, viruses, algae, pollen,

spores etc.). Their contribution in densely vegetated regions, particularly the moist tropics, could be even more significant. The presence of humic-like substances makes this aerosol light absorbing, especially in the UV-B region (Havers et al., 1998), and there is evidence that biogenic particles may be able to act both as cloud droplet and ice nuclei (Schnell and Vali, 1976). They may, therefore, be of importance for both direct and indirect climatic effects, but not enough is known since their atmospheric abundance may undergo large changes as a result of land-use change, and they deserve more scientific study.

1.4.1.6. Biomass Aerosols

Forest and bush fires have occurred from time to time across the globe. They are prolific sources of biomass aerosols (Fig 1.4). Forest fires produce large quantities of finely divided particles in the sub micrometer size range. The uncontrolled combustion of bush and forest debris has not been studied extensively for the nature of the particle produced. The mean particle diameter is approximately 0.3 μm; there are also few particles present above the 10 μm diameter.

Fig1.4. Biomass burning ejecting organic aerosols into the atmosphere

The composition of smoke from fires varies over a wide range, producing mostly volatile and non-volatile carbon material, with significant amounts of sulfate, nitrate and chlorine. But distinction is possible in the nitrate content in the smoke from grass burns and trees. One of the major components of these forest fires are the carbonaceous particles. Soot is one of the general components of all fires. Hot flaming fires emit relatively small amounts of aerosol with high soot content, while smoldering fires emit large amount of organic carbon with a relatively small share of soot component (Crutzen and Andreae, 1990).

Organic carbon (OC) is the largest single component of biomass burning aerosols (Andreae et al., 1983; 1984; Cachier et al., 1995; Artaxo et al., 1998). Organics are also important constituents, perhaps even a majority, of upper-tropospheric aerosols (Murphy et al., 1998). The presence of polar functional groups, particularly carboxylic and dicarboxylic acids, makes many of the organic compounds in aerosols water-soluble and allows them to participate in cloud droplet nucleation (Saxena et al., 1995; Saxena and Hildemann, 1996; Sempéré and Kawamura, 1996). Later field measurements have confirmed that organic aerosols may be efficient cloud nuclei and consequently play an important role for the indirect climate effect as well (Rivera-Carpio et al., 1996).

1.4.2. Anthropogenic

Throughout the globe man's domestic and industrial activities contribute a dominant share of the tropospheric particle burden.

1.4.2.1. Sulphates

Most of the SO_2 emissions globally result from fossil fuel burning. It also comes from industrial sources like oil refineries and power plants (*See* Fig. 1.5). For this reason, most of the aerosol produced from the oxidation of SO_2 is considered to be anthropogenic sulphate aerosol (ASA). The source strengths for this trace gas are fairly well known compared to other aerosol precursor gases, and recent

estimates differ by not more than ~20 to 30% (Quinn, 1992). SO_2 must be oxidized to SO_4^{-2} (sulphate) before it plays a role in aerosol formation. The oxidation can take place while SO_2 is still in the gas phase, or after SO_2 becomes dissolved in cloud droplets (aqueous production). In the latter case, the sulfate becomes aerosol after the cloud droplets evaporate. Both pathways produce sulphate aerosols in the submicron size range that are efficient light scatterers. Sulphate is known to condense onto larger aerosol particles with lower scattering efficiencies and shorter atmospheric lifetimes.

Fig.1.5. Industrial emission of anthropogenic sulphates

The calculated residence times of SO_2, defined as the global burden divided by the global emission flux, range between 0.6 and 2.1 days as a result of different deposition parameterizations (Quinn, 1992; Penner et al., 1998). Because of losses due to SO_2 deposition, only 46-82 % of the SO_2 emitted undergoes chemical transformations and forms sulfate. The residence time of sulfate is

mainly determined by wet removal and is estimated to be between 2.7 and 7.2 days.

1.4.2.2. Nitrates

Nitrates are secondary particles formed through chemical reactions involving gases and other particles in the atmosphere. The major anthropogenic sources include vehicles, factories, and emissions during agricultural practices. Aerosol nitrate is closely tied to the relative abundances of ammonium and sulphate. If ammonia is available in excess of the amount required to neutralise sulphuric acid, nitrate can form small, radiatively efficient aerosols. Forcing due to nitrate aerosol is important at the regional scale (ten Brink et al., 1996). Observations and model results both show that in regions of elevated NO_x and NH_3 emissions, such as Europe, India, and parts of North America, NH_4NO_3 aerosol concentrations may be quite high and actually exceed those of sulphate.

1.4.2.3. Black carbon Aerosols

Carbonaceous compounds make up a large but highly variable fraction of the anthropogenic component of atmospheric aerosol. Black carbon (BC) aerosols are of particular importance for the direct effect due to the light-absorbing character (Penner et al., 1991). The only known source of BC in the atmosphere is the combustion of carbonaceous fuels and not by any atmospheric reactions. These aerosols are formed as a by-product of incomplete combustion of fossil fuels and consist of a mixture of graphite and light absorbing particles and constitute the fine mode size particles. A significant amount of emissions may reach the free atmosphere due to fast vertical transport and resides there long enough due to their large life time in the upper atmosphere. The sink of these surface emissions is attributed to wet or dry deposition.

The most important function of black carbon in the atmosphere is the absorption of solar radiation. These anthopogenic emissions are a strong absorber in the visible and near infrared part of the spectrum, where most of the solar energy is distributed. Its light absorbing properties reduces atmospheric visibility (Wolf,

1981). The absorption of light by them offsets the effects of most other aerosols (such as sulphates), which have light scattering properties that counteract the global-warming effects of CO_2 and other greenhouse gases. These types of aerosols induces radiative heating (Blanchet, et al., 1986) and even in small quantities may dramatically affect the aerosol cooling properties especially above surfaces of high reflectivity or when incorporated in clouds (Liousse, et al., 1996).

Elemental carbon is hydrophobic and chemically inert (Crutzen, et al., 1984; Chen et al., 2001). But as the aerosol ages it gets internally mixed with other aerosols in samples and loses its hydrophobic property and act as CCN. Studies have shown that absorption of solar radiation by these within a cloud or in a clear region can result either in a local reduction of the cloud cover or can inhibit cloud formation respectively (Ackerman et al., 2000). Carbonaceous particles within clouds increase the absorption of solar radiation and decrease the albedo. They affect the cloud albedo by altering the hygroscopic properties of CCN (Penner et al., 1991; Liousse et al., 1996), and the solar heating caused by these absorbing aerosols can reduce cloudiness (Ackerman et al., 2000). It has been estimated by the IPCC that the global mean clear-sky radiative forcing of BC is about +0.1 Wm^{-2} (IPCC, 1996; Penner et al., 2001).

The dry deposition rate of BC is thought to be 0.1 cm s^{-1}. The mean globally averaged lifetime of BC is 7.85 days (Orgen, 1982). Yet, there is considerable uncertainty in the residence time of these fine mode carbon particles in the atmosphere. The fact that BC is found in Polar Regions suggests that the atmospheric lifetime is at least a week or more. Thus it seems reasonable to assume that the BC atmospheric lifetime to be between 3 and 12 days.

1.4.3. Source strength

The sources of atmospheric aerosol components vary significantly with region and time of year. This, together with the fact that the aerosol lifetime is relatively

short (about 5 days), implies that the concentrations of the components also vary significantly with location and time. Table 1.1 below presents Northern Hemispheric (NH) and Southern Hemispheric (SH) average sources for primary particulates according to aerosol size ($d < 2$ μm and $2 < d < 20$ μm). It is seen that carbonaceous aerosols together with mineral dust constitutes significant portion of the fine mode aerosols in the northern hemisphere.

Table 1.1. Annual source strength for emissions of gas phase aerosol (Tg/yr) (Tegen and Fung, 1995)

Source	NH	SH
Fossil fuel	19.9	1.1
Volcanoes	6.3	3.0
Biomass burning	2.9	2.7
Sea salt	23	31
Mineral dust (< 1μm)	90	17

The fine mode fraction of the atmospheric aerosol (defined as that portion with diameter less than 1μm) has been studied extensively because it contains the largest number fraction and is the most important fraction for determining the direct radiative forcing. The composition and number concentration of the sub-micron fraction is also important for determining the indirect effects of aerosols.

1.5. Classification of Aerosols

The aerosols can be classified by its shape, size, density and refractive index. For air quality studies the important characteristics that should be assessed is the aerosol mass concentration and from the radiative and optical point of view it is the Aerosol optical depth, size distribution, single scattering albedo, asymmetry factor and phase function. A brief description of the basic properties as well as its optical and radiative properties are given below

1.5.1. Aerosol Shape

Aerosols occur with different shapes. They can be classified as follows (Reist, 1984). *Isometric particles* are those for which all three dimensions are roughly the same. One common example is the spherical particles. *Platelets* are particles that have two long dimensions and one small third dimension. Leaf fragments are examples of this type of aerosols. *Fibres* are particles with great length in one dimension and much smaller dimensions in the other two. Threads or mineral fibres are examples of this type of aerosols.

1.5.2. Aerosol Size

The size of aerosol particles is usually given as the radius of the particle (assuming a spherical shape). Aerosols are usually assigned into one of the following three size categories (Whitby, 1978). Aitken particles, or *nucleation mode*: (0.001 - 0.1 μm radius), Large particles, or *accumulation mode*: (0.1 - 1 μm radius), Giant particles, or *coarse particle mode*: (1.0-100 μm radius). Table 1.2 shows the different particle size, its chief source and lifetime.

Table 1.2. Classification of aerosols based on size

Particle Size Range (μm)	**Classification**	**Chief Source**	**Life Time**
0.001-0.1	Aitken particles, or *nucleation mode*:	Gas to Particle Conversion	< 1 day
0.1 – 1.0	Large particles, or *accumulation mode*	Coagulation and Heterogeneous Condensation	Days to week
1.0 –100	Giant particles, or *coarse particle mode*	Mechanical Disintegration	In hours

The terms *nucleation mode* and *accumulation mode* refer to the mechanical and chemical processes by which aerosol particles in those size ranges are usually produced. The smallest aerosols, in the nucleation mode, are principally produced by *gas-to-particle conversion* (GPC), which occurs in the atmosphere.

Aerosols in the accumulation mode are generally produced by the *coagulation* of smaller particles and by the *heterogeneous condensation* of gas vapour onto existing aerosol particles. Most aerosol particles in the nucleation mode are comprised of sulphuric compounds, and are the result of the oxidation of sulphur containing precursor gases (like SO_2, H_2S, CS_2, COS) to sulphate (SO_4^{2-}), and subsequent condensation into particle form (homogenous GPC).

1.5.3. Aerosol Density

Particle density refers to the mass per unit volume of the particle. In dry state, the volume of the particles is exactly the sum of the volumes of all its water soluble and insoluble components. Generally, the mean bulk density of aerosols ranges between 1.0 and 3.0 g cm^{-3}. In the following table the densities of a few typical aerosol types are given (Hess et al., 1998). Table 1.3 shows the density of different aerosol species.

Table 1.3. Densities of different aerosol species

Aerosol species	**Density (gcm^{-3})**
Water insoluble	2.0
Water soluble	1.8
Sea-salt	2.2
Mineral dust	2.6
Soot	1.0
Sulphate droplets	1.7
Volcanic dust	2.8

1.5.4. Refractive index

Particle refractive index is an important parameter in determining the radiative properties of aerosols (d'Almeida et al., 1991) and depends on the chemical composition; and hence refractive index depends on the source of particles and the microphysics. The real part determines the scattering properties and imaginary part, the absorption characteristics. Particles originating from combustion processes usually have high absorption properties and hence high imaginary part of refractive index. The real and imaginary parts of refractive indices are maximum for soot particles and minimum for sea salt particles. Table 1.4 shows the refractive indices of different aerosol species.

Table 1.4. Refractive indices of different aerosol species

Wavelength(μm)	Water Soluble	Dust like	Soot	Sea salt
0.4	1.53- i0.005	1.53- i0.008	1.75- i0.46	1.5-i3.0E-08
0.55	1.53-i0.006	1.53- i0.008	1.75- i0.44	1.5- i E-08
0.7	1.53- i0.007	1.53- i0.008	1.75- i0.43	1.49- iE-07

1.6. Size Distribution

Atmospheric aerosol particles present a wide range of particle sizes and concentration. A suitable analytic function was sought, which accurately fits the size distribution observations.

1.6.1. Junge Power Law

Junge (1963) has given the power law distribution of the form

$$\frac{dn(r)}{d\log r} = cr^{-v} \qquad \ldots(1.1)$$

where *dn (r)* expresses the number of particles having a radius between *r* and *r+dr* per unit volume, *c* is a constant depending on the number density of particles and *v* is the power law index which gives the relative dominance of large aerosol particles over the smaller ones. The advantage of this distribution is that by knowing the values of *v* and *c*, we can determine the size distribution.

1.6.2. Log Normal

Aerosol size distribution can often be represented by a lognormal distribution function. This type of functions has the form

$$\frac{dn(r)}{d\ln r} = \sum \frac{N}{\sqrt{2\pi}\ln\sigma_i} \exp\left(\frac{-\ln\left(\frac{r}{r_i}\right)^2}{2\ln(\sigma_i)^2} \right) \quad \ldots(1.2)$$

Where r_i is the mode radius of the particle and σ_i the standard deviation. This type of functions is used to represent aerosol size distributions near the source regions where *i* represent each source.

1.7. Aerosol Size Transformation Processes

There are different processes, which transform aerosols particle of one size to another size range. The major aerosols transformation processes are coagulation, and condensation. Though these processes do not remove the aerosols mass from the atmosphere, and hence cannot be called removal mechanisms they are capable of producing changes in the aerosols number density size distribution and hence in their optical, radiative and environmental effects. Thus these processes are very important in aerosol science.

1.7.1. Coagulation

At high aerosols concentrations, two or more aerosol particles collide and coalesce together to form one larger particle; the process known as coagulation.

It is the result of particles coming into contact due to Brownian diffusion or due to electrostatic force. Coagulation is mainly controlled by the diffusion coefficient (μ) of particles which is in turn related to particle mobility (B) through the relation,

$$\mu = BK_BT \qquad ...(1.3)$$

Where, K_B is the Boltzmann's constant and T, the absolute temperature.

Coagulation is also enhanced in shearing or turbulent flows, as these induce fast relative particle motion. The factors favorable for coagulation are higher concentration and smaller particle sizes. The smaller the particles and greater the concentration, the greater is the rate of coagulation and hence this process limits the lower end of the aerosol size spectrum. Coagulating particles shift mass from smaller particle sizes to larger ones, and hence the total mass of the aerosol system remains conserved. The rate of coagulation is minimum when all the particles are of the same size and it increases rapidly as the size difference increases (McCartney, 1976; Pruppacher and Klett, 1978).

1.7.2. Condensation

Since most of the aerosols are in the sub micron range (r < 1μm), they present large amount of surface area. The condensation of vapours present in the atmosphere on these aerosols makes them to grow in size. The rate of condensation ultimately depends on the aerosols size and the concentration and diffusion coefficient of the vapour. Condensation of water vapour takes place on the aerosols with increasing relative humidity (RH) and evaporation of water present on the aerosols takes place with decreasing RH. The vapour pressure over a solution droplet is proportional to the product of vapour pressure of the pure solvent and the mole fraction of the solvent according to *Rault's law*. As the RH increases, to maintain the particle in equilibrium with the ambient RH, condensation takes place and conversely, as RH decreases evaporation takes

place. Thus, the aerosols particle grow as RH increases and shrink as RH decrease, however, the processes are not totally reversible.

With changes in the relative humidity (RH), the optical properties of the aerosol also change. Small hygroscopic particles respond quickly to changes in RH, absorbing and releasing moisture as fast as the RH changes. Condensation nuclei are the most active components of haze aerosols, as contrasted with particles that are not hygroscopic. Ordinary dust particles, are non-hygroscopic, which other types, such as sea salt, are highly hygroscopic. These hygroscopic particles acts as CCN, and are more active members. Their size depends on the ambient RH, availability of water, ability to coagulate by collisions. Physical parameter such as mean density, size distribution and refractive index undergo changes with changes in RH with consequent impact on the radiative properties of aerosols.

1.8. Residence Time

The residence time of aerosols depends on their size, chemistry and height in the atmosphere. Particle residence times range from minutes to hundreds of days. Aerosols between 0.1 - 1.0 μm (the accumulation mode) remain in the atmosphere longer, and hence it is more important in aerosol studies. The smaller aerosols (nucleation mode) are subjected to Brownian motion; so that, due to particle collision and coagulation the size of individual particles increases. The coarser particles (> 1 μm radius) have less residence time due to their higher sedimentation rates. The residence time varies from a few days at lower troposphere to few years in the stratosphere, due the lack of effective removal mechanisms. Thus residence time is a function of size, altitude and atmospheric conditions (Pruppacher and Klett, 1978).

The residence time of atmospheric aerosol particles at various levels in the atmosphere is gives in following Table 1.5.

Table 1.5. Residence time of aerosols in different altitudes

Level in the atmosphere	**Residence Time**
Below 1.5 Km	0.5 – 2 days
Lower Troposphere	2 days to 1 week
Middle and Upper Troposphere	1 – 2 weeks
Tropopause Level	2 weeks to 1 month
Lower Stratosphere	1 to 2 months
Upper Stratosphere	1 – 2 years
Lower Mesosphere	4 – 20 years

1.9. Vertical Distribution

The vertical distribution of aerosols show a rapid decrease of particle size from a range of 10^3-10^4 cm^{-3} at the ground level to a low value of 0.1- 19 cm^{-3} above 25 km. The maximum in large particles aloft is found between 12 and 25 km altitude depending on latitude. This layer of large particles is sometimes referred to as the *Junge layer* in the stratosphere. Recent studies using Lidar has reported maximum amplitude of aerosol extinction to peak around 29 km in the northern hemisphere (Thampi et al., 2009). Below 5 km over the continents and adjacent areas over the oceans, concentration is higher owing to the vicinity of the sources. Over the oceans there is almost a constant profile of aerosol concentration (Bigg et al., 1984). Concentrations of aerosols decrease exponentially with height, thus

$$N(Z) = N(0)\exp\left(\frac{-z}{H}\right) \qquad \ldots(1.4)$$

where *N(0)*, *N(z)* are the concentrations at heights 0 and *z* (km) above ground level, respectively. The scale height *H* typically is 10 km for continental (including desert) air in summer, 6 km for urban air, 2 km for continental air in winter, and 1 km over the marine subtropical high pressure regions. The higher values during the summer imply more deep tropospheric stirring of the aerosols

by thunderstorms. In places with a well defined, long lived inversion on top of a well mixed planetary boundary layer, the aerosol concentration tends to be homogenous in the atmospheric boundary layer (Hess, et al., 1998).

1.10. Aerosol Transport

Mesoscale or synoptic scale air mass types influences the aerosol properties (Smirnov et al., 1995). Aerosols get transported from its source region to distant places by means of prevailing winds. If wind is very persistent and the residence time of the aerosols is more then it gets transported to distant regions. In addition, transport of aerosols and aerosol precursor gases to the upper troposphere can impact the concentration of several trace gases, including water vapour, and the population of ice crystals in cirrus clouds. The air trajectories are also very potential in advecting aerosols from distinct source regions and causing changes in the optical characteristics at far off locations (Krishnamurthy et al, 1998, Moorthy et al., 2001).

Large-scale transport of dust occurs from Africa to south Indian Ocean, from West Asia to Arabian Sea, from China across the Pacific, from Australia over to Indian Ocean (Prospero et al., 1983; Uematsu et al., 1983; Tyson et al., 1996; Kaufman et al., 2000; Moorthy and Satheesh, 2000; Moorthy and Saha, 2000; Satheesh and Srinivasan, 2002). Since these particles are generated at the earth's surface, they are mainly confined within the troposphere. It has been observed that the northeast monsoonal low level flow can transport sulphates, mineral dust and other aerosols from the Indian subcontinent to the ITCZ (Inter Tropical Convergence Zone) within 6 to 7 days (Krishnamurthy et al, 1998).

1.11. Aerosol Removal

1.11.1. Wet deposition

Wet deposition includes rainout, and washout. Brief qualitative explanations of these are given as follows.

1.11.1.1. Rain out (nucleation scavenging)

Rainout or nucleation scavenging describes the removal of a cloud condensation nucleus. It is the most important natural removal processes of tropospheric aerosols. As this process takes place within the cloud, it is also known as in-cloud scavenging. In clouds producing rain, some of these drops grow to such a large size that they fall (gravitationally settle) to the surface as raindrops. The aerosol (condensation nuclei) deposited in this way is said to rain out.

1.11.1.2. Wash out (precipitation scavenging)

Washout or precipitation scavenging, describes the removal of aerosol by cloud droplets. In this processes an aerosol is incorporated into an already existing cloud drop. As the processes continue, the drop grows large enough to fall as rain. Then the particle is said to wash out. Both liquid (fog, cloud droplets and raindrops) and solid (ice crystal, snow, graupel and hail elements) precipitation can be involved in the removal process. A falling raindrop collects lot of fine aerosols along its path, which are also finally removed from the atmosphere along with the falling raindrop. Hence it is also referred to as below cloud scavenging or impaction scavenging.

The difference between washout and rainout is the required pre-existence of a collecting drop for washout.

1.11.2. Dry Deposition

Dry deposition pathways are the group of deposition mechanisms that transport pollutants (in this case particle) directly to the surface without the aid of precipitation. The two parameters determining the fall velocity are particle mobility and particle mass. The particle mobility decreases as the air density increases. Thus, the mobility is lesser in lower atmosphere where the atmosphere is denser and mobility increases with increase in altitude. Since the fall velocity is directly proportional to the particle mobility, at lower levels, the fall velocity is less compared to that at upper levels. In addition to particle mobility, the only

parameter determining the fall velocity is the particle mass. Hence large and heavier particles have higher fall velocity compared to finer and lighter ones. About 10 to 20% of the aerosol removal takes place through the sedimentation process (Wallace and Hobbs, 2006).

1.12. Effects of Aerosol

The presence of suspended particles in the atmosphere provides a variety of natural phenomena that are of interest and represent an important part of aerosol science. Besides its optical effects (such as scattering and absorption), it also affects the cloud microphysics and thus has an effect on precipitation. Moreover, finely divided particulate matter is a contributor to respiratory disease. Toxic chemicals and carcinogens, which originate from organic and inorganic compounds, pose a hazard to the well being of the modern world. Therefore these distinctive roles played by the aerosols make itself an important part of scientific research.

1.12.1. Optical Effects

Particulate matter in the air exerts an influence on the transfer of electromagnetic radiation through the atmosphere. This manifests itself in changes in visibility and coloration as a result of light scattering. The sky colour and haziness, is a direct result of the influence of suspended particles interacting with the visible light. Sunlight as it passes through the atmosphere undergoes various changes and they are grouped into the optical phenomena of light.

1.12.1.1. Scattering

It is the processes by which a scatterer in the path of an electromagnetic wave continuously (1) abstracts energy from the incident wave and (2) re-radiates into the total solid angle centered at the particle. For scattering to occur, the refractive index of the particle must be different from that of the surrounding medium (McCartney, 1976). Both scattering and absorption removes flux from a given

beam of light, but scattering does not produce net change in the internal energy states of molecules. But, absorption does produce changes in the energy states. The three major parameters of scattering are (i) particle size (ii) refractive index (iii) wavelength of the incident light.

Scattering can be broadly classified into two, *Elastic* and *Inelastic* scattering. In elastic scattering, the wavelength of the scattered radiation is at the same wavelength as that of the incident radiation while in the inelastic scattering, the wavelength of the scattered radiation is different from that of the incident radiation. The elastic scattering can be again classified into two, the *Rayleigh* and the *Mie* scattering, depending on the size of the particle relative to the wavelength of the incident radiation. The intensity distribution pattern for Rayleigh and Mie scattering is shown in Figure 1.6.

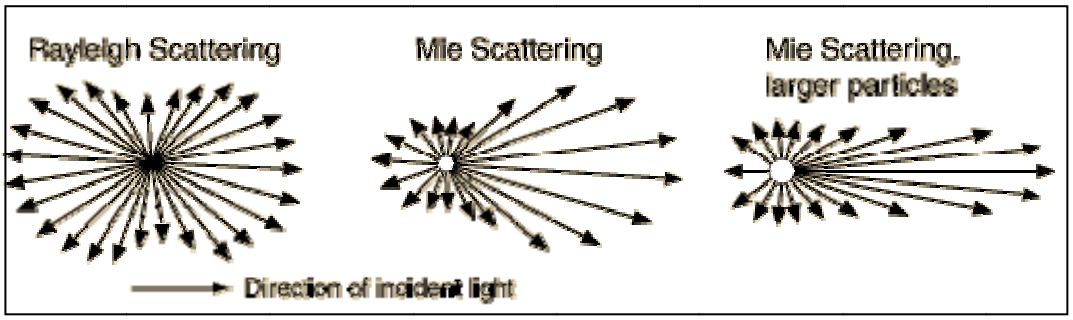

Fig1.6. Intensity distribution pattern for Rayleigh and Mie scattering

1.12.1.1.1. Rayleigh scattering

When the particle diameter is far smaller than the incident wavelength (< (1/10) λ) the scattering is called Rayleigh scattering. Scattering of this type varies directly as the second power of the particle volume and inversely as the fourth power of the wavelength, with equal amount of fluxes in the forward and back hemispheres. The principal Rayleigh scatters in the atmosphere are the molecules of atmospheric gases.

1.12.1.1.2. Mie scattering

As the particle size becomes comparable to the wavelength of the incident radiation Rayleigh theory becomes inadequate to explain the scattering phenomena. As the particle size increases, the scattering is no more symmetric and more radiation is scattered in the forward direction than in the backward direction, which is the most important property of the Mie scattering. Mie scattering is highly anisotropic with forward scattering dominating over back scattering. The scattered intensity has a much weaker dependence and is dependent on the size of scattering.

The basic process of aerosol – radiation interaction involves scattering and absorption of solar and terrestrial radiation and angular re-distribution of the scattered energy. In this perspective several terms are involved which can be explained briefly as follows.

1.12.1.1.3. Scattering cross section

Scattering cross section is defined as the cross section of an incident wave, acted on by the particle, having an area such that the power flowing across it is equal to the total power scattered in all directions.

1.12.1.1.4. Angular scattering cross section

Angular scattering cross section is defined as that cross section of an incident wave, acted on by the particle, having an area such that the power flowing across it is equal to the scattered power per steradian at an observation angle.

1.12.1.1.5. Total scattering cross section

Scattering cross section is defined as the cross section of an incident wave, acted on by the particle, having an area such that the power flowing across it is equal to the total power scattered in all directions.

Thus,

$$\sigma_{sc} = \int_0^{4\pi} \sigma(\theta) dw \qquad (1.5)$$

Where σ_{sc} is the scattering cross section, $\sigma(\theta)$ is the angular cross section and dw is the solid angle defined as the integrated vertical column of unit cross section.

Phase function defines the angular scattering properties or the way the scattered energy is re-distributed as a function of the scattering angle. Phase function P(θ), is defined as the energy scattered per unit solid angle in a given direction (E_θ) to the average energy in all directions (E_{sc}). It can be written as

$$P(\theta) = \frac{E(\theta)}{E_{sc}/4\pi} \qquad (1.6)$$

1.12.1.1.6. Scattering coefficient (β_{sc})

The aerosol scattering coefficient is defined as the total amount of flux scattered from a light beam by unit volume of particles in suspension per unit irradiance of the incident beam. The total scattering for a mono dispersion is given by

$$\beta_{sc} = N\sigma_{sc} \qquad (1.7)$$

where N is the number of aerosols in unit volume of air (cm^{-3}) and σ_{sc} is the scattering cross section of a single particle (cm^2). Scattering cross section (σ_{sc}) cross section of an incident wave, acted on by the particle, having an area such that the power flowing across it is equal to the total power scattered in all directions.

Since scattered radiation proceeds into the entire 4π radians surrounding the particle,

$$\sigma_{sc} = \sigma(\theta)\, d\omega \tag{1.8}$$

The *scattering efficiency factor* (Q_{sc}) is defined as the ratio of the scattering cross section to the geometric cross section of these particles. Q_{sc} is related to scattering coefficient β_{sc} by the relation

$$\beta_{sc} = N\pi r^2 Q_{sc} \tag{1.9}$$

The scattering and absorption efficiencies can be written as

$$Q_{sc,ab} = \sigma_{sc,ab} / \pi r^2 \tag{1.10}$$

Similarly, the *absorption coefficient* is given as

$$\beta_{ab} = N\, \sigma_{ab} \tag{1.11}$$

Where σ_{ab} is the scattering cross section of a single particle (cm^2).
Here the *absorption efficiency factor* (Q_{ab}) is defined as the ratio of the scattering cross section to the geometric cross section of these particles. In relation to scattering coefficient β_{ab} is given by the relation

$$\beta_{ab} = N\pi r^2 Q_{ab} \tag{1.12}$$

1.12.1.1.7. Extinction coefficient (σ_e)

Extinction is the overall effects of scattering and absorption. It indicates the fraction of energy removed, per unit path length, from an incident wave with energy flux density 1 by a collection of particles in suspension characterized by the particle size distribution. The processes of scattering and absorption are additive and hence the cross sections, coefficients and efficiency factors of

extinction can be obtained by adding the corresponding parameters of absorption and scattering.
Thus,

$$\sigma_{ext} = \sigma_{sc} + \sigma_{ab}$$
$$\beta_{ext} = \beta_{sc} + \beta_{ab} \quad (1.13)$$
$$Q_{ext} = Q_{sc} + Q_{ab}$$

1.12.1.1.8. Single scattering albedo

Single scattering albedo is the fraction of energy removed from the incident wave, which reappears as scattered radiation. The single scattering albedo equals 0 for a perfectly absorbing aerosol and equals 1 for a pure scatterer. It is a very important characteristic of aerosols. It is given as,

$$\omega = \frac{\sigma_s}{\sigma_e} = \left[\frac{\sigma_s}{\sigma_a + \sigma_s}\right] \approx 1 - \left[\frac{\sigma_a}{\sigma_e}\right] \quad (1.14)$$

where, σ_e σ_s σ_a are the extinction, scattering and absorption coefficients respectively.

For sulphate aerosols, $\omega \approx 1$, and hence they act as scatterers of solar radiation leading to increase in albedo and a net cooling of Earth's surface. For soot, ω is very small (≈ 0.2), and hence large amount of radiation is absorbed leading to local heating.

1.12.1.2. Aerosol Optical Depth (AOD)

Aerosol Optical Depth is the integration of the extinction coefficient over a path length through the atmosphere. The optical thickness or depth (τ), for a path length x is defined by

$$\tau = \int_0^x \beta(x) dx \quad (1.15)$$

Which implies that the coefficient $\beta_{,}$ (a constant which defines the ability of a unit volume of a suspension to scatter light of a specified wavelength totally), has a constant value over the distance *x*.

1.12.2. Physiological Effects

An aerosol component can be a health hazard, if it is able to get into the respiratory system. Aerosols generated by natural processes are transported to great distances with the help of wind. Submicron particles produced from viral and bacterial disease agents, radioactive products, smokes and fumes from vegetation fires and geothermal sources, affects the lungs and cause respiratory ailments like bronchitis and asthma (Uno et al., 1984). $PM_{2.5}$ particulate is all particles sized 2.5 microns and smaller. The observed human health effects of PM include breathing and respiratory symptoms, aggravation of existing respiratory and cardiovascular disease, alterations in the body's defense system against inhaled materials and organisms, and damage to lung tissue. PM_{10} is that includes only those particles smaller than 10 microns. Prolonged exposure may irritate healthy people's eyes, nose, throat, and lungs, and might cause more serious problems in sensitive populations. In addition to that it can cause cough, phlegm, wheezing, shortness of breath, bronchitis, increased asthma attacks, and aggravation of lung or heart disease.

1.12.3. Chemical Effects

Aerosols also can act as sites for chemical reactions to take place (heterogeneous chemistry). The most significant of these reactions are those that lead to the destruction of stratospheric ozone. During winter in the Polar Regions, aerosols grow to form polar stratospheric clouds. The large surface areas of these cloud particles provide sites for chemical reactions to take place. These reactions lead to the formation of large amounts of reactive chlorine and, ultimately, to the destruction of ozone in the stratosphere

1.12.4. Effect on Cloud properties

The global mean cloud cover is close to 60%; the global average volume fraction of clouds in the troposphere is 7-8%. Since most clouds occur in the lower atmosphere, which involves most of its mass, about 10% of the total mass of the troposphere is contained in cloud systems; the cloud volume fraction in the lower troposphere is about 15%. On the average, only one-tenth of these clouds are in a precipitating state. Moreover, the global average precipitation efficiency is about 50%, which means that half of the amount of water entering a precipitating system reaches the Earth's surface (Cotton and Anthes, 1989), while half of the water that has condensed in the atmosphere evaporates again. Water vapour condenses on aerosol particle that act as CCN. The mean CCN lifetime in the atmosphere is about one week, so that these particles go through about 5-10 cloud condensation-evaporation cycles before being removed from the troposphere.

The life cycle of a cloud- its formation, development (both microphysical and chemical), and dissipation- is linked in part to the nature of the aerosol on which the cloud forms. This property of the aerosols to act as CCN is dependent on their chemical composition and size. The CCN sources are, in general, secondary aerosols of either natural or anthropogenic origin. Non-sea-salt sulfate is considered to be the major natural source, while biomass/organic and sulfate aerosols are major anthropogenic sources. The ability of pure inorganic salts and acids such as nitrates, sulphates or sulphuric acid to act as CCN is relatively well investigated in experimental and modelling work. The indirect effect is the mechanism by which aerosols modify the microphysical and radiative properties; amount and lifetime of clouds (see *Fig 1.7)*. Key parameters for determining the indirect effect are the effectiveness of an aerosol particle to act as a cloud condensation nucleus, which is a function of the size, chemical composition, mixing state and ambient environment (e.g., Penner et al., 2001; 2004).

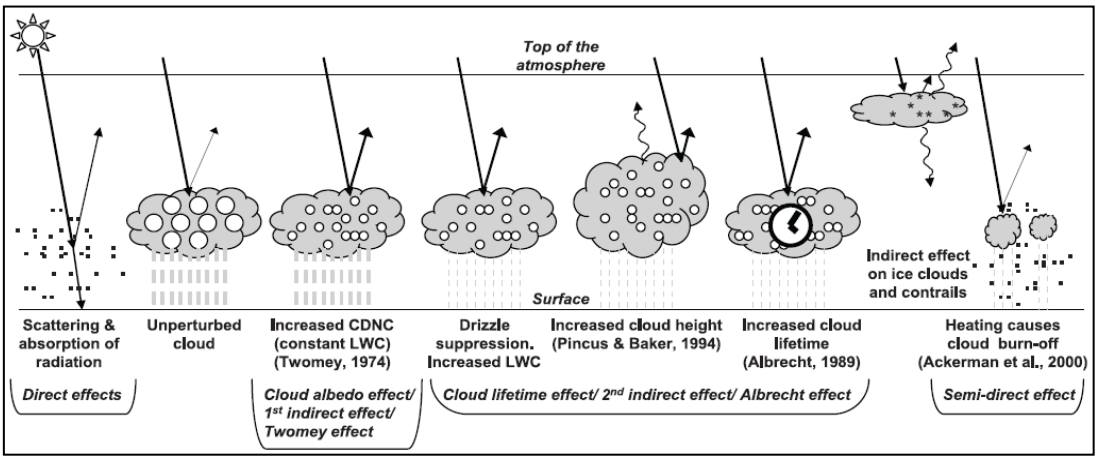

Fig.1.7. Schematic diagram showing the various radiative mechanisms associated with cloud effects that have been identified as significant in relation to aerosols. The small black dots represent aerosol particles; the larger open circles cloud droplets. Straight lines represent the incident and reflected solar radiation, and wavy lines represent terrestrial radiation. The filled white circles indicate cloud droplet number concentration (CDNC). The vertical grey dashes represent rainfall, and LWC refers to the liquid water content (IPCC, 2007).

The microphysically induced effect on the cloud droplet number concentration and hence the cloud droplet size, with the liquid water content held fixed has been called the *first indirect effect* (e.g., Ramaswamy et al., 2001), the *cloud albedo effect* (e.g., Lohmann and Feichter, 2005), or the *Twomey effect* (e.g., Twomey, 1977). The microphysically induced effect on the liquid water content, cloud height, and lifetime of clouds has been called the *second indirect effect* (e.g., Ramaswamy et al., 2001), the *cloud lifetime effect* (e.g., Lohmann and Feichter, 2005) or the *Albrecht effect* (e.g., Albrecht, 1989).

The liquid water content (LWC) is related to fluctuations in the vertical air velocity. Strong updrafts, which produce rapid cooling and high supersaturation cause high LWC. The average droplet radius in the marine clouds is approximately twice as large as in continental clouds. Thus marine clouds are characterized by relatively large droplet radii and small droplet number concentrations. Observations show that the residence time of air parcels in clouds is considerably shorter than the lifetime of clouds. This is a consequence of the rapid vertical transport of air through the clouds.

1.13. Radiative Forcing of Aerosols

Aerosols particles play an important role in radiation budget of the atmosphere. Because aerosols are regionally concentrated, absorbing aerosols can impose a large horizontal gradient in radiative heating, which can directly alter the general circulation, which in turn can perturb the precipitation patterns (Russel et al., 1999). Aerosols modify incoming solar and outgoing IR radiation. Change in radiation flux caused by aerosol is referred to as *aerosol radiative forcing*. The effect of aerosols on the top of the atmosphere (TOA) radiative fluxes is called top of the atmosphere radiative forcing and that on surface radiative fluxes is called the surface radiative forcing. The difference between the two is the atmospheric radiative forcing. Aerosol forcing is defined as the difference in radiative fluxes with and without aerosols. In a study done from an urban location; Babu et al., (2002) have demonstrated the significant role of carbonaceous aerosols over the urban land where it reduces the single scattering albedo, reversing the sign of Top Of Atmosphere (TOA) forcing.

Effects of aerosols on solar radiation can be broadly classified into two; (1) direct forcing and (2) indirect forcing.

1.13.1. Direct Radiative Forcing

The interactions of radiation with aerosols can be either on account of scattering or absorption. The scattering and absorption of visible radiation (short wave) by aerosols produces changes in climate by changing the planetary albedo. Absorption and re-radiation of IR enhances the atmospheric greenhouse warming. These two effects are called direct forcing of aerosols on radiation and climate. The presence of aerosol increases the surface reaching IR radiation and decreases the outgoing IR radiation. Since most of the aerosols are concentrated near the surface, absorbing aerosol component heat the lower atmosphere (Reddy et al., 1999; 2000).

The direct radiative effect of aerosols is also very sensitive to the single scattering albedo ω. For example, a change in ω from 0.9 to 0.8 can often change

the sign of the direct effect, depending on the albedo of the underlying surface and the altitude of the aerosols (Hansen et al., 1997c). Recent estimates for the direct forcing by anthropogenic aerosols are between -0.3 to -0.9 Wm^{-2} for sulphate aerosols, between -0.15 and -0.25 Wm^{-2} for biomass aerosols (from biomass fuel use and land clearing), and between +0.15 and +0.2 Wm^{-2} for fossil fuel and industrial sources of organic and black carbon aerosols (Penner et al., 1998). Thus, the climate forcing associated with anthropogenic aerosols could offset a substantial fraction of the warming associated with greenhouse gases Tegen et al. (1996).

1.13.2. Indirect Radiative Forcing

Aerosols can act as CCN for the formation of clouds. An increase in the concentration of aerosols can result in an increased concentration of cloud droplets, which in turn can increase the albedo of clouds (Twomey et al., 1984). This causes a decrease in the visible solar radiation reaching the surface. Thus cloud albedo has a significant role in determining the global energy balance. An increase in aerosols increases the cloud droplet concentration and reduces the mean droplet size. This is because the water vapour availability per aerosol is less when the aerosol number is more. This increases the cloud lifetime and thus inhibits precipitation. Changes in droplet concentrations due to carbonaceous aerosols from biomass burning and fossil fuel/industry lead to estimates of forcing that range from –1.2 to –1.6 Wm^{-2} depending on the magnitude of natural organics assumed in the calculation (Penner et al., 1999). Estimation of aerosols effect on radiation is more uncertain than that due to well mixed green house gases, because of their short life times, highly inhomogeneous spatial distribution and its complex nature of interaction with radiation (Hansen et al., 1997a; 1997b;1998; Haywood et al., 1999; IPCC, 2001).

1.14. Measurement Techniques

The variety of aerosol sources (natural and anthropogenic); wide size spectrum and their short life times result in a spatially and temporally heterogeneous aerosol field making aerosol characterization a real challenge. Due to their short residence times, aerosols are not uniformly mixed around the globe; consequently, their chemical and physical characteristics, including radiative properties, are subject to substantial regional variations (Penner et al., 2002). As such, no single technique or group of techniques is adequate for entirely characterizing aerosol properties over the extremely wide range of particle size, shape, altitude profile and chemical composition found in the atmosphere. In general, measurements of particles are done by: (a) in situ and (b) remote sensing. Both the techniques can be applied from different types of observation platforms like ground based, airborne and space borne. In situ measurements make direct measurements on the parameters at their location, while in remote sensing the parameters are deduced by measuring the impact of radiation on the interacting particle without direct contact with it (e.g., Aerosol Samplers). Remote sensing can be of two types: (a) active and (b) passive. Active sensors use its own radiation to illuminate the object (Eg. Lidar, Sodar), while in the case of the passive sensors, it measures the emission or reflection of the natural sources of energy (Sun, moon) from the earth (e.g. Radiometer).

1.15. Objective of the Study

The present study address the growing concern about the significant changes in the climatic and weather patterns due to the aerosol loading that have taken place in the Indo Gangetic Plain (IGP) which comprises most of the North Indian region (21^0 N – 29^0 N; 69^0 E – 89^0 E) as shown in Fig 1.8. This chosen region comprises of major industrial cities in India (New Delhi, Kanpur, Allahabad, Jamshedpur and Kolkata). It can be seen from Fig 1.8 that this region is bounded by the Himalayas in the north, Thar Desert in the west, the Vindhyan range in the south and Brahmaputra ridge in the east. Therefore, under favourable conditions

the aerosols reaching the location gets confined within the IGP resulting in the accumulation of aerosols.

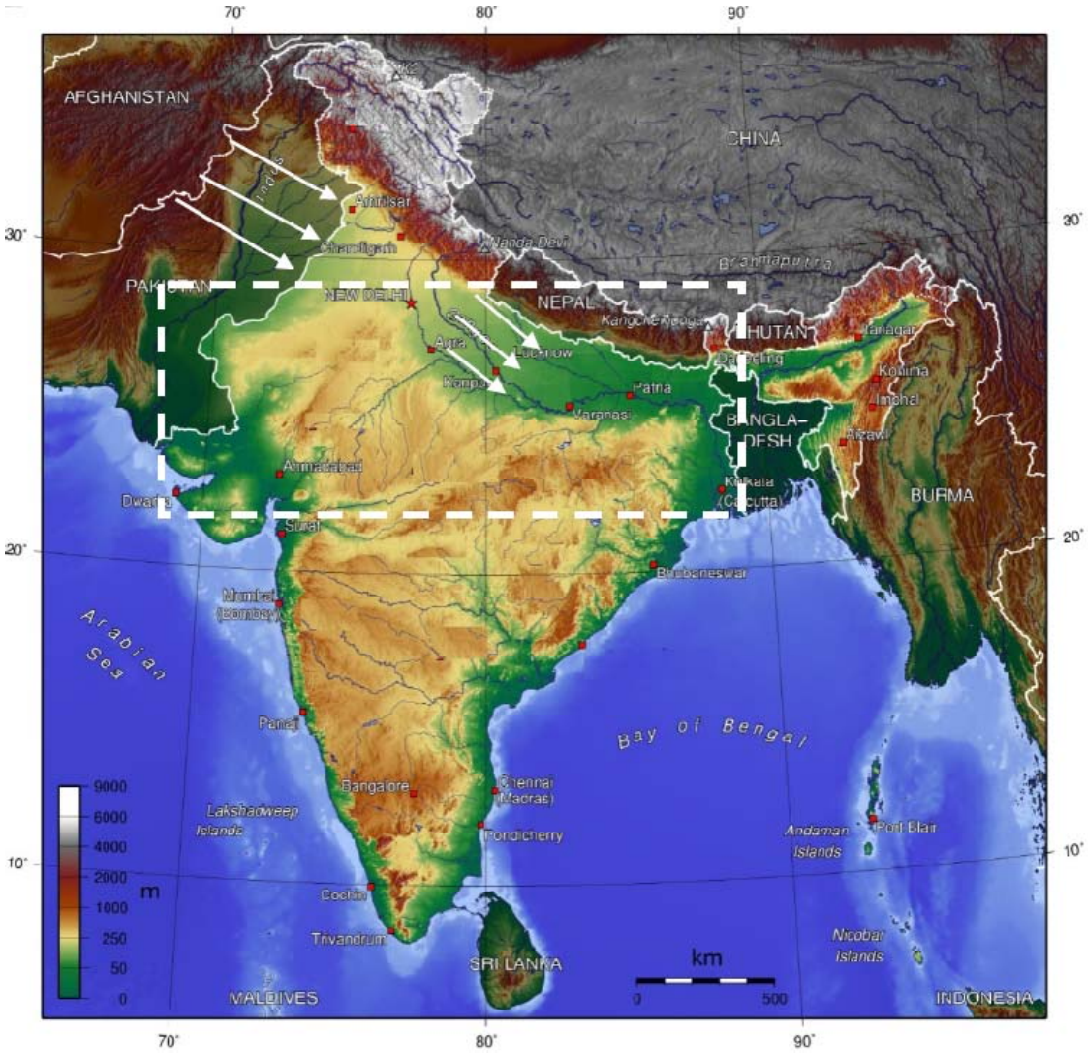

Fig.1.8. Map of India with area chosen for study. Major industrial and urban locations are shown

Northern and central parts of India are one of the most thickly populated areas in the world and have the most intensely farmed areas. The IGP has a major source of coal; therefore most of the industries including numerous thermal power plants that run on coal are located around this region. They inject copious amount of aerosols into the atmosphere. As a result of these factors there is an enormous concentration of industrial aerosols over IGP (Guttikunda et al. 2003). Apart from anthropogenic sources natural sources also contribute to the aerosol loading in the region. Sikka, (1997) has reported that dust storms in this region is maximum during pre-monsoon season, when large quantities of dusts are

transported from the adjoin Thar Desert and from arid regions of Arabian Peninsula and Mediterranean.

The topography and the meteorological conditions are favourable for the accumulation of aerosols that reaches this location. During the non-monsoon months (October to May) the weather in the location is dry with very little rainfall. Surface winds are weak during most of the time in this dry season. Atmospheric aerosols that reach the location get blocked by the Himalayan mastiff which results in a buildup of these aerosols in the region increasing their surface concentration. Rapid increase in population and urbanization has resulted in an excessive combustion of fossil fuels as well as biomass burning. Previous studies (Dey et al., 2004; Deepshikha et al., 2006; Nair et al., 2007; Aloysius et al., 2008) made in this location has pointed out the importance of study of aerosols in the region where it has been observed an increase in aerosol loading during recent years.

This complex combination of aerosol transport and anthropogenic factors mixed with the contribution from the natural sources, particularly in the pre-monsoon and post-monsoon seasons modify the optical properties as well as the cloud micro properties at this place. As a result of these effects the meteorological parameters in the location gets altered. Therefore, any change in weather which disturbs the normal hydrological pattern is alarming in socio-economic point of view. Even though this region is of great importance not many studies has been done on the aerosol indirect effects and its influence on precipitation. Hence the main focus of this work is to understand the interaction of these aerosols with meteorological parameters and cloud properties.

To understand the effects of aerosols in the geosphere-biosphere systems it is essential to characterise their physical, chemical and optical properties. As most of the aerosol sources are of terrestrial origin, the variability of their properties will be very large close to the surface. As mentioned in the first section aerosols are produced from different sources. Depending on the sources and also on the meteorological condition and geographical location (marine, continental, polar,

desert), there is considerable variation in the composition and physical properties of the particles. Thus, an understanding of the aerosol properties and its spatio-temporal distribution assumes significance.

Aerosols being highly dynamic both spatially and temporally, integration of all these measurements is very difficult, that too at short time scales. On the other hand, remote sensing measurements from satellites can quite well characterise the spatial and temporal heterogeneities of aerosol distribution on a global scale (King et al., 1999). The next chapter gives an overview of the retrieval of aerosol data from the satellite sensors for this study and also a description about the supplementary datasets used in the analysis.

CHAPTER 2
DATA AND METHODOLOGY

2.1. Introduction

A study on the time evolution of synoptic scale distribution of aerosols essentially requires detailed information on aerosols over a large geographical region on a routine basis. In order to reduce the uncertainty in our understanding of climate change, satellite measurements of atmospheric gases and aerosols are rapidly gaining in importance (Browell et al., 1998; King et al., 1999). The uncertainty in our understanding of the radiative effects of aerosols stems from the lack of accurate and repetitive measurements at global sales. In addition to improving our knowledge of the atmospheric aerosols in general, one of the principal drivers behind the study of atmospheric aerosols is the need to reduce this magnitude of uncertainty in the Earth's radiative forcing (Kaufman et al., 2002a). Unlike greenhouse gases which tend to be well mixed in the atmosphere and have long residence times, atmospheric aerosol concentrations are highly dynamic varying both spatially and temporally and as a result need to be continuously monitored at regional and global-scales. Typically, aerosols have short atmospheric residence times of the order of days to weeks before undergoing dry deposition through gravitational settling and turbulent mixing, and wet-deposition through precipitation. Aerosol particles are derived from relatively local sources although they can be distributed between continents and so their distribution and composition are highly variable worldwide. The main advantage of satellites therefore lies in their ability to measure global distributions of atmospheric constituents.

The application of satellite remote sensing for the determination of aerosol properties started about 30 years ago. One of the first retrievals of aerosol optical depth from space borne measurements of the spectral intensity of the reflected solar

light was performed using observations from the Multi Spectral Scanner (MSS) onboard the Earth Resources Technology Satellite (ERTS-1) (Griggs, 1975; Mekler et al., 1977) and the first operational aerosol products were generated using data from the radiometer on board the TIROS-N satellite launched on 1978. The Nimbus-7 was launched on 25 October 1978, carrying the Stratospheric Aerosol Measurement instrument (SAM) (McCormick et al., 1979) and the Total Ozone Mapping Spectrometer (TOMS) (Torres et al., 2002a). The TOMS series was extended with the Ozone Monitoring Instrument (OMI) launched in 2004. The primary aerosol data delivered from these sensors were Aerosol Index, a measure for absorbing aerosol, until an algorithm was developed to retrieve AOD as well (Torres et al., 1998; 2002b).

One of the first reliable retrievals of aerosol optical depth over land was made using the dual view of the Along-Track Scanning Radiometer (ATSR-2) (Veefkind et al., 1998), followed by retrievals using POLDER (Deuze et al., 2001) MODIS (MODerate Resolution Imaging Spectroradiometer (Kaufman et al., 1997a) and MISR (Multi angle Imaging SpectroRadiometer) (Martonchik et al., 1998). Retrieval techniques have improved to the extent that satellites are increasingly used for continuous observations of the aerosol distribution and composition on regional to global scales, complementary to ground-based observation networks and dedicated field campaigns, to assess the effects of aerosols on climate (Kaufman et al., 2002a; IPCC, 2007).

The next most important parameter required for studying the aerosol transport is the atmospheric wind field. Re-analyzed wind field generated using the global circulation model by the National Centre for Environmental Prediction (NCEP) and European Centre for Medium range Weather Forecast (ECMWF) are highly reliable and well suited for this purpose.

This chapter gives a brief outline of the data used in the present work and methodology to analyse the aerosol transport, distribution and its meteorological effects over a given locality.

2.2 The MODIS Sensor

The MODerate resolution Imaging Spectro-radiometer (MODIS) instrument was designed to remote sense the properties of aerosols and clouds (King et al., 1992). From polar orbit, approximately 700 km above the surface and a ± 55^0 view scan. MODIS views the Earth with a swath of about 2330 km, thereby observing the entire globe on a daily basis and repeating orbits every 16 days. MODIS measures radiance in 36 wavelength bands, ranging from 0.41 to 14.2 µm (Salomonson et al., 1989), with nadir on ground spatial resolutions between 250 m and 1 km. Its measurements are organized into 5 minute sections, known as *granules*, each 2300 km long. MODIS sensor is onboard two NASA satellites, *Terra* and *Aqua*. *Terra* has a descending orbit (southward), passing over the equator about 10:30 local time, whereas *Aqua* passes over the equator about 13:30 local time in an ascending orbit (northward). MODIS is a paddle broom (sometimes called a whiskbroom) electro-optical instrument that uses the forward motion of the satellite to provide the along-track direction of scan (Fig. 2.1).

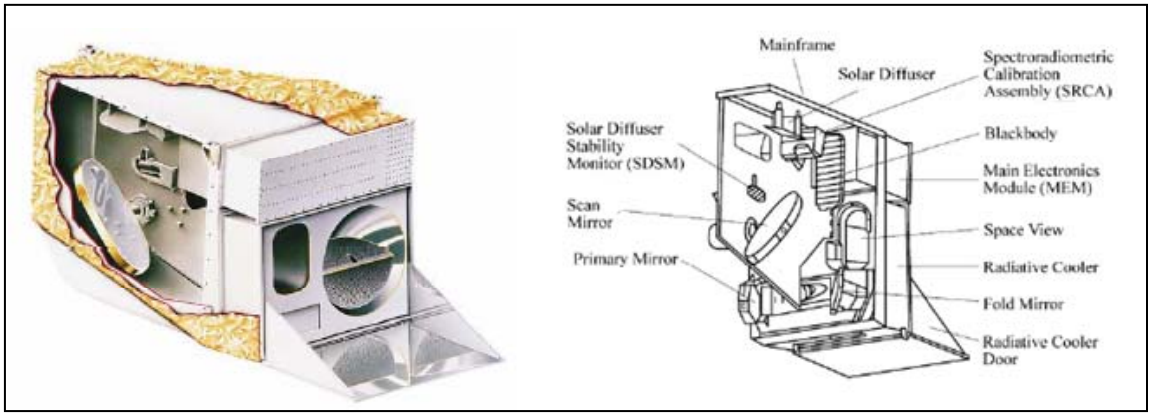

Fig. 2.1. A schematic diagram of the MODIS sensor

The combination of dark-target aerosol retrieval uses the seven 'land' wavelength bands (Table 2.1), which are all in atmospheric *windows* where the gaseous absorption are weak. Included in Table 2.1 are estimates of the central wavelength in each band which is obtained by the integration of the channel-averaged response functions. The MODIS channels 1, 2, 3, 4, 5, 6 and 7 are the channels at 0.65, 0.86, 0.47, 0.55, 1.24, 1.64 and 2.12 μm respectively. In addition, the aerosol algorithm makes use of radiance in other MODIS bands for cloud and surface screening. The 'noise equivalent differential spectral reflectance' (NeΔρ) represents the sensitivity to changes in the signal and is an inherent property of the instrument.

Table 2.1 Characteristics of MODIS channels used in aerosol retrieval

Band No.	**Bandwidth (μm)**	**Weighted central wavelength (μm)**	**Resolution (m)**	**NeΔρ($\times 10^{-4}$)**
1	0.620-0.670	0.646	250	3.39
2	0.841-0.876	0.855	250	3.99
3	0.459-0.479	0.466	500	2.35
4	0.545-0.565	0.553	500	2.11
5	1.230-1.250	1.243	500	3.12
6	1.628-1.652	1.632	500	3.63
7	2.105-2.155	2.119	500	3.06

The light transmitted from the Earth is reflected into the instrument telescope by a rotating two-sided scan mirror. One-half revolution of the scan mirror takes approximately 1.477 seconds and produces the across-track scanning motion. The light is then focused onto separate calibrated radiation detectors covered by narrow spectral band-pass filters. MODIS simultaneously senses in each band, 10 rows of 1km detector pixels, 20 rows of 500 m detector pixels and 40 rows of 250-m detector pixels. Each row corresponds to a single scan line of MODIS data that is nominally composed of 1,354 1km, 2,708 500 m, and 5,416 250 m observations (*see*

Fig. 2.2). The MODIS radiometric calibration uses two approaches, one for the 16 thermal emissive bands and a second for the 20 reflected solar bands. The sensor's digital counts are related to radiance by viewing a blackbody (BB) of known temperature and deep space (zero input radiance) each scan line. Since a number of the 16 thermal emissive bands are non-linear, a quadratic fit to each detector's response versus radiance is utilized. The response curves are determined pre-launch by scanning a variable blackbody temperature. The non-linear fitting coefficient is updated periodically post-launch by varying the temperature of the onboard blackbody.

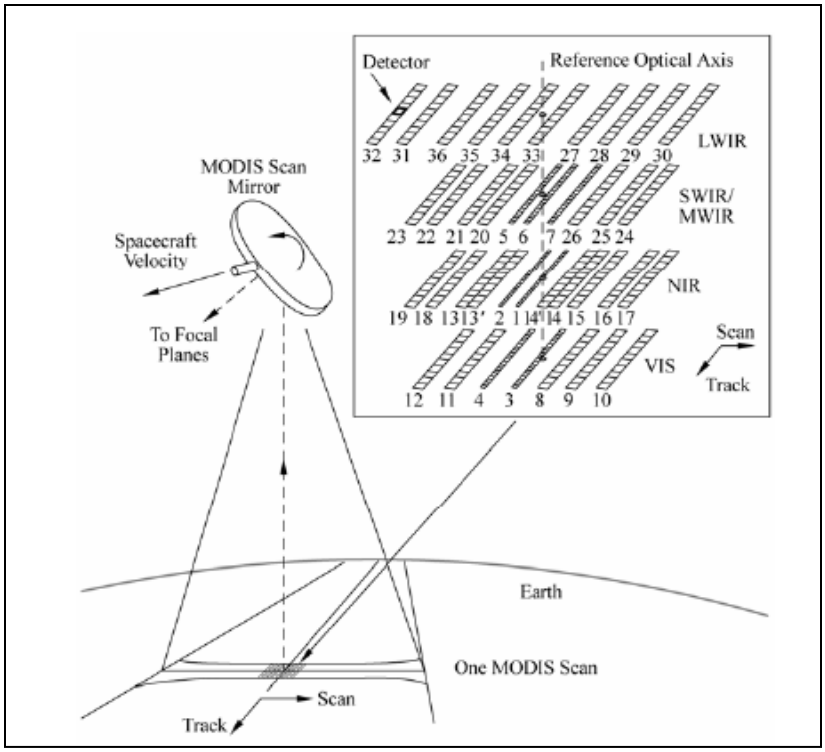

Fig. 2.2.Overview of MODIS sensing geometry. A scan of MODIS data is sensed over a half revolution of the MODIS double sided scan mirror and is focused onto four focal planes containing the 1 km, 500 m and 250 m bands. The instantaneous sensing of four co-registered focal planes is shown, illustrating the MODIS "paddle broom" sensing geometry

2.2.1. MODIS dark-target algorithm over land

Land surfaces do not provide the same uniform surface signal as the ocean. They are much more variable in their reflectance properties and therefore the algorithm must include additional steps to estimate the land surface contribution to the satellite-observed signal. If the surface is either completely dark or its reflectance can be accurately modeled or assumed, the atmospheric signal may be sufficiently decoupled from the combined surface/atmospheric signal.

The aerosol retrieval over land uses spectral reflectance in five of the channels listed in Table 2.1, specifically the 0.66, 0.86, 0.47, 1.24 and 2.12 μm channels. Preliminary steps of the retrieval include testing the spectral observations to screen the 10 km box for clouds (Gao et al., 2002; Martins et al., 2002), snow and ice (Li et al., 2005), and sub-pixel water bodies such as ponds or swamps (Remer et al., 2005). The pixels that remain are sorted by their relative reflectance (at 0.66 μm), such that the 20% of the darkest pixels and 50% of the brightest pixels are removed. The remaining pixels are expected to represent dark surface targets with the least amount of contamination from clouds (including cloud brightening and shadowing) as well as surface inhomogeneities. Therefore, 120 pixels remain from the original 400. These remaining pixels are averaged yielding one set of spectral reflectance values that are used to retrieve aerosol products representing 10 km. Primary aerosol products for dark-target algorithms include the total aerosol optical depth (τ) at 0.55 μm and an estimate of the fine aerosol weighting (η) to the total optical depth. During the course of the retrieval algorithm, certain criteria are evaluated and the final products are given Quality Assured (QA) values to indicate subjective ‘confidence’, ranging from 3 (high) to 0 (none).

2.2.2. Aerosol Product

The aerosol product (MOD04) is based on different algorithms for the remote sensing of tropospheric aerosol over land (King et al., 1999) and ocean (Tanre et al., 1997). Both algorithms try to match MODIS observed reflectances to a lookup table of pre-computed reflectance for a wide variety of commonly observed aerosol conditions, as summarized by King et al. (1999). Since the retrievals over ocean are beyond the scope of this study, only methodology about retrieval over land mass is only mentioned here. Over land, the prime difficulty is separating the reflectance measured by the satellite into an atmospheric part and a land surface part. This difficulty is overcome by estimating the visible surface reflectance from the MODIS-measured reflectance in the shortwave infrared wavelength (2.13 m) for dark targets, as described by Kaufman et al. (1997a). Removing the estimated surface reflectance from the total measured by the satellite, the atmospheric contribution is isolated by using lookup tables to determine the aerosol characteristics and optical thickness in the scene. Final land products include aerosol optical thickness at 0.47, 0.56, and 0.65 m at a 10-km spatial resolution. The spectral dependence of the reflectance across the visible wavelengths is then used to obtain a rough estimate of the fine mode (radius 0.6 m) fraction of the aerosol optical thickness at 0.56 m.

The accuracy of satellite estimates of aerosol optical thickness was first suggested based on theoretical analyses (Kaufman et al., 1997c; Tanre et al., 1997), and consisted of a bias of 0.05 over land and 0.03 over ocean due to uncertainty in the estimate of surface reflectance and 0.20 over land and 0.05 over ocean due to uncertainty in the aerosol absorption and scattering phase function. A number of papers describe the validation of MODIS aerosol products, primarily using the operational Aerosol Robotic Network (AERONET) sun photometers (Holben et al.,

1998). Over land, Chu et al. (2002) confirm the visible accuracy of and a reasonable spectral correlation.

The MODIS operational cloud products include cloud top pressure, thermodynamic phase, optical thickness, particle size, and water path, and are derived globally at spatial resolutions of either 1 or 5 km (referred to as Level-2 or pixel-level products).

2.2.3. Level-2 Cloud Products

The MODIS cloud products are generated on a granule basis; a granule is 5 minutes of data and typically consists of 2,030 along-track pixels. The suite of operational cloud products (Platnick et al., 2003) begins with cloud detection or masking. Infrared techniques are employed to estimate cloud top pressure, effective cloud amount (product of cloud fraction and cloud emittance), and cloud thermodynamic phase. In daytime data, cloud optical thickness and effective particle size are provided using solar reflectance techniques. The cloud products are archived in a single Hierarchical Data Format (HDF) file with the product designation MOD06.

2.2.4. Cloud Optical and Microphysical Properties

Cloud optical thickness is defined as the vertical integration of extinction coefficient. For water clouds composed of spherical particles, effective particle size is defined as the ratio of the third moment to the second moment of the particle size distribution. MODIS retrievals of cloud optical thickness and effective particle size are performed using a band that is practically non-absorbing for bulk water/ice (0.65, 0.86, or 1.2 μm) combined with three longer wavelength bands where bulk water/ice has significant absorption (1.6, 2.1, and 3.7 μm). Three separate effective sizes are provided in MOD06 corresponding to each of these absorbing bands. The cloud product (MOD06) algorithm combines infrared and visible techniques to

determine the physical, radiative and microphysical properties of clouds. Cloud optical thickness and effective radius are derived globally using six visible and near-infrared bands at 1 km spatial resolution. Finally, the cloud product contains a cirrus reflectance product at a visible wavelength for use in removing cirrus scattering effects from the land surface, and it utilizes an additional band at 1.38 μm.

2.2.5. Level 3 Atmosphere Products

Once the Level-2 granule-level cloud products have been produced, spatial and temporal composites are aggregated to daily, eight-day, and monthly files. Statistics are sorted onto a 1° × 1° equal-angle grid (row by column) containing 180 × 360 individual cells. There are three Level-3 atmosphere product (MOD08), each covering different time interval (daily, eight-day and monthly), that contain statistics derived from four Level-2 atmosphere products: aerosol (MOD04), Precipitable water (MOD05), cloud (MOD06), and atmospheric profiles (MOD07). For the daily product, every Level-2 granule that overlaps any part of the data day, defined as being from 0000 to 2400 UTC, is included in the temporal compositing process. A granule that spans either 0000 UTC or 2400 UTC may be included in two consecutive MOD08 daily products. The eight-day product is derived from the daily Level-3 products summarized over eight consecutive days. The eight-day intervals are reset at the beginning of each year similarly to the Level-3 products produced by the MODIS ocean and land discipline groups. The monthly product provides a summary of the daily products obtained over a calendar month.

Cloud fraction (from the cloud mask) and cloud top properties (i.e., cloud pressure and IR phase) are processed for both day and night and are provided in the Level-3 products as daytime only, nighttime only, and combined day and night. Cloud optical and microphysical properties are summarized for daytime only since they are not derived at night. The cloud fraction derived from the cloud mask is currently provided in the scientific datasets (SDS) names beginning with “Cloud_Fraction”.

An example of the Level-3 monthly product is shown in Fig. 2.3 of cloud effective particle radius for liquid water clouds from MODIS Terra in April 2003. Effective radius is seen to be generally smaller over the continents compared to oceanic regions.

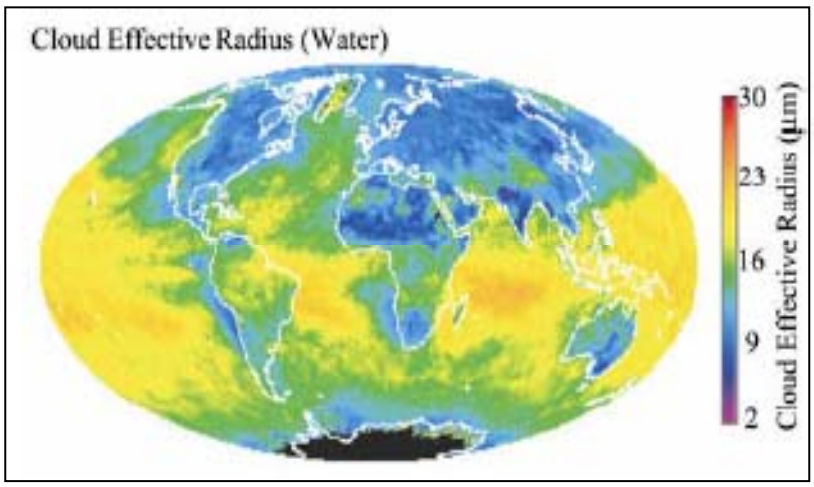

Fig 2.3. Level-3 monthly product of cloud effective particle radius for liquid water clouds from MODIS Terra in April 2003.

2.2.6. MODIS Aerosol Retrieval method and its Accuracy

The MODIS aerosol retrieval algorithm is comprised of two different schemes to retrieve aerosol properties over land and ocean. The details of the algorithm can be found in Kaufman et al. (1997a), Chu et al. (1998) for land and Tanré et al. (1997) and Tanré et al. (1999) for ocean. The enhancements and modifications of the schemes were described in Chu et al. (2003) (land), Levy et al. (2003) (ocean) and Remer et al. (2005) (land and ocean). Since this study is made over land area, the retrieval methodology over land is described here.

Over land, the dark target approach (Kaufman et al., 1997a) is adopted to retrieve aerosol optical depth based upon the reflectances at 0.47, 0.66, and 2.1 μm wavelengths. Aerosol optical depths are derived at 0.47 and 0.66 μm wavelengths

from the mean reflectances of clear pixels of 10 km x 10 km areas. The use of 10 km x10 km box is mainly to accommodate surface variability in order to better select dark pixels at the global scale. Cloud-free pixels are first selected by MODIS cloud mask (Ackerman et al., 1998), followed by the removal of water and snow/ice pixels using positive Normalized Difference Vegetation Index (NDVI) at 250 m resolution and Near real-time Ice and Snow Extent (NISE) snow mask. Surface reflectances of the selected (i.e., cloud-free, water-free, and snow/ice free)pixels at 0.47 and 0.66 μm are estimated by a fixed relationship based upon the measured reflectance at 2.1 μm (Kaufman et al., 1997b; Kaufman et al., 2002). To further eliminate the contaminations by residual clouds, water, and snow/ice, 20 -50 percentile is used to calculate the mean surface reflectance and reflectance at top of the atmosphere. The selection of urban/industrial or biomass-burning aerosol model (both dominated by fine-mode particles) is based upon geographic locations and seasons of emission sources.

The determination of the fraction of fine-mode aerosol is based upon the ratio of path radiance between 0.66 and 0.47 μm similar to Ångström exponent except that path radiance ratio is not affected by the assumption of aerosol models. The final AOD is obtained by the linear combination of AODs of fine and coarse mode aerosols. AOD, fine-mode fraction, and Ångström exponent are the primary parameters obtained from aerosol retrieval and also can be validated by AERONET sun/sky measurements. The secondary aerosol parameters include reflected/transmitted fluxes and column mass concentration derived from lookup tables. The dark target method and fixed relationship of land surface reflectance has achieved satisfactory success over vegetated surface with retrieval errors within $\Delta\tau_\alpha = \pm 0.05 \pm 0.20\ \tau_\alpha$ (τ_α denotes AOD) at 0.47 and 0.66 μm (Chu et al., 2002; Chu et al., 2003; Remer et al., 2005) except in the coasts, mountain tops, and partial snow melting regions.

2.3. Detection of Aerosols using Ultraviolet observations

Observational evidence as well as important theoretical analyses, indicate that the absorption of solar radiation by soot-containing and organic aerosols may contribute to warming the atmosphere. In addition to the well-documented climate role of aerosol absorption, recent research indicates that absorbing aerosols may have an effect on the hydrological cycle as it has the potential of inhibiting cloud formation and preventing or delaying the onset of precipitation. The development of the capability to detect aerosol absorption from space using near Ultraviolet (UV) observations was one the most important breakthroughs of the last decade in aerosol remote sensing from space. The technique, developed from analysis of observations by the Total Ozone Mapping Spectrometer (TOMS) instrument has been extensively used for the global mapping of desert dust sources, transport patterns and as an important tool for validation of transport models. Aerosol absorption can be measured from space in the near UV by taking advantage of the interaction between Rayleigh scattering and particle absorption. The result of this radiative transfer interaction is a unique signal that clearly detects the presence of absorbing aerosols under most observing conditions: clear skies over water and land surfaces (including deserts), mixed with clouds or above them, and aerosols over ice and snow covered surfaces.

The Total Ozone Mapping Spectrometer (TOMS) data represent the primary long-term, continuous record of satellite-based observations available for use in monitoring global and regional trends in total ozone over the past 25 years. TOMS also provides measurements of tropospheric aerosols volcanic SO_2, ultraviolet irradiance, erythemal UV exposure, and effective reflectivity from the Earth's surface and clouds. The data are produced by the Laboratory for Atmospheres at NASA's Goddard Space Flight Center.

Four TOMS instruments have been successfully flown in orbit aboard the Nimbus-7 (Nov. 1978 - May 1993), Meteor-3 (Aug. 1991 - Dec. 1994), ADEOS (Sep. 1996 - June 1997), Earth Probe (July 1996 - 2004) satellites. The TOMS series was extended with Ozone Monitoring Instrument (OMI) onboard Aura satellite launched in July 2004. Version 8 TOMS data products are available from the Goddard Earth Sciences Distributed Information and Services Center (GES DISC). These include level 3 gridded data (1.0° x 1.25°) as well as level 2 instrument resolution data (between 50 km x 50 km and 26 km x 26 km pixel at nadir). For the present study, the data from the Earth Probe TOMS and Aura OMI instruments are used.

2.3.1. The TOMS sensor

Absorbing aerosols data obtained from the TOMS instruments is used to obtain estimates of the quantities of aerosols in the troposphere that absorb ultra-violet light. In particular, desert dust and smoke from fires absorb at the UV wavelengths used by TOMS. Smoke detected by TOMS comes from a variety of ground based sources, such as biomass burning whether naturally occurring or caused by the agriculture, oil industry fires or industrial smoke. The TOMS sensor detects smoke particles regardless of source or season and is reliable over land or water. Data from TOMS can be used to detect the presence of both UV absorbing aerosols and non-absorbing aerosols. The technique uses the ratio of the upwelling radiance (or spectral contrast) between the 340 nm and 380 nm channels (I_{340}/I_{380}). Absorbing aerosols in the UV spectrum include smoke produced by biomass burning, black carbon from urban and industrial activities, agricultural dust, mineral dust coming from arid and semi-arid regions (desert dust) volcanic aerosols and ash. Carbonaceous aerosols generated by biomass combustion consist of a mixture of material with varying radiative properties; the absorbing fraction will contain elemental or graphitic carbon. Non-absorbing aerosols are primarily sulfate (H_2SO_4) aerosols (Herman et al. 1997; Torres et al. 1998). A schematic diagram of Earth probe space craft and TOMS sensor is given in Fig 2.4.

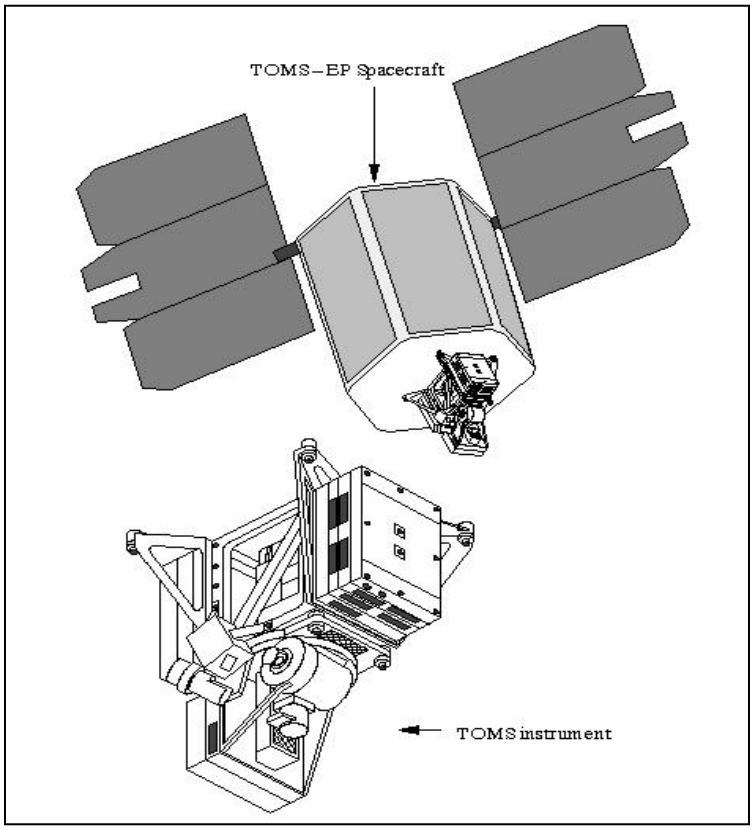

Fig 2.4 The TOMS- Earth Probe space craft and its sensor

The spectral contrast in UV wavelength is useful over both land and water because the UV reflectivity of these surfaces is low and nearly constant, unlike for the visible wavelengths. Gaseous absorption of UV is weak at the 340, 360 and 380 nm wavelengths. Backscattered radiation at these wavelengths is primarily controlled by Rayleigh (molecular) scattering, surface reflection (Earth's surface), and scattering from aerosols and clouds (Mie scattering). The inclusion of these wavelengths in the TOMS instrument provided a means for detecting the presence of aerosols. In a clear molecular atmosphere (no aerosols and clouds), molecular (Rayleigh) scattering at a given wavelength will scale inversely with λ^4. This mathematical relationship causes up to a 50% difference in the backscattered UV radiance between 340 and 380 nm in a pure atmosphere (ie. a strong spectral contrast). Mie scattering can also make reflectivity (R) spectrally dependent. In accordance with Hsu et al (1996), the UV absorbing aerosols cause R (reflectivity) to increase with

wavelength (e.g. $R_{380} > R_{340}$). For this reason, the presence of aerosols and clouds adds a radiance component that is weakly wavelength dependent; they reduce the I_{340}/I_{380} spectral contrast that would be observed due to the molecular atmosphere alone. In other words, the Mie scattering caused by the aerosols or clouds reduces the spectral contrast expected due to Rayleigh scattering alone. The detection of aerosols from TOMS data involves a quantity called a *residue*.

The N-value residue at l_{340} is defined as:

$$\Delta N\lambda = -100\left[\log_{10}\left(\frac{I_{340}}{I_{380}}\right)_{\text{meas}} - \log_{10}\left(\frac{I_{340}}{I_{380}}\right)_{\text{calc}}\right] \quad \ldots(2.1)$$

where I_{meas} is the backscattered radiance at that wavelength measured by the TOMS and I_{calc} is the model calculated radiance assuming an atmosphere of Rayleigh scatterers (pure molecular atmosphere) bounded by a Lambertian surface (which necessitates exclusion of data affected by sea glint, snow or ice). The model employed is a modified version of Dave (1978) Lambert equivalent reflectivity (LER) model, constructed to give nearly zero *residue* in the presence of clouds.

When UV absorbing aerosols are present in the atmosphere, the spectral contrast (I_{340}/I_{380}) is smaller than predicted by the LER model and positive residues are produced by the equation above. Non-absorbing aerosols produce greater spectral contrast and thus result in negative residues. ΔN_{340} values scale almost linearly with single scatter albedo (thus optical depth) and with altitude. Absorbing aerosols in the boundary layer of the troposphere are not readily measured by TOMS because aerosol absorption at one height in the atmosphere affects molecular scattering below the aerosol layer and the underlying Rayleigh scattering produces only a small signal. Starting at altitudes of at least 1 km, absorbing aerosols become readily detected by the residue technique. In the middle latitudes, most of aerosol transport

occurs between 3-5 km altitude (or higher in the case of volcanic ash) thus middle latitude aerosols are well detected.

2.3.1.1. TOMS Aerosol Index

Measurement of TOMS aerosol data are given in units called the *aerosol index*. The aerosol index (AI) is defined as the difference between the observations and model calculations from a pure molecular atmosphere with the same surface reflectivity and measurement conditions. The index can be interpreted in terms of optical depth if the index of refraction, particle size distribution, and the height of the aerosol layer are known from other measurements.

2.3.2. The OMI sensor

The Ozone Monitoring Instrument (OMI) was launched on July 15, 2004 on the National Aeronautics and Space Administration's (NASA) Earth Observing System *Aura* satellite. Placed in a polar sun synchronous orbit at an elevation of 700 km, it makes one complete orbit around the globe in 93 minutes 53 seconds in an ascending node with an equatorial crossing at 13:42 local time. The flight of this sensor is just a few minutes behind the MODIS as a part of the NASA A-Train constellation. Therefore, these two sensors provide an ideal means to identify the transport and distribution of aerosols.

Ozone Monitoring Instrument was designed to replace the TOMS sensor and employs the same retrieval algorithm with TOMS (Torres et al., 1998). It has a spatial resolution of 13 x 24 km at nadir and measures back scattered radiances in near UV region. As in the case of TOMS, OMI measures the back scattered radiances in the near UV region, and using these measurements computes an absorbing AI, which is a qualitative measure of the presence of absorbing aerosols over all terrestrial surfaces. The present work uses the OMI-AI Level 3 global

gridded product (1^0 x 1^0 spatial resolution) to analyse the distribution of aerosols over the study region.

The OMI instrument is an ultraviolet-visible imaging spectrograph that uses two-dimensional charge-coupled device detectors to register both the spectrum and the swath perpendicular to the flight direction. The swath which is 115 wide enables global daily ground coverage with high spatial resolution**.** The high resolution spectrograph measures the upwelling radiance at the top of the atmosphere in the ultraviolet and visible (270-500 nm) regions of the solar spectrum. It has a 2600 km wide swath and provides daily global coverage at a spatial resolution varying from 13 x 24 km at nadir to 40 x 135 km at the extremes of the swath. The OMI near-UV aerosol products consist of the well known Absorbing Aerosol Index (AI) as well as the quantitative parameters Aerosol Optical Depth (AOD) and Single Scattering Albedo (SSA).

In order to meet the science objectives, measurements are needed that combine both a good spatial resolution of km and daily global coverage. This is realized by implementation of a unique optical design of the telescope system and the use of CCD detectors, which enables an instantaneous field of view of 115, corresponding to a 2600 km broad swath on the Earth's surface, while at the same time the desired spatial resolution is obtained. This spatial resolution is required to optimize the probability of observing cloud-free ground pixels, which is important for obtaining the best tropospheric trace gas amounts and to enable OMI to monitor tropospheric pollution phenomena, like biomass burning and industrial pollution, on urban or regional scale.

For the OMI instrument the following subsystems can be identified. The optical bench is the heart of the instrument. The two CCD detectors located in the two detector modules, which are in turn located on the optical bench, produce the

recorded spectra and transfer these via a video line to a separate electronics and instrument control unit, the electronics unit (ELU), which digitizes the measured signals. The ELU transfers the measurement data and exchanges the instrument commands to and from the instrument on one hand and to and from the so-called Interface Adapter Module (IAM) on the other hand. The latter forms the interface between the OMI systems and the EOS Aura spacecraft. The optical layout of the instrument is shown in Fig. 2.5.

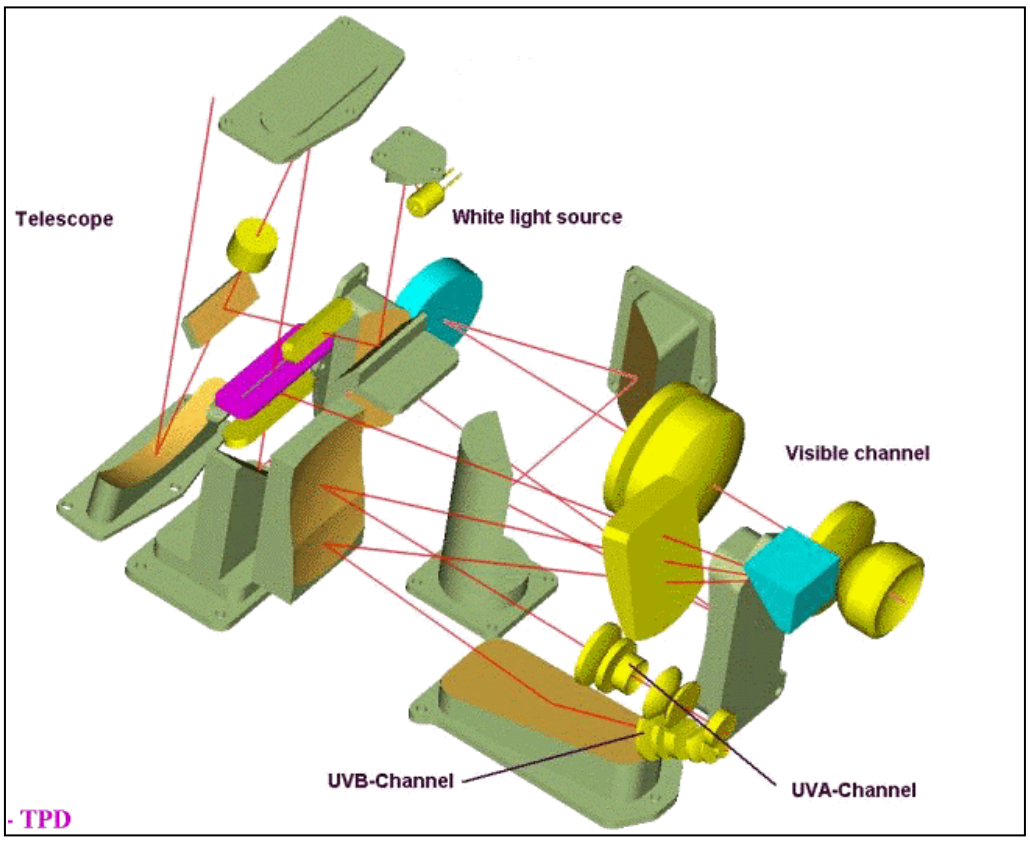

Fig. 2.5. The optical layout of the OMI sensor

The Earth radiance enters the telescope, which consists of two bare aluminum spherical mirrors, and is imaged on the 44-mm long and 300 m broad entrance slit. The telescope is of a special design that provides an instantaneous field of view of

0.8 in the flight-direction (along-track) and of 115 in the swath direction (cross-track). These fields of view yield an overall ground coverage of about15 km (along track) by 2600 km (across track) at an altitude of 700 km (*see* Fig. 2.6). This is sufficient to provide daily global coverage of the Earth, at all latitudes. The cross-track resolution is either 24 km (global mode) or 12 km (spatial zoom-in mode) at nadir, depending on the electronics settings.

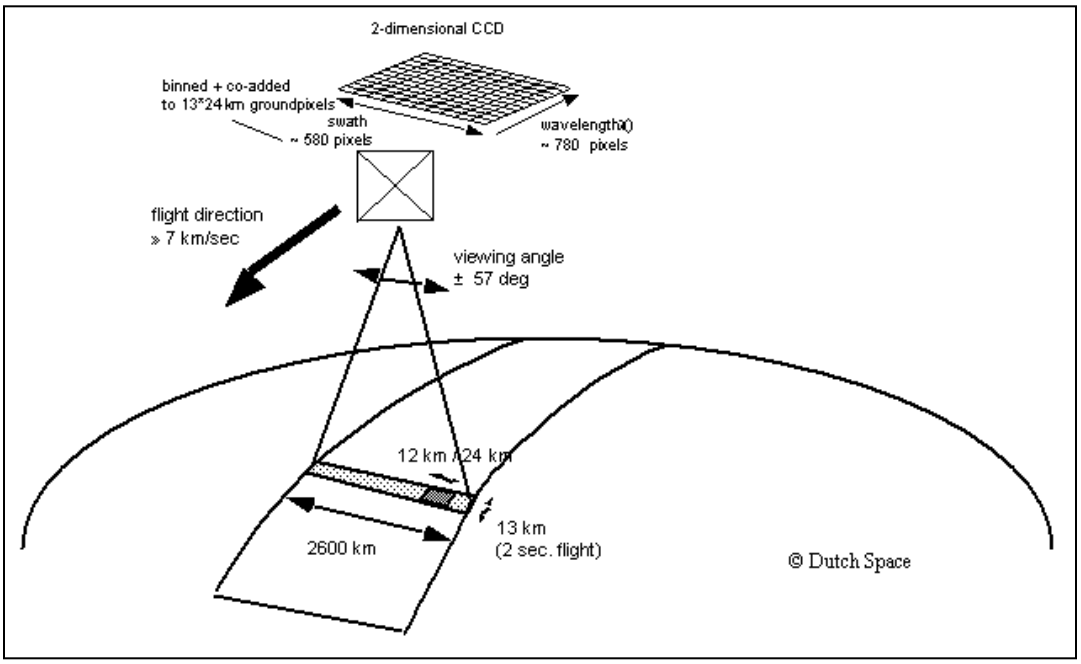

Fig. 2.6. Schematic overview of the measurement principle of the instrument

2.4. The Atmospheric Infrared Sounder

The Atmospheric Infrared Sounder (AIRS) was launched on the Aqua research satellite, a major component of NASA's Earth Observing System, in May 2002. Together with two microwave sounders – the Advanced Microwave Sounding Unit (AMSU) and the Humidity Sounder for Brazil (HSB) - it forms the AIRS Sounding Suite, which makes up about half of the Aqua payload. This AIRS sounding suite is

the most advanced atmospheric sounding system to date, with measurement accuracies far surpassing those of current weather satellites (Aumann et al., 2003). From its sun synchronous polar orbit, the AIRS system provides more than 300,000 all-weather soundings covering more than 90% of the globe every 24 hours.

The AIRS is an infrared grating spectrometer that operates in the thermal infrared portion of the spectrum, from 3.7 μm to 15.4 μm. It has 2378 channels covering about 3/4 of this range, with a spectral resolution ($\lambda/\Delta\lambda$) of about 1200. Radiometric sensitivity is typically about 0.25 K. This system measures upwelling thermal radiation emitted from the atmosphere and the surface. Its scan mirror rotates around an axis along the line of flight and directs infrared energy from the Earth into the instrument. As the spacecraft moves along, this mirror sweeps the ground creating a scan swath that extends roughly 800 kilometers on either side of the ground track. Within the instrument, an advanced, high-resolution spectrometer separates the infrared energy into wavelengths. This is essentially accomplished by inverting the radiative transfer equation (RTE), which models the spectral intensity for a given distribution of the geophysical parameters.

Each infrared wavelength is sensitive to temperature and water vapor over a range of heights in the atmosphere, from the surface up into the stratosphere. By having multiple infrared detectors, each sensing a particular wavelength, a temperature profile, or sounding of the atmosphere, can be made. While prior space instruments had only 15 detectors, AIRS has 2378. This greatly improves the accuracy, making it comparable to measurements made by weather balloons. The major advantage of this instrument is that makes use of the properties of both microwave and infrared sounder. A microwave radiation has the capability to penetrate through most cloud systems and can provide full coverage under most weather conditions; while, an infrared sounder provide adequate vertical resolution and reasonable measurement accuracy.

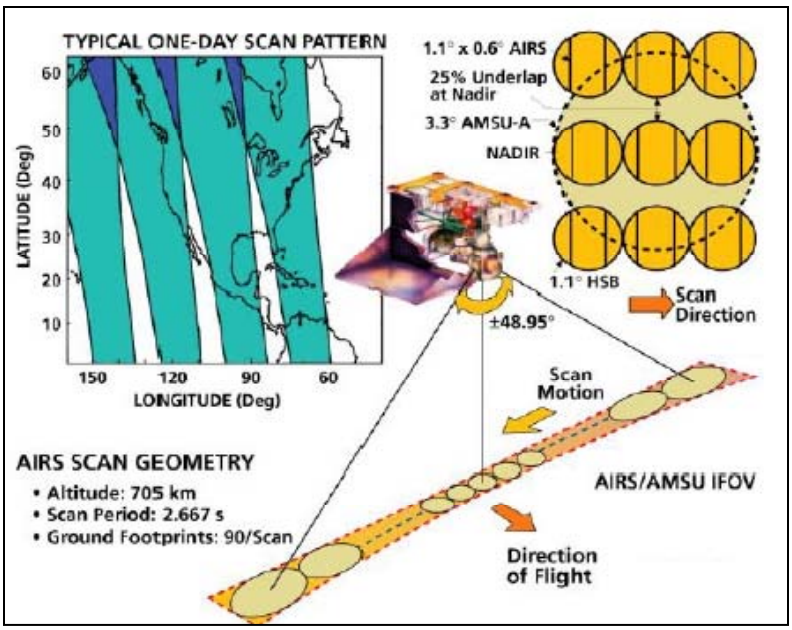

Fig. 2.7. AIRS viewing geometry and coverage

Data from AIRS and the microwave instruments are combined to provide highly accurate measurements in all cloud conditions resulting in a daily global snapshot of the state of the atmosphere. The AIRS in combination with microwave sounder observe the entire atmospheric column from earth's surface to the top of the atmosphere and provide real time measurements of temperature and water vapour profiles. For the present study vertical temperature profiles are used which has a vertical resolution of 1 km in the troposphere and an accuracy of 1^0 K.

Fig 2.7 illustrates a typical scan pattern of AIRS, where the larger circle represents the region defined by the microwave field of view and the smaller circles are defined by the smaller infrared field-of-view circles. The construction and operation of the instruments in the AIRS suite are arranged so that the entire global swaths scanned can be divided into such clusters. Each of the clusters illustrated in Fig. 2.7 are about 45 km in diameter that is situated directly below the satellite and larger near the edges of the scan swath. An inversion of the radiative transfer equation is employed as described before to compute the atmospheric profiles along with other

parameters (such as the surface temperature). In practice, the cloud clearing and inversion of the RTE are combined in an iterative process that is repeated until conversion is achieved between radiances predicted with the RTE and those observed. Its ability to provide simultaneous observations of the Earth's atmospheric temperature, water vapor, ocean surface temperature, land surface temperature and infrared spectral emissivity makes AIRS/AMSU a very useful space instrument to observe and study the response of the atmosphere to increased concentration pollutants.

2.5. HYSPLIT model

The Air Resources Laboratory's HYbrid Single-Particle Lagrangian Integrated Trajectory (HYSPLIT) model is a complete system for computing both simple air parcel trajectories and complex dispersion and deposition simulations (Draxler and Hess, 1998). The model calculation method is a hybrid between the Lagrangian approach, which uses a moving frame of reference as the air parcels move from their initial location, and the Eulerian approach, which uses a fixed three-dimensional grid as a frame of reference. In the model, advection and diffusion calculations are made in a Lagrangian framework following the transport of the air parcel, while pollutant concentrations are calculated on a fixed grid.

The initial version of the model used only rawinsonde observations and the dispersion was assumed to consist of uniform mixing during the daytime and no mixing at night. In the next revision, variable strength mixing was introduced based upon a temporally and spatially varying diffusivity profile. In Hysplit_3, the use of rawinsonde data was replaced by gridded meteorological data from either analyses or short-term forecasts from routine numerical weather prediction models. The current version (Hysplit_4) has substantially updated algorithms for stability and mixing and is capable of handling multiple and nested meteorological data and

concentration output grids. Version 4 is a result of a joint effort between the National Oceanic and Atmospheric Administration (NOAA) Air Resources Laboratory and Australia's Bureau of Meteorology. New features include improved advection algorithms, updated stability and dispersion equations, a new graphical user interface, and the option to include chemical transformation modules. All simulations used the default configuration of modeling the horizontal dispersion through the growth of pollutant ''puffs'' and the vertical dispersion by a Monte Carlo particle approach. The meteorological data are vertically interpolated to the dispersion model's internal terrain following coordinate system, which is on the same horizontal grid as the input data.

Air concentrations are computed on a user-defined grid by summing the masses of all particles in each concentration grid cell divided by the cell's volume, averaged over 24 h, which corresponds to the sample collection period. The concentration grid was defined with a horizontal resolution of 0.58 and a depth of 10 m. Surface grid cell concentrations represent the layer averaged from the ground to 10 m.

2.5.1. Meteorological input data

Tracer transport and dispersion was calculated using meteorological data fields produced by the NCEP–National Center for Atmospheric Research reanalysis project (Kalnay et al. 1996). The reanalysis data were obtained from NCEP 4 times per day on the model sigma surfaces on a global Gaussian grid of 1.9 degree resolution. To reduce the data volume and because the dispersion model requires the data to be on a conformal grid, the data points from the global grid were bilinearly interpolated to a regional Mercator grid. The Mercator grid parameters were selected to ensure that the Mercator grid points were in almost identical locations with the Gaussian grid points, which minimizes the importance of the interpolation technique. Each final processed data file contains 1 month of data (surface pressure,

air temperature, true-direction wind components, and vertical velocity) on 28 model sigma surfaces, with the first 7 levels within 150 hPa of the surface.

The meteorological input data in the model are the zonal (u) and meridional (v) wind components, temperature (T), height (Z) or pressure (P), the pressure at the surface (P_0) and vertical velocity (w). If wet deposition processes are to be included, then the rainfall field is also included in the model.

2.5.2. Calculation of the Trajectories

Once the basic (u,v,w) meteorological data have been processed and interpolated to the internal model grid, trajectories can be computed. Trajectories are computed by means of time interpolation of the meteorological fields in the advection algorithm. The advection of a particle or puff is computed from the average of the three-dimensional velocity vectors for the initial position *P(t)* and the first-guess position *P (t + ⊿t)*. The velocity vectors are linearly interpolated in both space and time. The first guess position is

$$P\,(t + \Delta t) = P(t) + V(P, t)\,\Delta t \qquad \ldots (2.2)$$

and the final position is

$$P\,(t + \Delta t) = P(t) + 0.5\,[V(P, t)\,\Delta t + V(P\,, t + \Delta t)]\,\Delta t \qquad \ldots (2.3)$$

The trajectories can be computed either in backward in time or forward in time. Trajectories are terminated if they exit the model top or intersect the ground. Here, 0.5 denotes the advection distance per time step.

The Real-time Environmental Applications and Display sYstem (READY) is a web-based system, developed by the Air Resources Laboratory (ARL), for accessing and displaying meteorological data and running trajectory and dispersion model products on ARL's web server. The primary use of READY is to run HYSPLIT, ARL's transport and dispersion model. Users can produce air parcel trajectories that follow the movement of the wind patterns defined by the meteorological models run operationally by the NOAA National Centers for Environmental Prediction (NCEP). Meteorological data (forecast and archived) are available to HYSPLIT on global and regional scale grids. Users also can model the dispersal of pollutants with HYSPLIT by tracking thousands of particles across the domain, as opposed to one or two particles for trajectories. In this way, pollutant plumes can be produced from such sources as wildfires, chemical or radiological releases, or volcanic eruptions.

Another application of READY is for users to be able to produce meteorological products for any location in the world based on the meteorological data produced by NCEP. These products include meteorograms (time series of meteorological variables), vertical profiles, wind roses and time-series of atmospheric stability. In the present analysis READY is used to run the HYSPLIT model to compute the trajectories to identify the source locations of the aerosols transported towards the study region.

2.6. Reanalysis Data

A reanalysis is the product of a state-of-the-art data assimilation system fed with several years (or decades) worth of observations and ocean boundary conditions. This reconstruction of the weather over the entire globe (for global reanalyses) takes the form of gridded datasets which feature no gaps and consequently attract users outside the specialized weather community. As part of the data assimilation system, a highly realistic model from numerical weather prediction is used to propagate the atmospheric state in time. That state (*background*) is updated, at regular intervals,

typically 6 or 12 hours, with observations, to form the *analysis* at that time. This update step typically uses variational data assimilation, whereby a cost function is minimized iteratively. The atmospheric model also provides constraints (radiation, dynamics and physics) that help enforce a physically realistic analysis. These constraints also ensure that the analyzed variables are consistent with one another; for example, the extratropical mass field is weakly balanced against the wind field, and water amounts cannot be negative. With a four-dimensional variational (4DVAR) assimilation system as in ERA-Interim, that consistency between the analyzed variables and within analyzed fields is also found in space and time within each analysis window.

Reanalyses have been advocated since the 1980s, with the First Global Atmospheric Research Program Global Experiment (FGGE) demonstrating the concept (Bengtsson et al., 1982). Pioneering reanalysis projects include the NCEP/NCAR reanalysis (Kalnay et al., 1996) and the ERA-40 reanalysis (Uppala et al., 2005).

2.6.1. ERA - Interim

The ECMWF Reanalysis (ERA) -Interim reanalysis covers the time period from 1 January 1989 to the present and features a horizontal resolution of about 80 km. The model and analysis (4DVAR with a 12-hour window) uses 60 vertical levels between the surface and about 65 km altitude. The time resolution of the products is 3 hours for the surface fields and 6 hours for the upper-air fields. The atmospheric model time-step is 30 minutes. Each 12-hour analysis window is decomposed into 30-minute time-slots.

ERA-Interim products can be accessed from the following webpage, where latest dataset updates and some information about product quality can also be found at *http://www.ecmwf.int/research/era*. The previous major reanalysis conducted at ECMWF was ERA-40 and covered the time period from 1957 to 2002 (Uppala et

al., 2005). ERA-Interim is not a replacement for ERA-40. However, as the name suggests, it proposes an improved dataset until a full-fledged reanalysis is carried out to supersede ERA-40. ERA-Interim improves on several deficiencies reported in ERA-40, in particular (1) the water cycle, which was too wet in the tropics in ERA-40, and (2) breaks in some of the ERA-40 products time-series, coinciding with the introductions of new satellites in the assimilation. Overall, these various improvements come from developments on the data assimilation system and the atmospheric model.

Another major improvement as compared to previous reanalysis exercises at ECMWF has been the continuation of the ERA-Interim product into the present. This offers users with the possibility to build applications addressing today's weather and seasonal time-scales, while benefiting from a dataset that has a depth of more than 20 years.

2.6.2. NCEP Reanalysis Data

The reanalysis, begun in 1991, was intended to address the problem of apparent climate changes in long term data sets due to changes in the data assimilation system (Kalnay et al., 1996; Kistler et al., 2001). Data from many different source (including rawinsondes, balloons, aircraft, ships, surface stations and satellites) were put through a quality check, fed into an assimilation model that includes parameterizations for all major physical processes, and finally examined again for self consistency. The model used in the NCEP reanalysis has 28 vertical levels extending from the surface to ~ 40 km, with vertical resolution of ~ 2 km.

The analysis scheme is a three-dimensional variational (3DVAR) scheme cast in spectral space denoted spectral statistical interpolation (Parrish and Derber 1992). The assimilated observations are upper air rawinsonde observations of temperature, horizontal wind, and specific humidity; operational Television Infrared Observation

Satellite (TIROS) Operational Vertical Sounder (TOVS) vertical temperature soundings from NOAA polar orbiters TOVS temperature soundings over land only above 100 hPa; cloud-tracked winds from geostationary satellites; aircraft observations of wind and temperature; land surface reports of surface pressure; and oceanic reports of surface pressure, temperature, horizontal wind, and specific humidity.

Gridded variables, the most widely used product of the reanalysis, have been classified into three classes (Kalnay et al. 1996): *type A variables,* including upper air temperatures, rotational wind, and geopotential height, are generally strongly influenced by the available observations and are therefore the most reliable product of the reanalysis. *Type B variables,* including moisture variables, divergent wind, and surface parameters, are influenced both by the observations and by the model, and are therefore less reliable. *Type C variables,* such as surface fluxes, heating rates, and precipitation, are completely determined by the model (subject to the constraint of the assimilation of other observations).

Although the reanalysis data assimilation system is maintained constant, the observing system has evolved substantially. The evolution of global observation system can be divided into three phases. The early period starts from the 1940s to the International Geophysical Year in 1957, when the first upper-air observations were established; the modern rawinsonde network from 1958 to 1978; and the modern satellite era from 1979 to the present. Although the reanalysis data assimilation system is maintained constant, the observing system has evolved substantially. The evolution of global observation system can be divided into three phases. The current products include, gridded reanalysis fields at a horizontal resolution of $2.5^0 \times 2.5^0$ resolution, 8-day forecasts every 5 days, and the binary universal format representation (BUFR) archive of the atmospheric observations. The products can be obtained from NCAR, NCEP, and from the National Oceanic

and Atmospheric Administration/ Climate Diagnostics Center (NOAA/CDC) (*http://wesley.wwb.noaa.gov/Reanalysis.html*). Unlike the operational data sets, reanalysis data with the benefit of advanced quality control and error correction gives a more reliable data. The meteorological variables used in the present study are air temperature, wind, and pressure at different levels.

These datasets retrieved from above mentioned sources are effectively utilised to determine the objective of this work, and the results are discussed in subsequent chapters.

CHAPTER 3

TRANSPORT AND DISTRIBUTION OF ATMOSPHERIC AEROSOLS AS INFERRED BY SATELLITE MEASUREMENTS

3.1. Introduction

The processes whereby air motions carry physical or chemical properties from one region of the atmosphere to another are collectively referred to as *transport*. Many of the particles in the atmosphere are emitted or produced at the surface. Transport of these aerosols begins in the atmospheric boundary layer (ABL), the dynamically variable layer just above the surface. Air within the ABL is characterised by horizontal winds having a high degree of turbulence. During intense convection air from the ABL moves vertically into the free troposphere. Dust aerosols are considered to be one of the major sources of tropospheric aerosol loading and constitute an important parameter in climate aerosol forcing studies (Kaufman et al., 2001; Slingo et al., 2006). These aerosols have a significant role in the earth system by altering the radiation balance in the atmosphere through the scattering and absorption of radiation (Tegen et al., 1997; Haywood and Boucher, 2000; Harrison et al., 2001; Sokolik et al., 2001) and suppressing precipitation (Rosenfeld, 2000). This property of dust aerosols has initiated research in the detection and mapping of dust aerosols and has become a subject of extensive study in several part of world (Moulin et al., 1998; Prospero, 1999; Li et al., 2008).

The impact of these aerosols in the Earth system depends mainly on particle size, shape and mineralogy that are initially determined by their source (Mahowald et al., 2005). During transport, the size distribution of these dust particles shifts rapidly to smaller particles because of the rapid fallout of large particles (i.e., 5–10 μm diameter and greater); at distances of a few hundreds of kilometers or more from the

source, (e.g., Duce, 1995) although some very large particles can be carried great distances (Betzer et al., 1988; Carder et al.,1986). The smaller aerosol particles have higher lifetime in the atmosphere and influence the atmospheric conditions at distant locations away from its source.

Observations and numerical models show that aerosol scattering of ultraviolet (UV) radiation in the boundary layer accelerate photochemical reactions and smog production, while the presence of UV-absorbing aerosols in the atmosphere affects the radiation balance (Haywood and Shine,1995; Ardanuy et al., 1992). The atmospheric loading of UV absorbing aerosols is the sum of several large annually cyclic sources of aerosols distributed over broad areas by tropospheric wind circulation. Satellite imagery shows that dust aerosols often cover very extensive areas are more persistent and occur more frequently than those associated with pollutant aerosols (Husar et al., 1997). In such a scenario, the use of satellite observations becomes the most efficient way to determine aerosol physical properties on the temporal and spatial scales needed to understand and monitor their effects on the earth–atmosphere system.

Continuous measurement of dust aerosols in the visible wavelength is challenging because of the intense surface reflection over deserts as well as arid regions. So, an approach to retrieve aerosol properties using measurements in the near-ultraviolet spectral region has emerged (Torres et al., 1998). The aerosol detection capability in the near UV became apparent with the development of the Total Ozone Mapping Spectrometer aerosol index (TOMS AI), as a by-product of the TOMS version 7 ozone algorithm (McPeters et al., 1996). The main advantages of the near-UV approach are the high sensitivity to particle absorption, and the capability of retrieving aerosol properties over most terrestrial surfaces including deserts. Therefore, one can clearly observe the occurrence of large dust events over the

continents and subsequently follow the movement of large-scale plumes (Herman et al., 1997).

During the summer months, dust is observed daily for periods of a week to several months. The largest sources of UV absorbing aerosols in the atmosphere are from biomass burning and wind borne desert dust from events that last a week or longer. Every year large quantities of dust are injected into the atmosphere over the deserts during this time. Strong winds can blow sand from these desert regions into the free troposphere, from where then it is advected over large distances (e.g. Prospero and Carlson, 1972; Prospero et al., 2002; Israelevich et al., 2003; Kubilay et al., 2005). The majority of the desert dust originates at the latitude of the Sahara and Sahel regions (near 10^0 N – 28^0 N) and is a belt stretching from the western coast of Africa passing through central Asia (Arabian Peninsula) to north-western India (Thar Desert). The prevailing upper level winds are favourable in bringing the dust laden air from arid locations in Africa, the Mediterranean and from the Thar Desert.

Long-range transport of desert dust mainly takes place in the upper troposphere (e.g. Prospero and Carlson, 1972; Hamonou et al., 1999; Murayama et al., 2001, Amiridis et al., 2005), where the aerosol lifetime is of the order of two weeks. The Indian subcontinent which is bounded by Himalayan ranges and Tibetan plateau to its north creates a favourable condition for the conglomeration of aerosols. The dry conditions generally existing during the non-monsoon months helps in the piling up of dust aerosols. An increase in these aerosols can influence climate by modifying the concentration of climate influencing constituents.

3.2. Data and Analysis

The present analysis is for 10 years for the years ranging from 2000-2009. The decadal variability of aerosol loading is studied using the Aerosol Index (AI) dataset

obtained from the Earth Probe TOMS and Ozone Monitoring Instrument (OMI) onboard NASA's *Aura* satellite. The TOMS AI dataset is used for the years 2000 to 2004. For the remaining years 2005 - 2009 OMI data sets are used. Both these sensors measure the backscattered UV radiance in three longest wavelength bands (340, 360 and 380 nm) where the gaseous absorption is weak. The net aerosol effects on back- scattered radiation are primarily governed by aerosol absorption of both *Rayleigh* and *Mie* scattered radiation as well as scattering and absorption of radiation reflected by underlying surface (Torres et al., 1998).

The algorithm for detection of aerosol and clouds from backscattered UV radiance measurement is based on the residue theory described in Herman et al. (1997) and Torres et al. (1998). The residue method is based on the principle that for fixed 380 nm radiance the I_{340}/I_{380} spectral contrast is largest for non-absorbing aerosol and clouds and deceases with increasing absorption. From the backscattered radiance measurements in the UV region of the spectrum, the retrieval algorithm computes an absorbing AI which is a qualitative measure of the presence of UV absorbing aerosols, such as mineral dust and smoke.

Desert dust has a direct effect on the AI because of its wavelength dependent imaginary part of the refractive index in the UV (de Graaf et al., 2005). The AI is positive for absorbing aerosols and negative for non-absorbing, while values of AI near zero indicate the presence of clouds. The wind speed at 700 hPa is obtained from NCEP/NCAR reanalysis data. The 700 hPa level was chosen due to the fact that the main dust activity is around this level. The aerosol pathway is determined using the Air Resources Laboratory's HYbrid Single-Particle Lagrangian Integrated Trajectory (HYSPLIT) analysis. It is a complete system for computing air parcel trajectories. The calculation method is based on Lagrangian approach, which uses a moving frame of reference as the air parcels move from their initial location.

3.3. Results and Discussion

3.3.1. Seasonal variation of Aerosol Index

Fig. 3.1 shows the spatial plots of AI over the Indian subcontinent for the 10 years taken into consideration. The analysis is for the pre-monsoon and post-monsoon seasons for each year. From the figure, it can be seen that aerosol concentration is higher during the pre-monsoon season than during post-monsoon season. The area of highest loading is extended from North West India towards the IGP. A close scrutiny of figure shows that aerosol concentration is higher in the belt 70^0 E- 89^0 E and 21^0 N – 29^0 N.

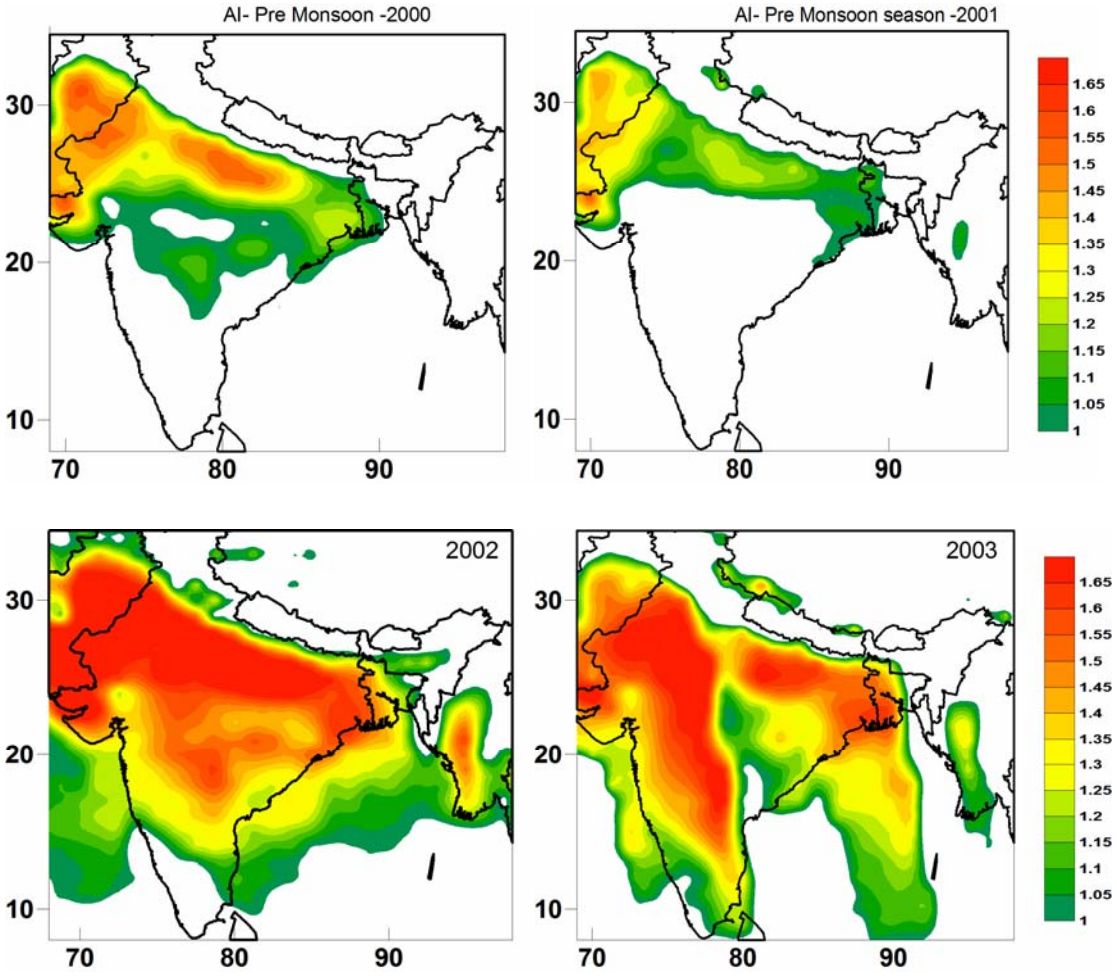

Fig. 3.1(a). Aerosol Index during the pre-monsoon season over the Indian subcontinent

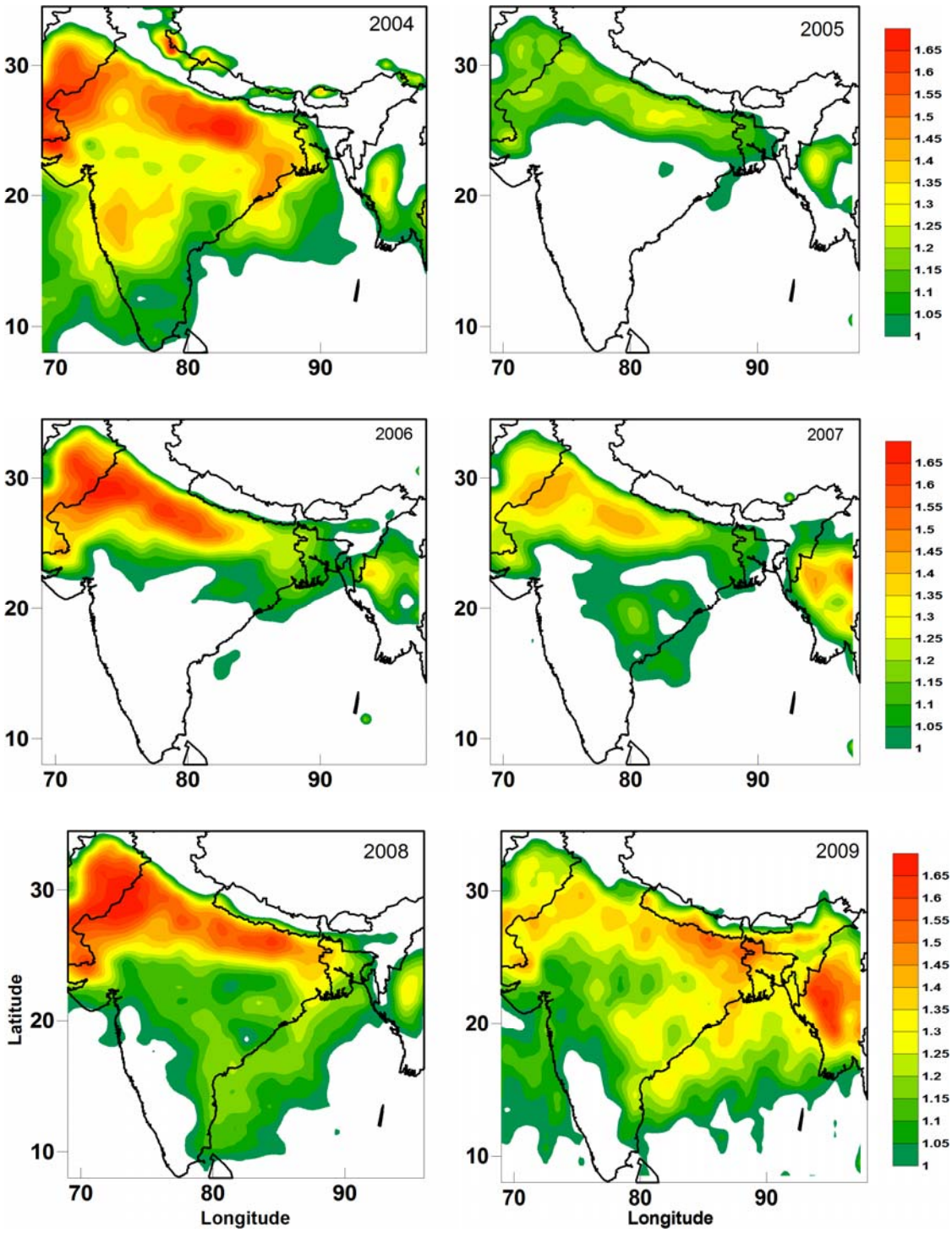

Fig. 3.1(a). Aerosol Index during the pre-monsoon season over the Indian subcontinent (continued.)

Pre-monsoon season aerosol loading is characterised with a high aerosol loading in the magnitude between 1 and 1.65 over the region. Such an enormous accumulation of aerosols is seen in this region and analysis shows that such a large build up of aerosols occurs during most of the years compared to the surrounding regions. Absence of rainfall which is an effective removal process may one of the major reasons for the piling up of aerosols. Also, prevailing upper levels winds are westerlies bringing copious amount of dust aerosols from the Middle East (Prospero et al., 2002) and adjoining Thar Desert regions (Moorthy et al., 2007). These aerosols on reaching North Indian plains mixes with the anthropogenic aerosols produced from industries and incomplete combustion of fossil fuels and biomass (Habib et al 2006). Moreover, surface winds are very weak so that effective dispersion of aerosols in the location fails, increasing the surface concentration of aerosols. These aerosols are mainly confined over IGP probably due to the topography of the region. Therefore, the natural as well as the anthropogenic sources combined with the dry conditions that exist during the season enhances the buildup of absorbing aerosols. The influence of wind will be discussed in detail in final section of this chapter.

Higher values of AI are seen in the even years of 2000, 2002, 2004, 2006, 2008. In the year 2003, aerosol concentrations were higher which may be possibly due to drought conditions existed in the year 2002. In the pre-monsoon season of the year 2002 a high AI value of about 1.6 existed in most parts of IGP and central India. The dry conditions that existed during the year enhance the production of absorbing aerosols, so that concentrations of these aerosols continued through the following year which is evident from the higher values in 2003. Except for the year 2003, it can be seen that a higher concentration of absorbing aerosols occur in every alternate years starting with the year 2000.

A majority of the absorbing aerosols gets washed away in the monsoon season which spans for almost four months from June to September. As a result, during post monsoon season the AI value diminishes compared to pre-monsoon season. In the post-monsoon season also, the North Indian region and IGP have the most accumulation of absorbing aerosols compared to the surrounding regions (Fig. 3.1(b)). In the post-monsoon season, the AI values are higher in the odd years of 2001, 2005, 2007 and 2009. In the year 2003, AI values were very less throughout the country during the post-monsoon season.

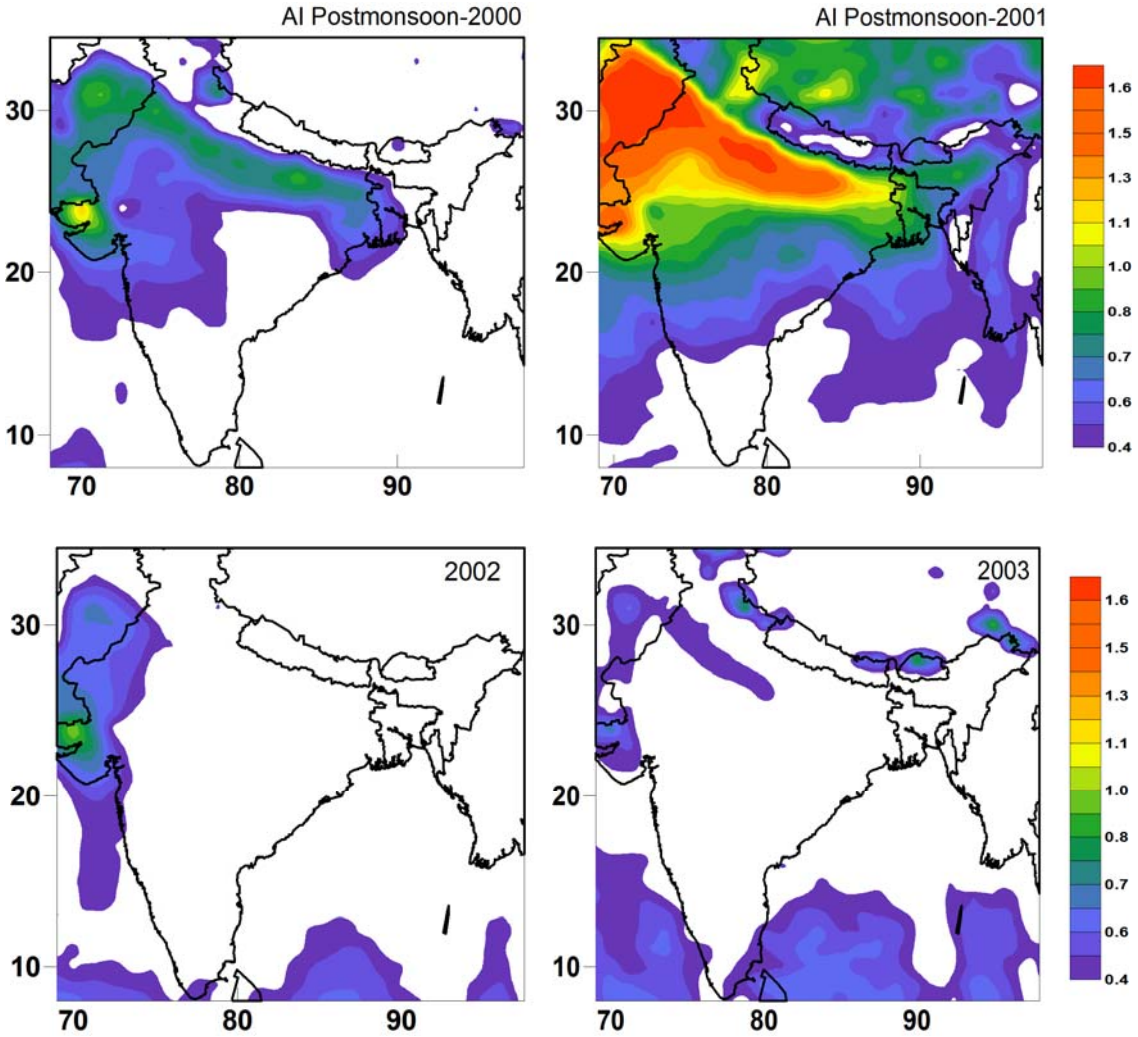

Fig. 3.1(b). Aerosol Index during post-monsoon season over the Indian subcontinent

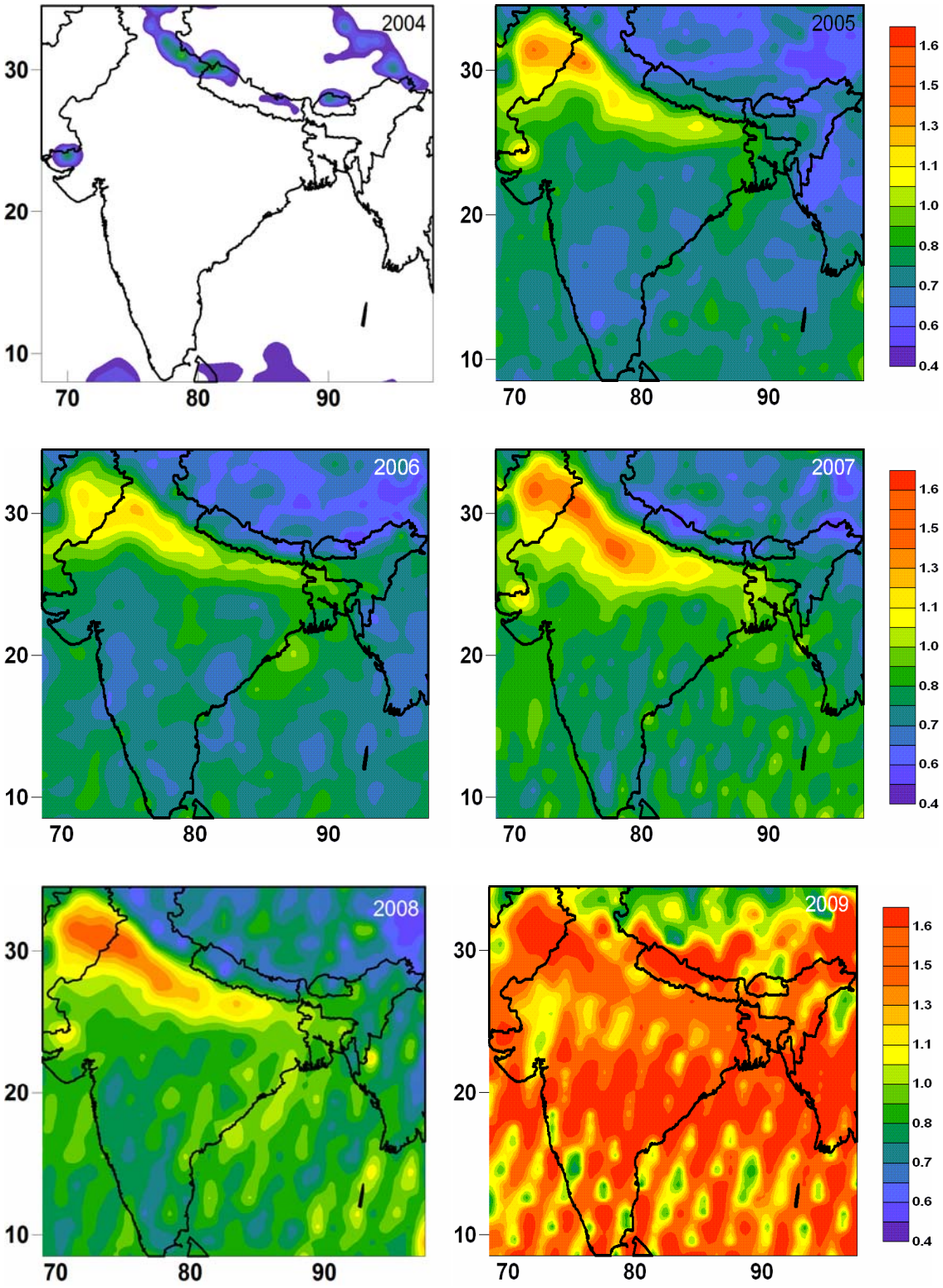

Fig. 3.1(b). Aerosol Index during post-monsoon season over the Indian subcontinent (continued)

3.3.2. Influence of wind speed on Aerosol Index

Prevailing winds at 700 hPa during pre-monsoon and post-monsoon seasons are illustrated in fig. 3.2(a) and 3.2(b) respectively. From the analysis of wind speed and direction for the pre-monsoon season, it is seen that strong and persistent winds are present at 700 hPa (~ 3km) over the region. Winds are westerlies at a magnitude of 8 – 12 ms^{-1} and have their pathways through major dust sources over the 30^0 latitude belt. Therefore, the dust aerosols present in the source region get transported by these upper level winds and get deposited in the north Indian region. These airmass are continental in nature and the absence of effective removal mechanisms (eg. rainfall) creates a favourable condition for their loading in the atmosphere. Also, the surface winds are weak that enables the deposition of aerosols. Therefore, absorbing aerosols resulting from long distance transport and anthropogenic sources (eg. combustion of fossil fuels and emission from industries) contribute to the large concentration of absorbing aerosols in the location. By the month of June, the prevailing winds shift its direction and become south westerlies and south easterlies which are predominantly composed of marine aerosols.

As a result, the contribution of absorbing aerosols in the total aerosol loading decreases and gets replaced by maritime airmass. The intense wind associated with the monsoonal circulation along with the rainfall removes the aerosol content in the atmosphere. Therefore, the total aerosol concentration in the atmosphere decreases. During the post-monsoon season, the majority of winds are the North easterlies with a weak westerly component. Since there are no prominent dust sources towards the east of the study region, the concentration of aerosols remains low.

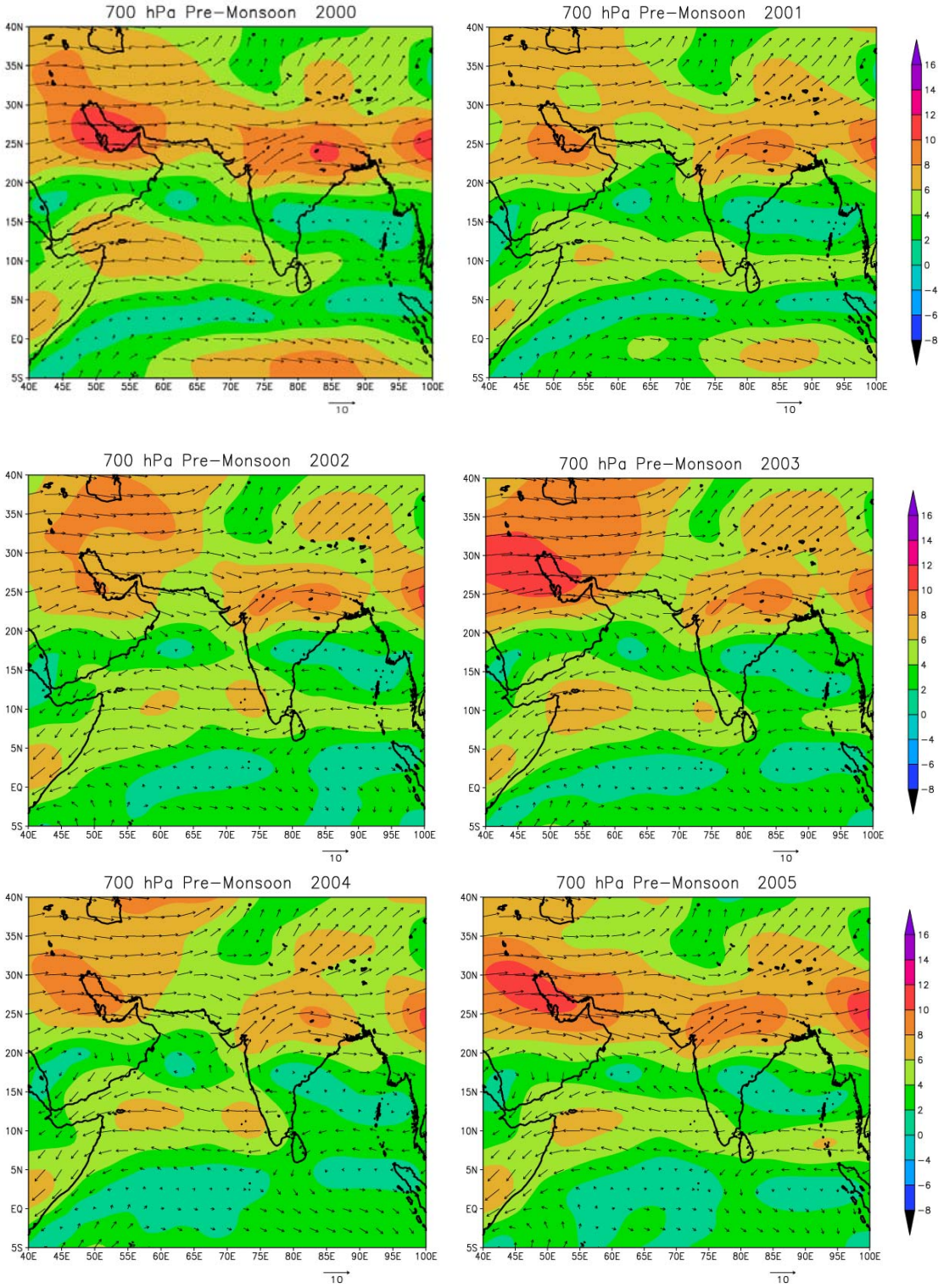

Fig. 3.2(a). Prevailing winds at 700 hPa during pre-monsoon season for the years 2000 to 2009

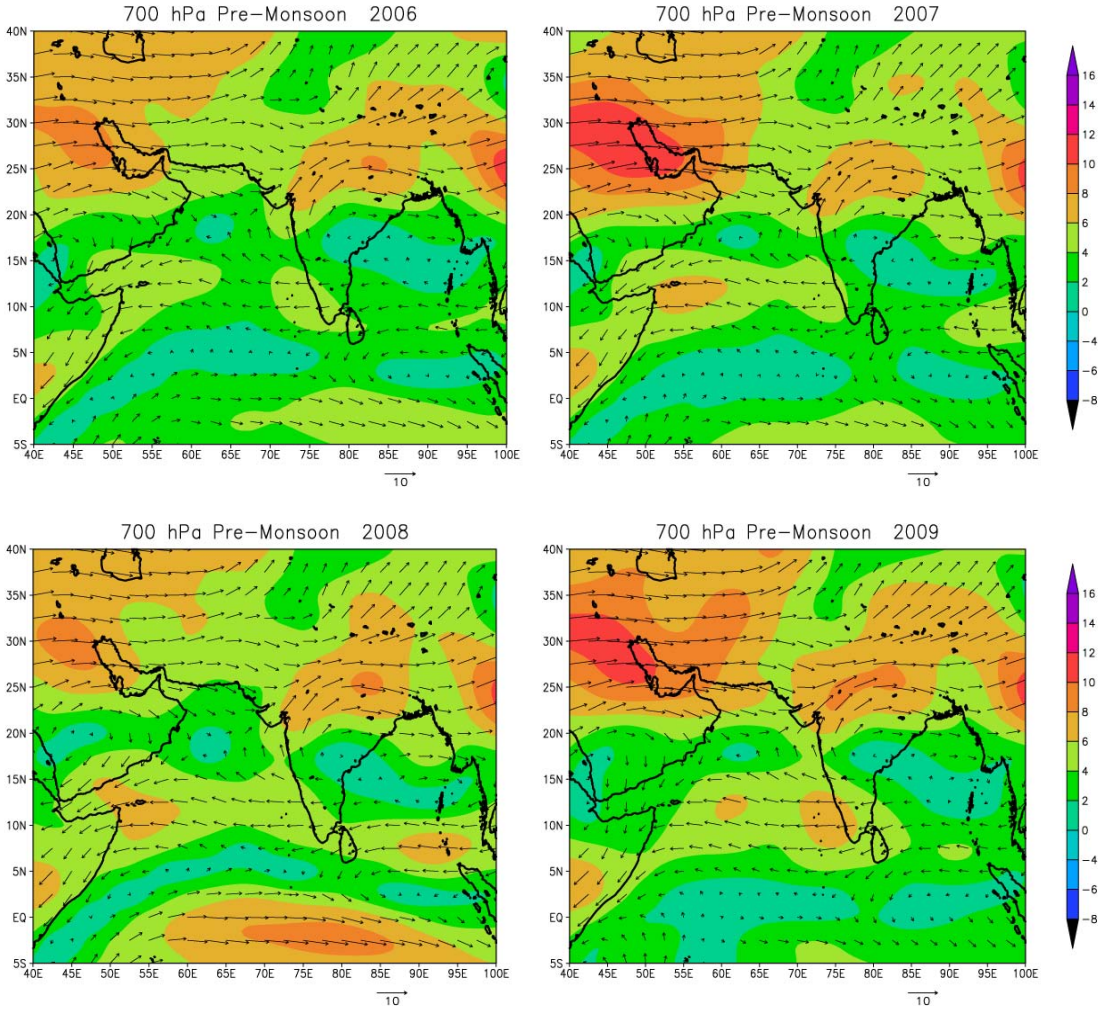

Fig. 3.2(a). Prevailing winds at 700 hPa during pre-monsoon season for the years 2000 to 2009 (contd.)

During the post-monsoon season (Fig.3.2 (b)), in contrast to pre-monsoon season the zonal winds at 700 hPa level gets weaker. The magnitude of winds is in range of 2 to 4 ms^{-1}. At 700 hPa level, south westerly winds of greater intensity (> $4ms^{-1}$) dominates the circulation system over the study region. This high velocity wind obliterates the weaker westerly dust laden winds. Since, these westerly winds are coming from pristine oceanic regions and constitutes marine airmass results in the dilution of the concentration of absorbing aerosols over the study region. This may be the possible reason for a reduction in concentration of absorbing aerosols during the post-monsoon season.

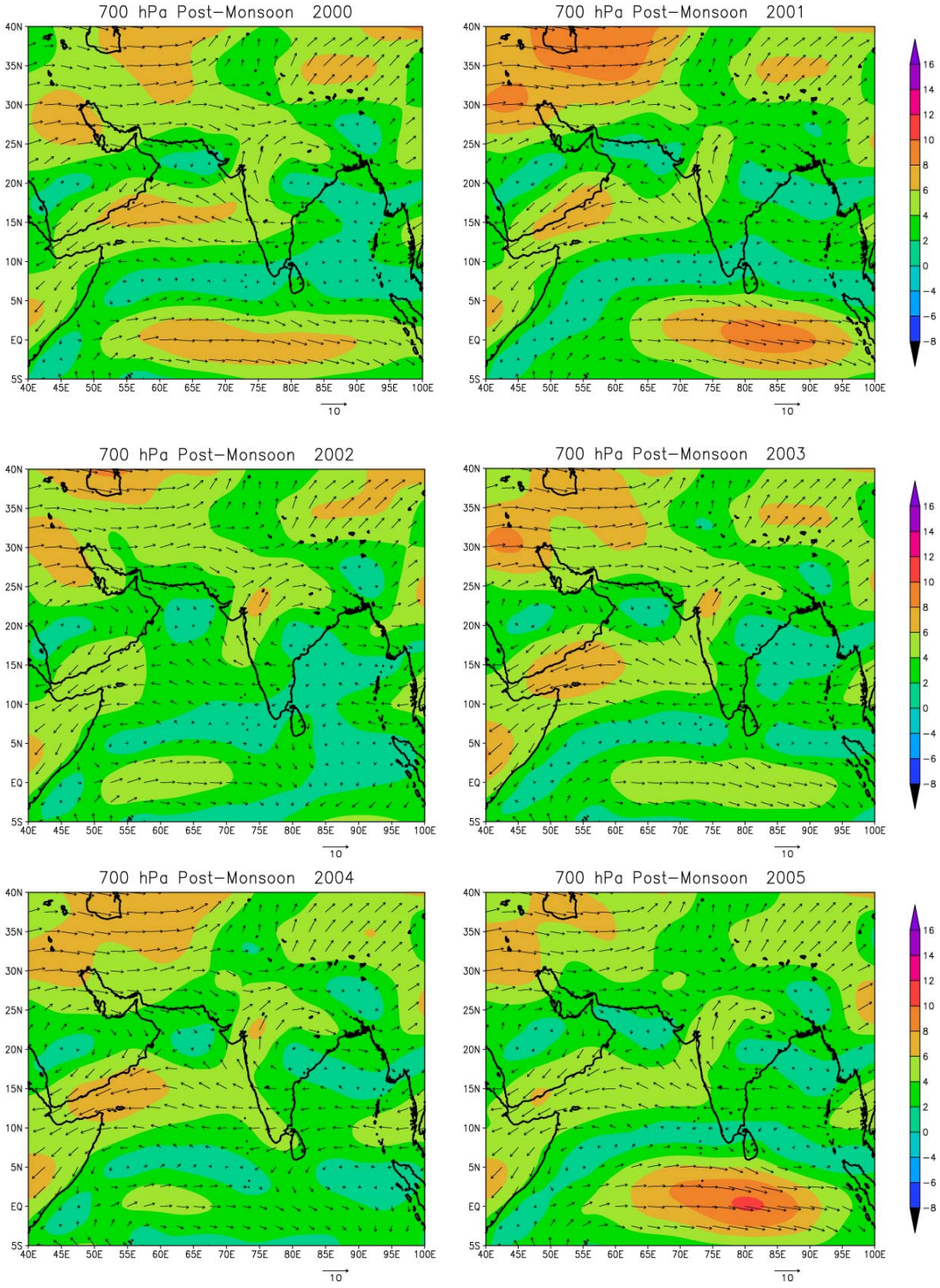

Fig. 3.2(b). Prevailing winds at 700 hPa for post-monsoon season during the years 2000 to 2009

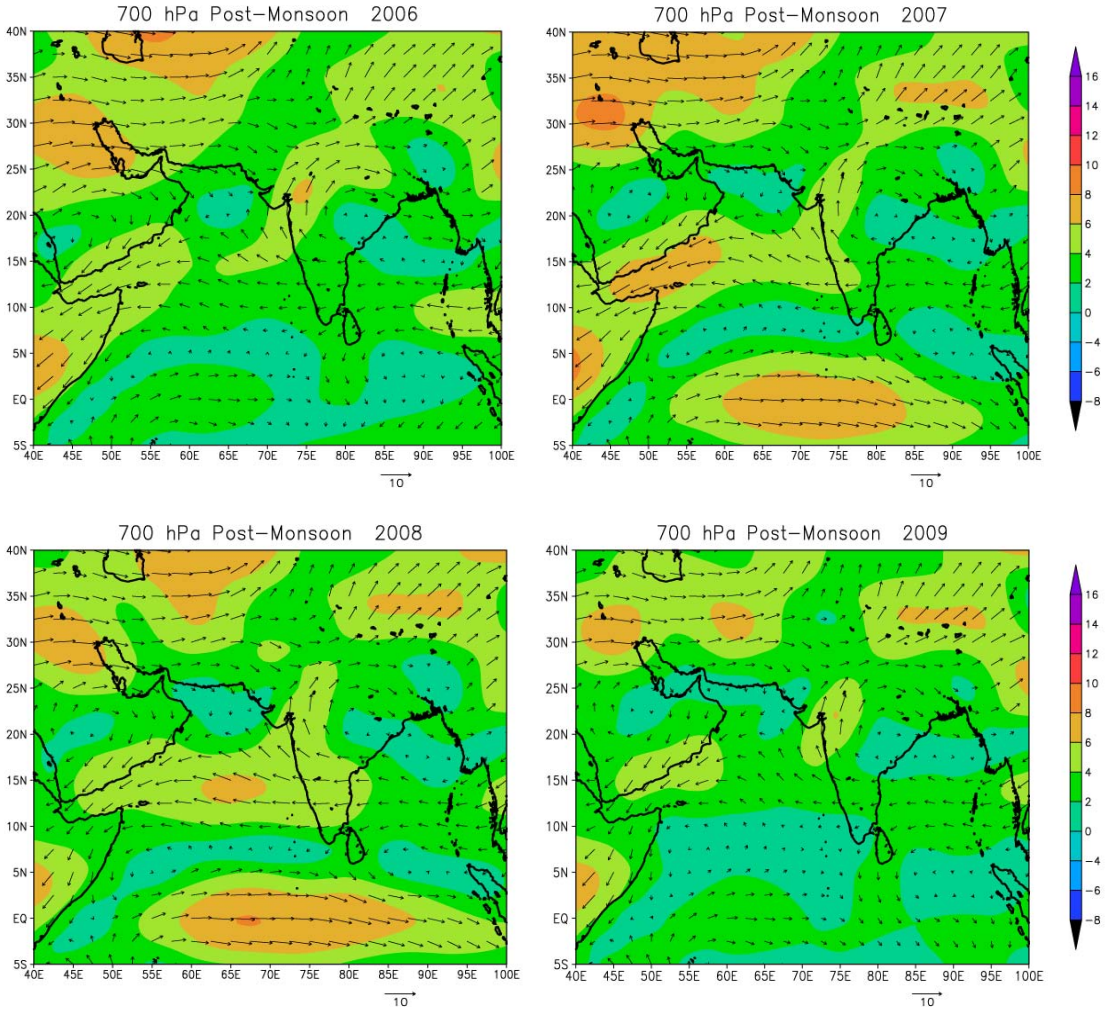

Fig. 3.2(b). Prevailing winds at 700 hPa for post-monsoon season during the years 2000 to 2009 (contd.)

3.3.3. Back Trajectory Analysis

Hysplit back trajectories are used to find the source of aerosols that reaches the Indian region. Back trajectories for both pre-monsoon and post-monsoon seasons are shown in figures 3.3(a) and 3.3(b). From the analysis it is found that during the pre-monsoon months the pathways of the trajectories are through the arid regions of Mediterranean, Arabian and Thar Desert regions. These are the major source of dust aerosols and contribute to the aerosol loading over the Indian regions. A major quantity of aerosols reaching the place is from desert locations in central Asia.

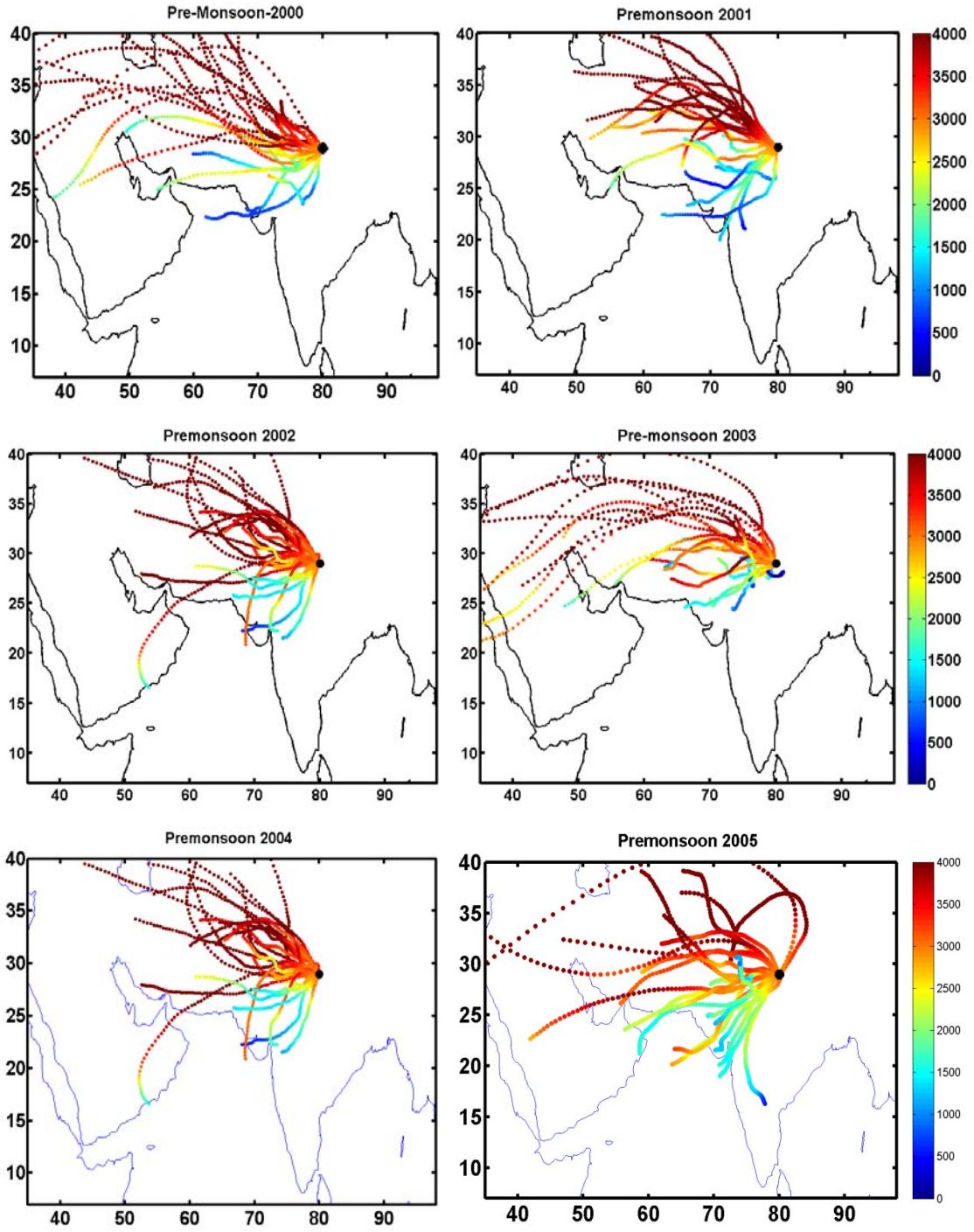

Fig 3.3(a). Back trajectories of aerosol particles reaching the location during the pre-monsoon season. Colour bar indicates altitude in meters.

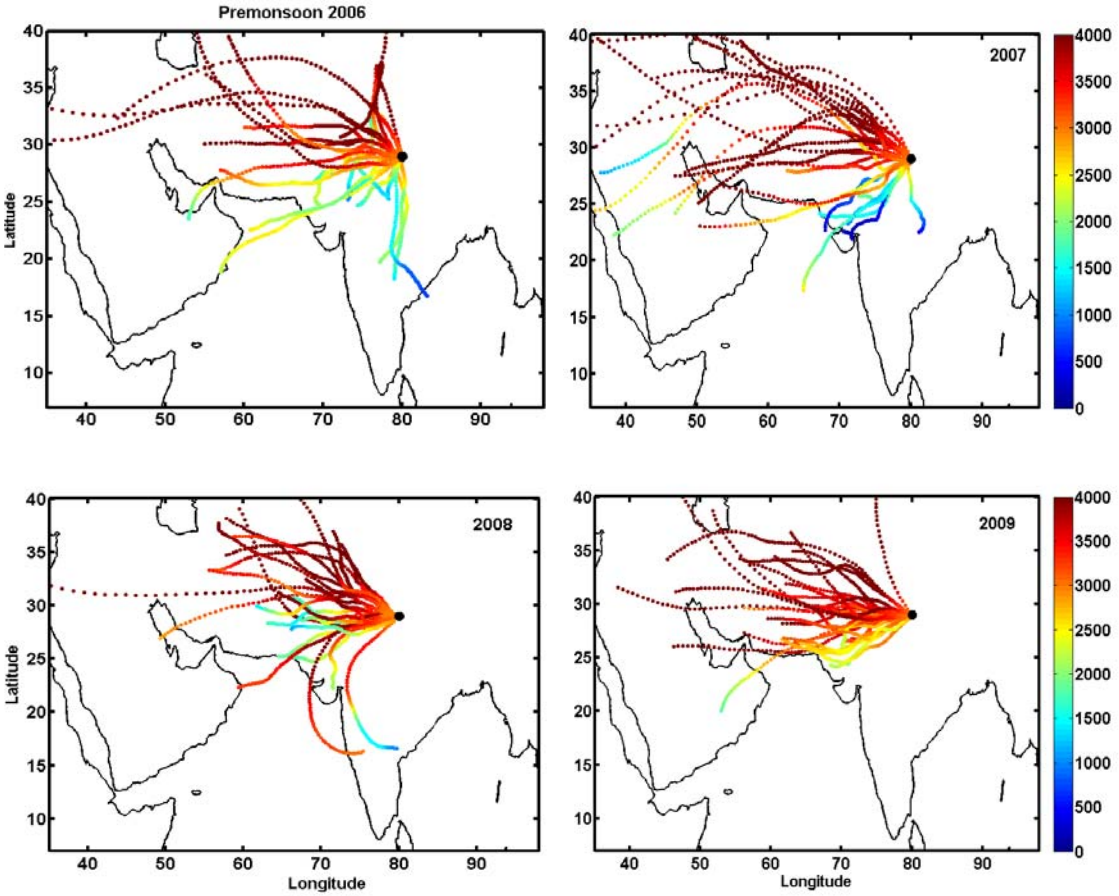

Fig 3.3(a). Back trajectories of aerosol particles reaching the location during the pre-monsoon season. Colour bar indicates altitude in meters (Continued).

From the above figures it can be seen that the aerosol transport occurs at 3 to 7 km above the surface and are advected towards the north Indian region by means of prevailing winds where they get blocked by Himalayan ranges and gets deposited. In the back trajectory analysis, it clearly shows that aerosol transport takes place in the Northerly direction. There is also a westerly component of the airmass during the time. Another importance feature is that most the transport occurs between 1.5 to 5 km levels, which are also another factor for the less aerosol concentration in the region. This is the characteristics of the airmass for almost all the years except for 2006, during which the airmass are predominantly easterlies. These results are in accordance with those reported by Herman et al. (1997) Gautam et al. (2009) in

which increased biomass burning and dust activity contributes to the aerosol loading in the Indian subcontinent.

During the post monsoon season, winds are so weak and the trajectories are passing through the North western parts of India. These regions have no major sources of dust aerosols and thus, the loading of dust aerosols are less. During the post monsoon season of 2000 aerosols that reaches India is a result of long distance transport from locations as far as from the Sahara desert. From their source regions they reach an altitude of 9 km where they have a highest life time before depositing over India.

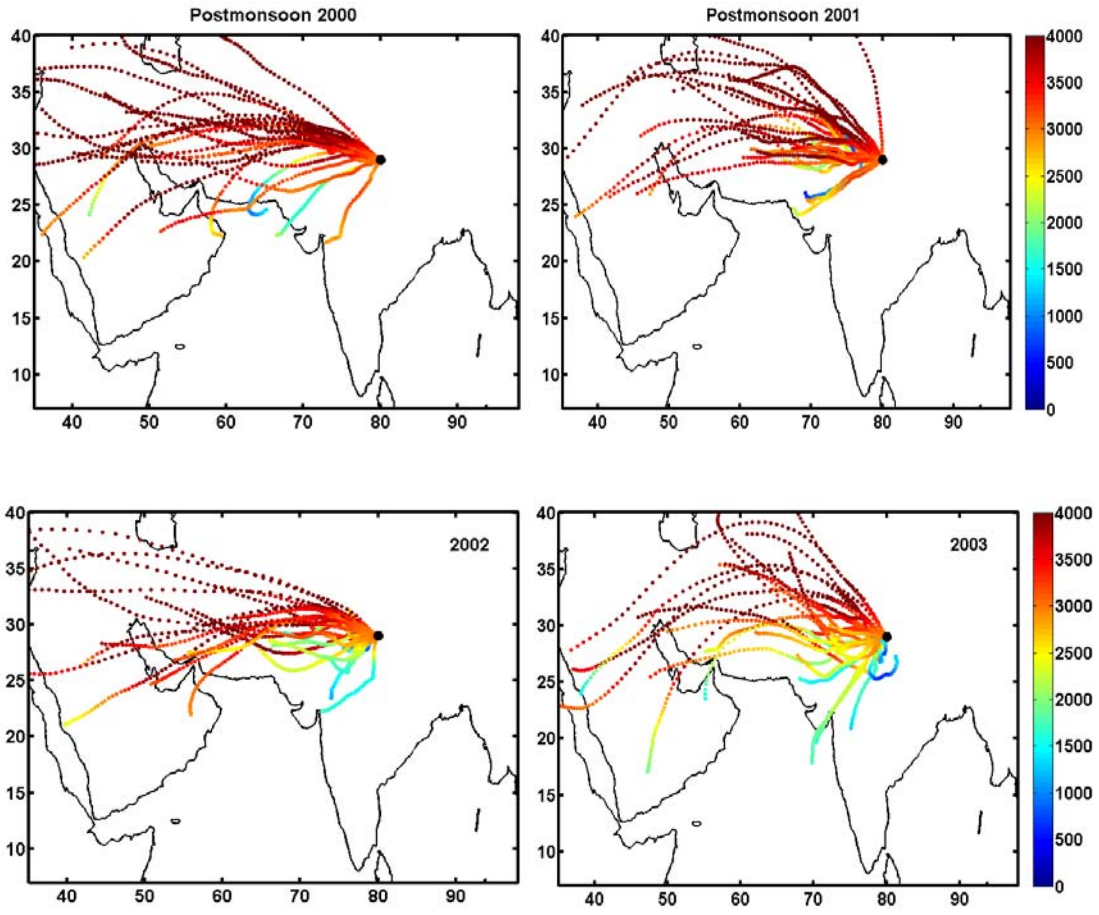

Fig 3.3(b). Back trajectories of aerosol particles reaching the location during the post-monsoon season. Colour bar indicates altitude in meters.

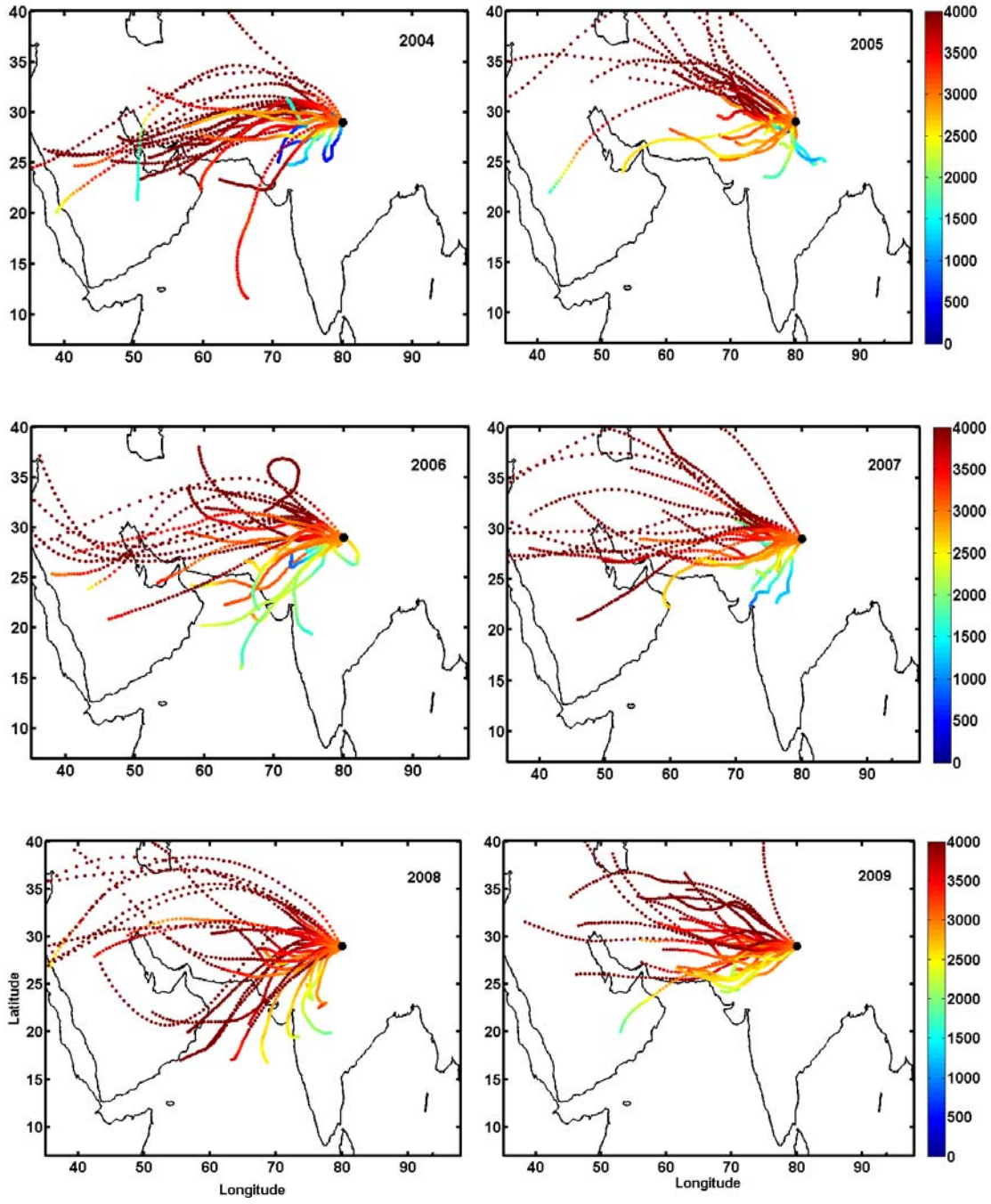

Fig 3.3(b). Back trajectories of aerosol particles reaching the location during the post-monsoon season. Colour bar indicates altitude in meters (Continued).

3.3.4. Effect of El-Nino and La-Nina

The El Niño Southern Oscillation (ENSO) is the largest known global climate variability signal on interannual time scales. It is a quasi-periodical fluctuation between warm El-Niño and cold La- Niña states of the Pacific sea surface temperatures and has a recurrence oscillation period of approximately 2 to 7 years (Philander, 1990). El Niño and La Niña events are denoted respectively by negative and positive trends in the Southern Oscillation Index (SOI). Whilst the largest ENSO signature exists in and over the tropical Pacific, it also affects global atmospheric circulation on a wider scale through the so-called "teleconnection" effects (Diaz and Kiladis, 1992; Xue and Shukla, 1997; Dawson and O'Hare, 2000). It is well known that El-Nino and La-Nina oscillations contribute significantly to the climate variability throughout the globe with El-Nino being dry and warm and La-Nina generally wet and cool. Moreover, the regional temperature, precipitation and circulation patterns vary between El-Nino and La-Nina years. This in turn affects the production and propagation of dust aerosols as well as on the extent of biomass burning which are main sources of aerosols in the Indian region. The ENSO impact on the transport, deposition and variability of these aerosols over the Indian subcontinent is less understood.

It is evident from figures 3.1(a) and 3.1(b) that it is during the years 2000, 2002, 2003, 2004, 2008 pre-monsoon season and 2009 post-monsoon season has a large concentration of absorbing aerosols. Moreover, the following monsoon seasons for 2002 2004 and 2009 were drought years (www.tropmet.res.in/~kolli/mol/Monsoon/ /Historical/air.html). Table 3.1 gives the warm (El-Nino) and cold (La-Nina) events during the years 2000 to 2009. The Oceanic Niño Index (ONI) has become the de-facto standard that NOAA uses for identifying El Niño (warm) and La Niña (cool) events in the tropical Pacific (Trenberth, 1997). It is the running 3-month mean SST anomaly for the Niño 3.4 region (i.e., 5^{o}N-5^{o}S, 120^{o}-170^{o}W). Events are defined as 5 consecutive months at or above the $+0.5^{o}$ anomaly for warm (El Niño) events and at or below the -0.5 anomaly for cold (La Niña) events. The threshold is further

broken down into Weak (with a 0.5 to 0.9 SST anomaly), Moderate (1.0 to 1.4) and Strong (≥ 1.5) events. For an event to be weak, moderate or strong it much have equaled or exceeded the threshold for at least 3 months. Based on these criteria, El-Nino and La-Nina events are classified into weak, moderate and strong phases and are given in Table 3.2.

During the year 2002, ONI shifts from cold phase to warm phase in the pre-monsoon months. This warm phase became intense by post-monsoon season and it persisted till the pre-monsoon season of the year 2003. High positive ONI indicates a moderate El-Nino condition in those years. After a weak phase in the post-monsoon season of 2003, the warm phase again became active in the pre-monsoon season of 2004 which continued into the post-monsoon season of the same year. Years 2004 and 2006 are defined as weak El-Nino years. Cold phases of ONI are seen in the pre-monsoon season of the years 2000, 2001, 2008 and in the post-monsoon season of the year 2007. The year 2000 is a weak La-Nina year 2007 and 2008 are moderate La-Nina years.

Table 3.1. Warm and cold phases of oceanic Nino Index

Year	DJF	JFM	FMA	MAM	AMJ	MJJ	JJA	JAS	ASO	SON	OND	NDJ
2000	**-1.6**	**-1.4**	**-1**	**-0.8**	**-0.6**	**-0.5**	-0.4	-0.4	-0.4	**-0.5**	**-0.6**	**-0.7**
2001	**-0.6**	**0.5**	-0.4	-0.2	-0.1	0.1	0.2	0.2	0.1	0	-0.1	-0.1
2002	-0.1	0.1	0.2	0.4	**0.7**	**0.8**	**0.9**	**1**	**1.1**	**1.3**	**1.5**	**1.4**
2003	**1.2**	**0.9**	**0.5**	0.1	-0.1	0.1	0.4	0.5	0.6	0.5	0.6	0.4
2004	0.4	0.3	0.2	0.2	0.3	**0.5**	**0.7**	**0.8**	**0.9**	**0.8**	**0.8**	**0.8**
2005	**0.7**	**0.5**	0.4	0.4	0.4	0.4	0.4	0.3	0.2	-0.1	-0.4	-0.7
2006	-0.7	-0.6	-0.4	-0.1	0.1	0.2	0.3	0.5	0.6	0.9	1.1	1.1
2007	0.8	0.4	0.1	-0.1	-0.1	-0.1	-0.1	-0.4	**-0.7**	**-1**	**-1.1**	**-1.3**
2008	**-1.4**	**-1.4**	**-1.1**	**-0.8**	**-0.6**	-0.4	-0.1	0	0	0	-0.3	-0.6
2009	-0.8	-0.7	-0.5	-0.1	0.2	**0.6**	**0.7**	**0.8**	**0.9**	**1.2**	**1.5**	**1.8**

Table 3.2. Intensity of El-Nino and La-Nina phases (http://www.cpc.noaa.gov/products/analysis_monitoring/ensostuff/ensoyears.shtml)

El-Nino			**La-Nina**		
Weak	Moderate	Strong	Weak	Moderate	Strong
2004	2002	2009	2000	2007	
2006	2003			2008	

It is seen that during the El-Nino (2002, 2003, 2004, 2006, and 2009) events the region experiences an intense accumulation of absorbing aerosols. For the year 2009, the AI values are less (1.25 to 1.3) compared to other years because El-Nino intensifies after the pre-monsoon season. During El-Nino years generally dry and warm conditions prevail globally, while La-Nina years are characterized by unusually wet and cool conditions. Dry conditions create a positive feedback for the production and propagation of dust aerosols. These conditions also leads to increased biomass burning which further enhances the loading of absorbing aerosols in the atmosphere.

But during La-Nina years (2000, 2007, 2008) the AI values exhibits lesser concentration as compared to El-Nino events. As mentioned before, AI values depend upon the presence of absorbing aerosols in the region. Most of the absorbing aerosols reaching the location are through long distant transport by zonal winds. Since, El-Nino and La-Nina events results in the modification of zonal winds in the equatorial regions, changes in the intensity of wind patterns will definitely influence the transport and deposition of these aerosols and in turn the concentration of absorbing aerosols in the study region.

Fig 3.4 depicts the composite of prevailing zonal winds at 700 hPa during El-Nino and La-Nina years respectively. The figure clearly shows that winds at that level is stronger over the source locations in Arabian Peninsula during El-Nino events compared to La-Nina events. Strong winds are blowing eastwards towards the

Indian region during El-Nino years. High intensity of winds with a magnitude of 8 to 12 ms^{-1} is blowing eastwards during the time. The wind vectors are closely spaced signifying high intensity. These high velocity winds are spread across vast areas of Arabian Desert regions which is one the major source of dust aerosols. These intense zonal winds are capable of transporting aerosols in large quantities towards the study region. However, during La-Nina years winds are generally weaker with a magnitude of 6 to 10 ms^{-1}. High velocity winds are confined to a small area and the weaker magnitude of upper level winds contribute to lesser quantity of aerosols transported eastwards towards the study region.

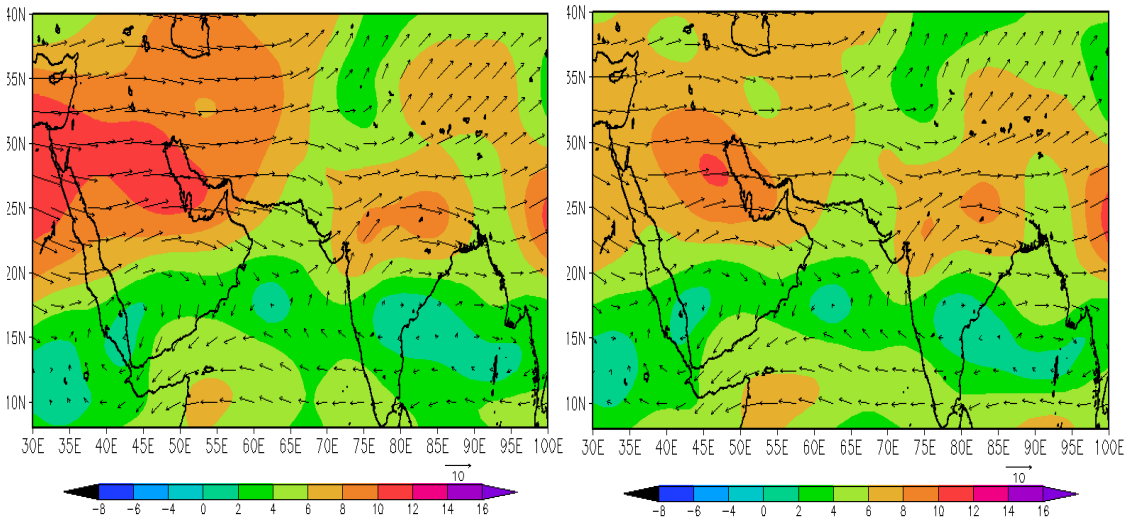

Fig. 3.4. Composite of prevailing winds at 700 hPa during El-Nino and La-Nina years respectively

Fig 3.5 illustrates composite of El-Nino and La-Nina years in the altitude longitude zonal wind (u) and vertical velocity (ω) averaged over the latitude (7^0 N – 30^0 N). From the figure, it can be seen that an intense vertical motion exists over the Arabian Peninsula (35^0 E - 55^0 E) which is indicated by larger vertical wind velocity. The dust aerosol that moves along with these vertical winds reaches upper levels of the atmosphere and merges with the prevailing wind at 700 hPa level. As mentioned before winds at these levels are of prime importance as major dust

transport occurs at this level. Dust aerosols that reach this level moves eastwards along with the direction of the upper level winds towards the Indian region. Over the Indian region these winds gets subsided that results in the deposition of aerosols which is carried along with these winds. As a result, these absorbing aerosols get deposited in the region over IGP.

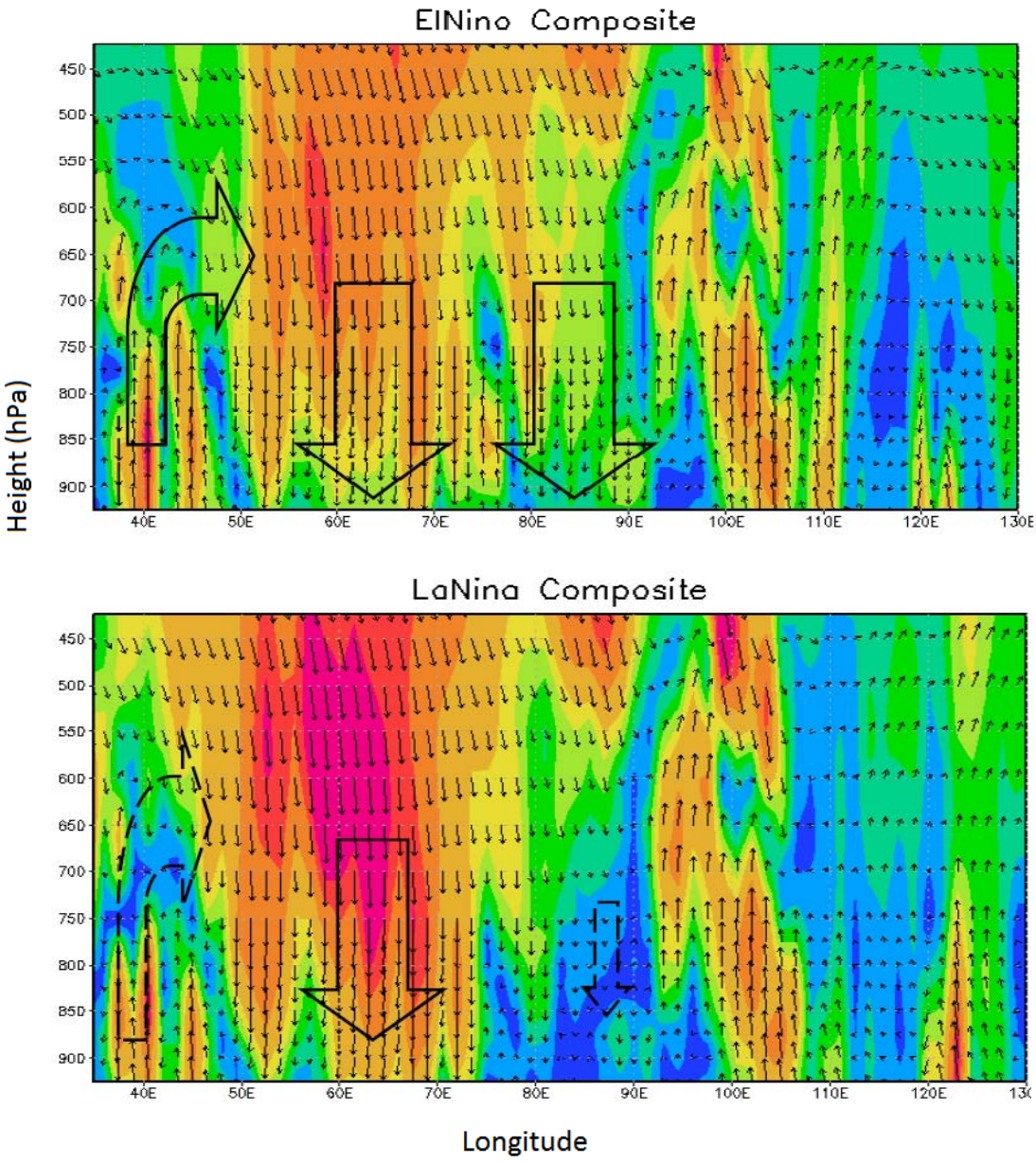

Fig.3.5. Height-longitude plot of the u wind and omega averaged over the latitude (7^0 N – 30^0 N)

The Fig.3.5 illustrates that the convergence of upper level wind starts from the 200 hPa level and the winds that are descending are so intense that along with these winds they brings down the aerosols to the surface level. The descending winds are stronger during El-Nino years in comparison to La-Nina years. Due to higher intensity of subsiding winds from upper levels, the aerosol reaches the lower atmosphere in larger quantities resulting in an increased aerosol concentration. This accumulation of aerosols is indicated by high AI values during the El-Nino years. However, circulations show a different characteristic during the La-Nina years. La-Nina composite plot shows that the even though upward circulation is strong over the dust aerosol source regions in Arabian Peninsula, when it reaches the 700 hPa level they weaken so that the quantity of dust transported eastwards is considerably less. This zonal circulation cell completes with the subsidence of upper level winds at 70^0 E – 75^0 E longitude. But, the downward limb of the circulation is so weak over the Indian region in the longitudinal belt extending from 75^0 E to 100^0 E, so that subsiding air becomes weak as it approaches 750 hPa levels. As the descending winds gets weaker the quantity of aerosols reaching the lower levels decreases. This explains the lower AI values over the North Indian region during La-Nina years. Also, a wet and cool condition that occurs during La-Nina years decreases the production and propagation of these absorbing aerosols.

The effect of the convergence of upper levels winds and the consequent enhancement of AI can be seen in Fig 3.6. As illustrated in the figure high concentration of aerosols can be seen at Indian region during El-Nino years. During this time AI values ranges from 1.25 to 1.65 over most parts of India. Peak values of 1.65 are observed at North India especially over the IGP. A secondary maximum of 1.45 is seen over West Bengal region. Dry conditions that existed during El-Nino create a favourable condition for the enhancement of these aerosols. Convergence of upper level winds which is a main carrier of aerosols was very intense during the time. All these factors contribute to the high AI values during El-Nino years. As

mentioned before, La-Nina years are characterized by wet conditions. Wind system shows a weak downwelling of upper level winds over India. Therefore, aerosol loading in the regions becomes substantially less as indicated in the Fig 3.6. The AI values ranges from 1 to 1.45 over the central and north India. Very lower AI values (< 1) are seen in the peninsular India. Peak AI values of 1.45 are over North West India and IGP.

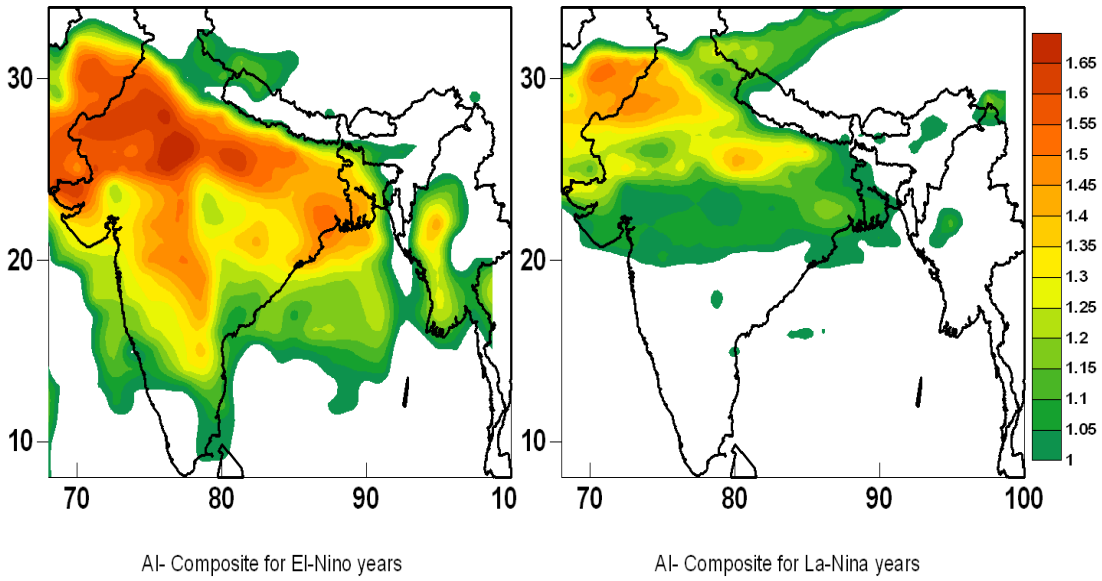

Fig. 3.6. Aerosol Index composites for El-Nino years and La-Nina years over the Indian subcontinent

Back trajectory analysis shows that major share of the aerosols that reaching the Indian region during La-Nina is from south westerly and northerly directions (Fig 3.7). Therefore the amount of UV absorbing aerosols will be significantly less quantity. But, during El-Nino conditions most of the aerosols reaching the location can be traced back from major source areas over the Arabian and African desert regions. These aerosols that get transported from source locations reaches up to an altitude level of 3 to 4 km from the surface. At these levels aerosols travel long distance without settling. Himalayan range acts as a barrier for these prevailing winds so that the air mass that carry aerosols get subsided over the region.

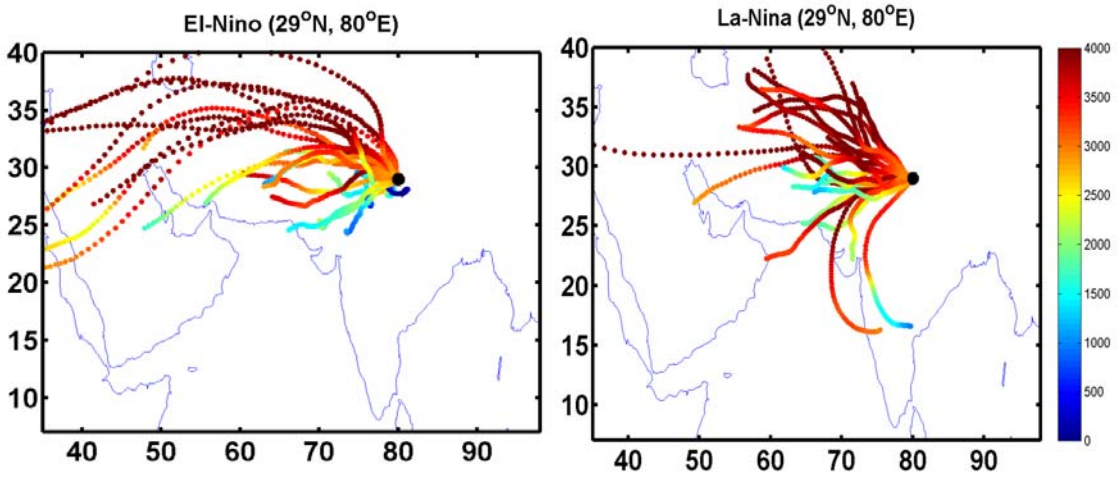

Fig 3.7 Back trajectory analysis for El-Nino and La-Nina composites

The back trajectory analysis shows that aerosols that reaching this location has its origin in major arid zones in Arabian Peninsula and West Asia which are the major sources of dust aerosols. Most of the airmass has a westerly component indicates that dust sources in the adjacent locations influence the aerosol concentration over India. The other source location of aerosol is from the Thar Desert. The trajectory path way that takes place at 1 km and 1.5 km is due to the combustion of fossil fuels and biomass burning. Therefore, aerosols resulting from sources at distant locations as well as due to enhanced combustion of carbonaceous fuels and biomass burning contribute to higher aerosol loading in El-Nino conditions. The dry conditions prevailing during El-Nino favours the production of these types of aerosols.

But, during La-Nina years the aerosol pathway is not along the major aerosol sources. Back trajectory analysis indicates that the components of aerosol pathways are in northerly and south westerly directions. Due to the weaker zonal winds, the long range transports of aerosols from desert locations are less. Most of the aerosols reaching the location are from nearby locations. Weaker westerly winds may have contributed to lesser quantity of aerosols reaching the place. Hence the transport of aerosols is marginal compared to El-Nino years. All these factors may have contributed to less concentration of aerosols in the region during La-Nina year.

3.4. Conclusions

Transport and deposition of aerosols is more during the pre-monsoon season than in post-monsoon season for all the years taken into consideration. Aerosols reaches the Indian subcontinent as a result of long distance transport by mean of prevailing winds at 700 hPa (~ 3km). These aerosols get deposited in the longitudinal belt ranging from 70^0 E to 90^0 E. The piling up of aerosols increases the concentration in the atmosphere as indicated by higher values in AI during pre-monsoon season. The following monsoon season washes out the aerosols present in the atmosphere so that AI will be lower during the monsoon season. During post monsoon season, the prevailing westerlies are not stronger as in the case of pre-monsoon. The AI values were higher in the pre-monsoon season during the years of 2000, 2002, 2004, 2006 and 2008 with an exception of the year 2003. Since winds are one of the major factors for the transport and distribution of aerosols, weakening and strengthening of zonal winds has an influence in the concentration of aerosols in the region.

It is during the El-Nino years the Indian subcontinent shows an enhancement of aerosol concentration. It is seen that during El-Nino years, the zonal winds are of higher intensity particularly over the source regions of Arabian Peninsula. These strong zonal winds carry aerosols eastwards towards Indian region and get subsided over the Indian subcontinent. The descending of upper level winds is so strong during those El-Nino years that most of the aerosols in the upper levels reach the lower atmosphere increasing the aerosol concentration. But during La-Nina events the situation reverses. The zonal wind at 700 hPa weakens and also the subsidence of upper levels winds are weakens there by less subsidence of upper level winds. Therefore, the aerosol concentration becomes decreased during La-Nina years. Aerosol Index composite during El-Nino years shows that higher aerosol concentrations over most parts of India, while La-Nina years are characterized by less AI values.

CHAPTER 4

BIENNIAL VARIABILITY OF ATMOSPHERIC AEROSOLS AND ITS RELATION WITH QBO

4.1. Introduction

The Quasi-Biennial Oscillation (QBO) in the zonal winds is a well known primary mode of interannual variability in the tropical lower stratosphere. These equatorially symmetric easterly and westerly wind regimes alternate regularly with a mean period of 24-30 months (Lindzen and Holton, 1968; Baldwin et al., 2001; Mohanakumar, 2008). Along with these oscillations warm and cold stratospheric temperature anomalies accompany these wind regimes as they propagate lower into the atmosphere (Gray et al., 1992). The driving force for the QBO is the vertical transfer of momentum from troposphere to stratosphere by the vertically propagating gravity waves, such as Kelvin waves, mixed-Rossby gravity waves and inertia-gravity waves (Holton and Lindzen, 1972; Dunkerton, 1997). There is considerable variability of the QBO period and amplitude, easterly phase being stronger than the westerly phase.

The QBO circulation requires a westerly shear zone with a warm temperature anomaly created by anticylonic vorticity anomalies in the tropical upper troposphere, subsidence and warming at the equator. This temperature anomaly is accompanied by a meridional circulation pattern in which a horizontal component of this circulation having an equatorward motion aloft and poleward motion at the lower levels, thus completing the circulation cell. The reverse scenario occurs during the easterly phase. The wave driving the QBO provides the necessary energy required for this thermodynamic circulation. Therefore, this circulation which

maintains the QBO induced temperature anomaly have a direct effect on atmospheric constituents in the tropics.

Reid and Gage (1985), has found a significant dependence on the phase of the QBO in zonal winds of the tropical stratosphere and tropical tropopause height based on radiosonde data obtained from nine tropical stations. Later studies (Huesmann and Hitchman, 2001; Ribera et al., 2008) has reported the correlation between the stratospheric phenomenon such as QBO and the evolution of the pressure and temperature at the tropical tropopause. A warming (cooling) of the tropical tropopause occurs during QBO positive (negative) phase for which the radiosonde data has shown that tropopuase height will be lower (higher). The relationship between the QBO, tropopause height, temperature and pressure are studied extensively (Angell and Korshover, 1964; Randel et al., 2000). Their results showed a good agreement with all these parameters and are either in-phase or out of phase with respect to the equatorial QBO. From all these reported studies we can infer that these stratospheric oscillations affect the dynamcis of most of the tropospheric variables.

Using in situ measurements, Saha and Moorthy (2005) noted that AOD over peninsular India shows enhancements from climatological mean for every alternate years and suggested that large scale atmospheric dynamcis to be one of the possible reasons for this varying magnitudes. A similar variation in monthly mean AOD has been reported by Beegum et al., (2009) over four tropical stations in Asia and Africa. It has been postulated by Kane (1992) that winds at 50 hPa are responsible for the periodicities in the concentration of trace elements and surface aerosols in the range of 2-4 years. Moreover, numerous studies indicate that QBO plays an important role in the distribution of aerosols and chemical constituents such as ozone, water vapour and methane (Trepte and Hitchman, 1992; Hitchman et al., 1994; Cordero et al., 1997; O'Sullivan and Dunkerton, 1997; Randel et al., 1998).

It is interesting to note that how much a stratospheric phenomenon like QBO influences aerosol concentrations which is predominantly confined to troposphere. There are not many studies done on the relation between QBO and atmospheric aerosol concentrations. Therefore our study focuses on how much the changes in QBO phase influences the prevalence of atmospheric aerosols in the northern Indian region where most of the earlier studies (Guttikunda et al., 2003; Dey et al., 2004; Tripathi et al., 2006; Nair et al., 2007) have reported large amount of aerosols in the region. Such a study is relevant in a region where a majority of the people in the billion population of India resides.

4.2. Data and analysis

Monthly mean MODIS (MODerate resolution Imaging Spectroradiometer) data onboard *Terra* and *Aqua* satellite is used to determine the aerosol properties for the years 2000 to 2009 (10 years) over the chosen location. MODIS monthly data is available in 36 spectral bands from visible to thermal infrared (29 spectral bands with 1km, 5 spectral bands with 500 m, and 2 spectral bands with 250 m, nadir pixel dimensions). The *Terra* and *Aqua* spacecrafts has an equatorial crossing time of 10:30 and 13:30 (local time) respectively. Due to its larger swath widths and instrument-scanning angle of 110° a nearly global image is produced (Levy et al., 2003). This sensor measures the land aerosol characteristics using the algorithm based on 'dark target' approach (Kaufman and Sendra, 1988; Kaufman et al., 1997; Remer et al., 2006), therefore does not retrieve over bright surfaces such as snow, ice and deserts. The aerosol properties are derived by the inversion of the MODIS-observed reflectance using pre-computed radiative transfer look-up tables based on aerosol models (Remer et al., 2005; Levy et al., 2007). The initial versions of the MODIS algorithms have been under continued development and have recently received an improved aerosol determination, *via* processing to Collection 5 (C005) Level 3 products (Levy et al., 2007).

The C005 Level 3 (spatial resolution 1°×1°) MODIS products are obtained from Giovanni website (*http://giovanni.gsfc.nasa.gov/*). MODIS retrieves the column aerosol concentration (in cloud free, solar glint free) conditions that is represented as aerosol optical depth (AOD). Overall, the uncertainty of the MODIS-derived AOD is ±0.05 ± 0.2 AOD over the land (Kaufman et al., 1997a; Chu et al., 2002). The MODIS-derived AOD are validated against the *in situ* AOD observed at AERONET stations, which shows that AOD retrievals in the visible wavelengths are generally within the pre-launch uncertainty (Jethva et al., 2007; Remer et al., 2008). An inter comparison of MODIS derived AOD with AERONET observations over India are found to be in reasonably good agreement with the ground-based sun photometer observations of AOD over the Gangetic plain (Jethva et al., 2005; Aloysius et al., 2008).

The tropopause temperature and pressure are obtained from the Atmospheric InfraRed Sounder (AIRS) onboard MODIS *Aqua* sensor. The AIRS sounding suite is the most advanced atmospheric sounding system to date, with measurement accuracies far surpassing those of current weather satellites. The AIRS is an infrared grating spectrometer that operates in the thermal infrared portion of the spectrum, from 3.7 μm to 15.4 μm. From its sun synchronous polar orbit, the AIRS system provides more than 300,000 all-weather soundings covering more than 90% of the globe every 24 hours. This system measures upwelling thermal radiation emitted from the atmosphere and the surface. By analyzing an observed spectrum it is possible to infer the vertical distribution of temperature and water vapor. This is accomplished by inverting the radiative transfer equation (RTE), which models the spectral intensity for a given distribution of the geophysical parameters.

The AIRS and Advanced Microwave Sounding Unit (AMSU) form an integrated temperature and humidity sounding system for numerical weather prediction and climate studies. Due to its hyper spectral nature, AIRS can provide near-radiosonde-

quality atmospheric temperature and moisture profiles with the ability to resolve some small-scale vertical features (Aumann et al., 2003). It retrieves temperature profiles with a vertical resolution of 1 km in the troposphere at an accuracy of 1K, and water vapor profiles with a vertical resolution of 2 km in the troposphere at an accuracy of 15%. In addition to temperature, profiles of ozone, CO and other minor gases are also produced. The dataset available for this study ranges for the period from October 2002 to December 2009.

The QBO of zonal winds at 50 hPa and 30 hPa are used to determine the phase change of zonal winds at these levels. High resolution radiosonde data of zonal wind in the lower stratosphere from an equatorial station where the QBO is a maximum is used for this study. It is made possible by using the Singapore wind data obtained from the Monthly Climatic Data of the world published by National Climatic Data Center, Asheville, USA.

4.3. Results and discussions

The monthly mean zonal winds averaged over the two altitude levels, viz., 50 and 30 hPa levels representing stratospheric QBO and the monthly mean AOD for the period ranging from March 2000 to December 2009 are depicted in Fig 4.1. The figure shows that the aerosol concentration undergoes a biennial variation with peak values for every alternalte years. Analysis of this behaviour of aerosols in relation to QBO shows that aerosol concentration is more during westerly phase (positive phase) of QBO, and lesser values during the easterly phase (negative phase) of QBO. It is observed that the AOD attains a maximum value in the month of July during almost all the years. Starting from 2000, the peak values of AOD are observed for the even years 2002, 2004, 2006 and 2008 for the month of July. While, for the odd years lower values are observed. In the drought years of 2002 and

2004, dry conditions are favourable for enhanced aerosol concentration resulting in very high values during those years.

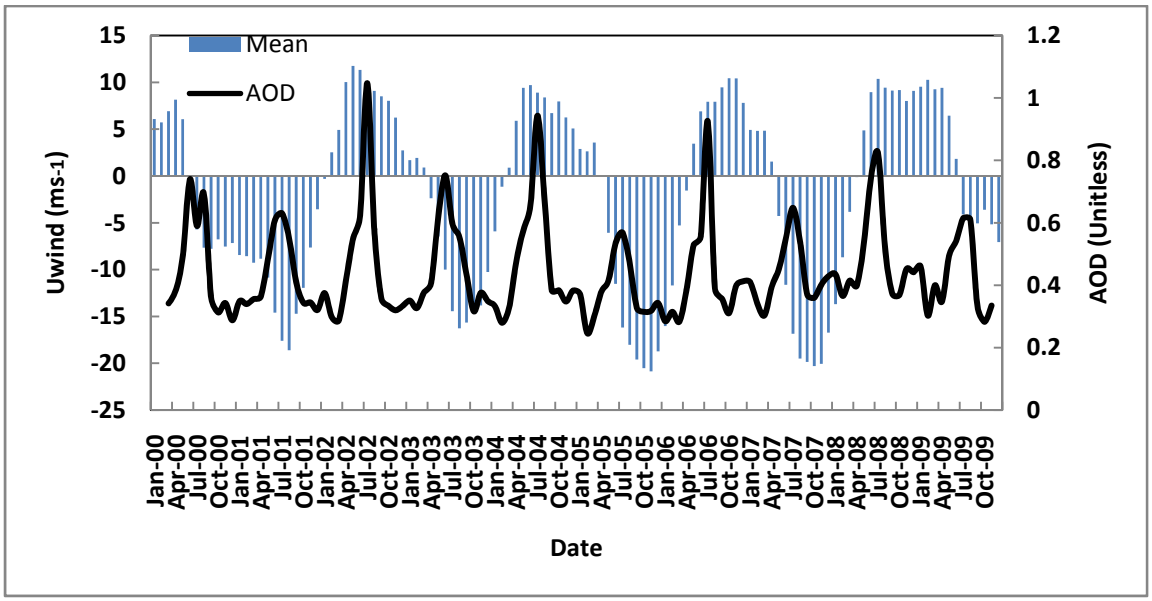

Fig 4.1. A comparison between monthly mean zonal winds at 50hPa and 30 hPa ((50hPa + 30 hPa)/2) and monthly mean AOD.

The QBO winds were in the westerly phase during the years 2002, 2004, 2006 and 2008. The westerly phase has maximum duration in the year 2008 which extended till the pre- monsoon season of 2009. The amplitude of the westerly phase shows a maximum in the year 2002. The AOD shows a decreasing pattern with the weakening of the zonal wind amplitude. It is seen that the amplitude of the easterly phase is about twice as strong compared to the westerly phase. The easterly phase has the maximum duration in the year 2001 and maximum amplitudes in the years 2005 and 2008. It can be seen that during both phases of QBO, higher values of AOD coincides with maximum amplitude of QBO zonal winds and declines with weakening amplitudes.

4.3.1. Meridional Circulations

The maximum values of monthly mean AOD has a periodicity of 24 months and the duration between a maximum and minimum AOD has a periodicity of about 12 months. A close evaluation suggests that the monthly mean AOD has a correspondence with the QBO. Stratospheric QBO, which is driven by vertically propagating Kelvin waves, contribute a westerly force, and Rossby gravity waves, that contribute an easterly force. These waves, which is the main driving mechanism of the QBO has maximum amplitude at the equator (Holton and Lindzen, 1972). The QBO's secondary meridional circulation (SMC) which is superimposed upon the Brewer Dobson Circulation consists of an increase of the upwelling in the easterly shear phase and a suppression of the upwelling in the westerly phase (Plumb and Bell, 1982).

According to Trepte (1993), divergence of the SMC occurs in the easterly jet, above the easterly shear and below the westerly shear, and convergence occurs in the westerly jet (see Fig 4.2). As a result, during the westerly phase of QBO, the divergence from the equatorial troposphere would enhance the aerosol loading , thereby increasing the AOD to higher values. Moreover, it is also seen that the QBO westerly phase lasts longer than the easterly phase. During this prolonged duration of westerly phase, the aerosols in the upper troposphere gets transported to lower levels in the atmosphere resulting in a build up of aerosols.

But, during the easterly phase the intrusion of tropospheric air into the lower stratosphere, may result in a much less aerosol content and thereby a decrease in AOD. The lower aerosol content may be possibly because the easterly phase induces anomalous motion that leads to a cooler, higher tropopause near the equator (Gray et al., 1992). Therefore these aerosols undergo mixing to a greater extent thereby reducing their concentration in the atmosphere. But during the westerly phase the

lower tropopause confines these aerosols to the shorter extent thereby increasing their concentrations in the atmosphere.

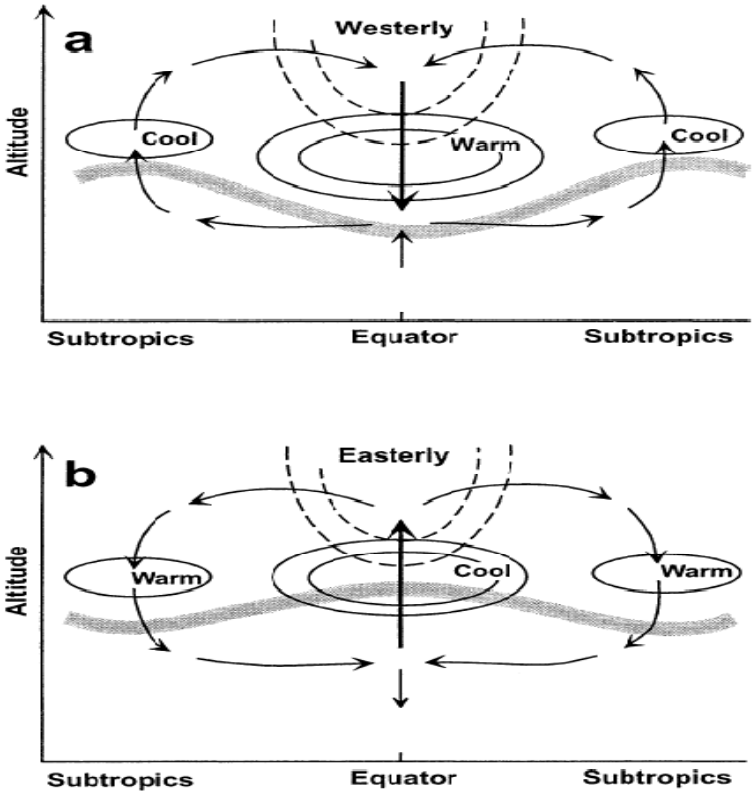

Fig. 4.2. Schematic representation of the mean meridional circulation driven by the QBO, after Trepte (1993). Dashed contours indicate isopleths of zonal velocity; solid contours represent anomaly isotherms. The thick, gray lines represent the tropopause. (a) Warm anomaly during descending zonal mean westerly shear; (b) cold anomaly during descending zonal mean easterly shear (Adapted from Collimore et al. 2003).

The QBO modulates the transport of aerosols in two distinct ways. The QBO modulates diabatic transport. There is local meridional diabatic circulation in the tropics and subtropics associated with the equatorial QBO winds (Plumb and Bell, 1982). In periods with westerly QBO shear, there is equatorward motion at upper levels, relative downwelling at the equator at the level of maximum shear and

poleward motion at lower levels. At the peak of the westerly circulation, the QBO secondary circulation is convergent with wind flowing towards the equator. In periods with ascending easterly QBO shear, the pattern of the meridional circulation is reversed with relative upwelling at the equator.

These patterns of meridional circulation induce corresponding QBO associated patterns in aerosol distribution. This flow reverses at peak of the easterly circulation. The aerosols in the tropical regions are rapidly transported zonally with mean stratospheric winds while, meridional transport is determined by large scale stirring and mixing (Plumb, 1996). Secondly, it is suggested that the QBO winds modulates isentropic mixing through their influence on extratropical planetary wave propagation and breaking. The large scale transport and isentropic mixing of aerosol, coupled with the process of particle condensational growth, coagulation and sedimentation is more effective during the westerly phase than in the easterly phase of QBO.

4.3.2. Vertical Distribution of Aerosols

Gautam et al (2009) has reported a increased concentration of aerosols during the pre-monsoon and summer seasons at elevated altitudes. During the westerly phase aerosols originating from the Thar Desert contribute to aerosol loading in the vertical levels. Higher deplorisation suggests the presence of large concentrations of dust and other anthropogenic aerosols in the 5 km levels. Together with pre-monsoon westerly winds and enhanced convection, these aerosols move aloft from the Desert regions towards the Gangetic region. High deplorisation values across the elevated dust transport levels (3-5 km) validates this analysis. This signifies the increased aerosol concentration during the westerly phase of QBO. The sulphuric acid or water droplets that compose the majority of the stratospheric aerosol can also act as condensation nuclei as they enter the upper troposphere, thereby affecting cloud formation and precipitation patterns (Twomey, 1991). During winter and spring, synoptic disturbances, traveling the lower stratospheric westerlies, transport

aerosol in to the tropical troposphere. Large aerosol loading occurring in the pre-monsoon season during westerly phase is concurrent with a quasi-horizontal advection, diffusion and gravitational sedimentation over the tropical regions increasing the AOD.

4.3.3. Tropopause Characteristics

Horizontal and seasonal variations in tropical tropopause temperature and thermodynamic properties are broadly associated with the distribution of convection and large scale vertical motion. The effect of the QBO in zonal wind on tropopause pressure level, height and temperature are presented in Fig 4.3. In the figure, anomalies in tropical tropopause pressure, height and temperature over the chosen location for the years 2002 to 2009 are illustrated. It is seen that the elevation of the tropopause level (positive anomalies of pressure) is associated with negative phase of QBO. During the positive phase of QBO, the tropopause is characterized by less than normal pressure levels which represent a higher tropopause. The height of the tropopause reflects the temperature of the underlying troposphere, and it decreases with decreasing atmospheric stability, suggesting an indirect response to convection.

The analysis of temperature anomalies at tropopause level together with the analysis of its QBO served to identify positive (negative) tropopause temperature anomalies during westerly (easterly) phase of QBO. It can be seen from Fig 4.3. that positive temperature and pressure anomalies are seen during the westerly phase of QBO. The present study is in agreement with those results obtained by Heusmann and Hitchman (2001), in which a positive correlation between the QBO and temperature at the tropopause level was detected using data from the NCEP reanalysis. During QBO easterly phase, strong negative tropopause temperature anomalies are observed in the months of January to May, which indicates a warming of the tropical troposphere.

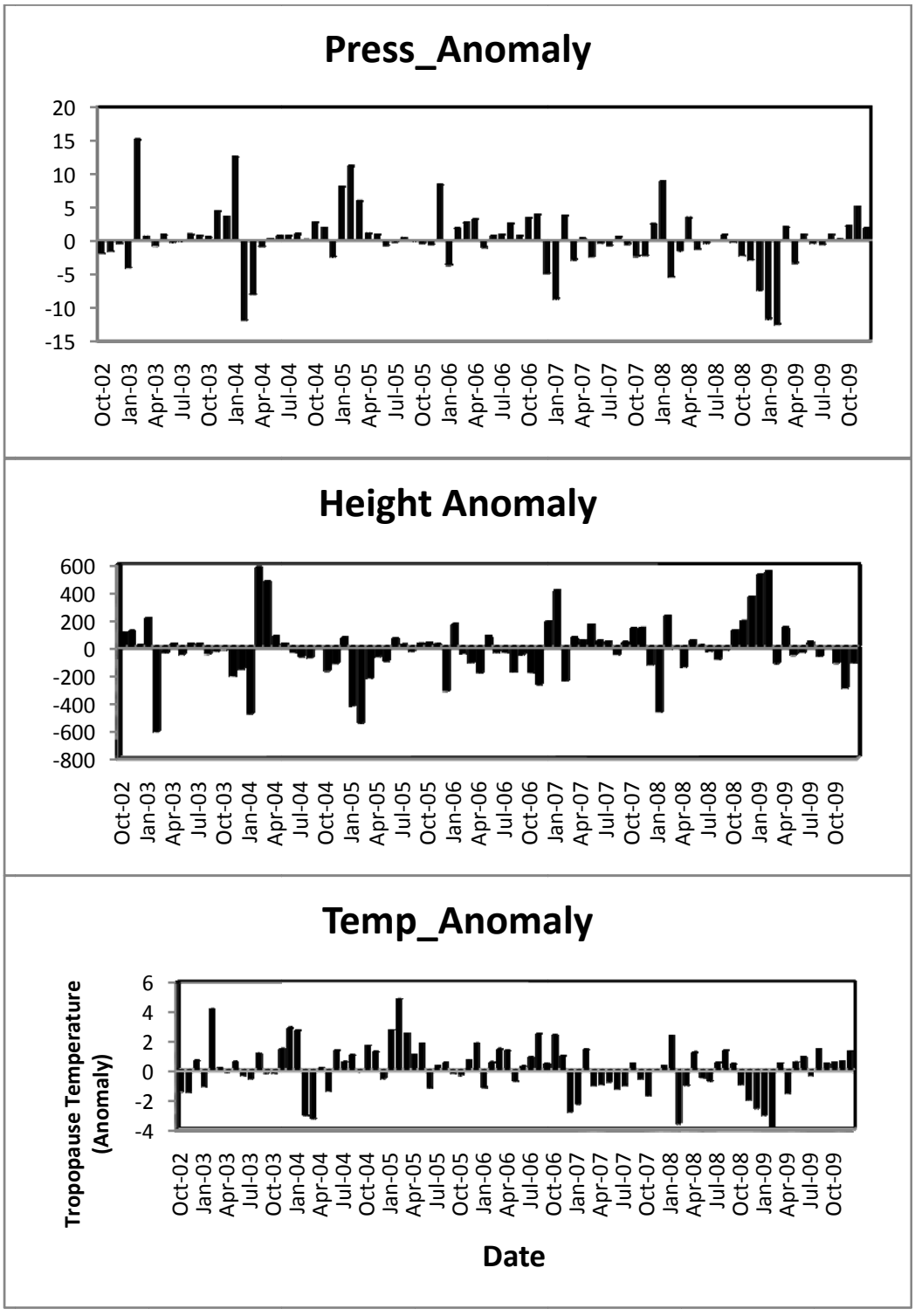

Fig 4.3. Anomalies of tropical tropopause (a) pressure (b) height (c) temperature respectively for the years 2002 to 2009. The anomalies are averaged from 22^0N to 29^0N and 69^0E to 89^0E.

Ribera et al., (2008) has reported that at tropics the QBO induces a secondary circulation that modulated the height and pressure of the tropopause. This may be the possible cause of the variations in tropopause characteristics with the changes in stratospheric zonal winds.

The modulation of QBO mean meridional circulation of the stratosphere induces changes in pressure and temperature of the tropopause (Salby and Callaghan, 2004). They showed that the changes in the Brewer-Dobson circulation generate anomalies in the tropopause temperature and height. During the westerly QBO phase, anticlockwise circulation anomalies are found in the low tropical stratosphere. These anomalies lead to downwelling and warming the tropical stratosphere region. In westerly shear zones due to sinking motion and the associated adiabatic warming implies a maximum temperature at the equator. The opposite holds in easterly shear zones. The variations in tropopause temperature and pressure anomalies bring about changes in troposphere height. Therefore, as mentioned above, during the downwelling of this positive phase, an increase in tropopause temperature and pressure and a decrease in tropopause height are seen. As a result the AOD increases.

But, during the easterly phase of QBO, cyclonic circulations create an upwelling in the tropical tropopause so that a negative temperature and pressure anomalies persist at tropical tropopause. Therefore, the tropopause height increases and the AOD decreases. The warming of the tropical tropopause layer would push the tropopause layer to higher latitudes and thereby to lower pressures. As the troposphere warms, the free troposphere or the upper troposphere gets warmer by a larger amount than the surface (Santer et al., 2005). Using global models, Gettelman et al., (2009) has established this theory and reported that warming of the troposphere results in a heating of the tropopause. The resulting increase in convection causes the effective mixing of the constituents in the troposphere (eg. aerosols) and lowering its concentration.

Since more than 90% of the total volume of aerosols lies in the troposphere the dilution in its concentration reduces the AOD values in the atmosphere. But, when tropical tropopause layer cools the tropopause shrinks to lower altitudes (higher pressures) so that atmospheric aerosols are confined to a smaller area in troposphere. As a result, the aerosol concentrations increases which is indicated by high AOD values in the atmosphere. As mentioned above, this occurs during the westerly (positive) phase of the QBO. It can be noted that increasing concentrations can be observed during the months when the prevailing winds in the tropopause are westerlies. These winds are capable of bringing dust aerosols from the arid regions (eg. Arabian Peninsula, Mediterranean and Thar Desert) to the study location and thereby increasing the surface concentration.

Therefore, the variations in AOD have an association with the waxing and waning of the tropical tropopause. Stratospheric QBO in zonal winds is one of the primary mechanisms for this variation in tropical tropopause layer as a result of which AOD undergoes a biennial variability in response to positive and negative phases of the QBO. It is suggested that positive temperature anomalies in response to QBO are the resultant of a complex forcing due to aerosols and green house gases.

4.4. Conclusions

The time series of monthly mean AOD over the Indian region shows a biennial variability which is seen to be associated with the positive and negative phases of QBO in stratospheric zonal winds. Further analysis reveals that QBO modulates the tropical tropopause layer by which the tropopause undergoes an oscillation in tropopause characteristics (height, pressure and temperature). The warming (cooling) of the troposphere during the positive (negative) phase of QBO enables intense convection thereby resulting in an increase (decrease) in concentration of atmospheric aerosols. Equatorial QBO, which is predominantly a stratospheric phenomenon, induces changes in the tropospheric characteristics that in turn modify

the distribution of tropospheric constituents including concentrations of atmospheric aerosols. Moreover, the increasing concentrations are observed when the winds are westerlies suggesting the transport of dust aerosols from the arid regions of Arabian Peninsula and Thar Desert.

Therefore it is evident from Chapter 3 and Chapter 4 that North Indian region which comprises of IGP is influenced by significant loading of aerosols as a result of the complex interactions between meteorological parameters and tropopause dynamics. The aerosols reaching the location by means of zonal, meridional and vertical transport accumulates due to the typical characteristics of the region. This enhanced piling up of aerosols in significant quantities during the non-monsoon months has a potential role in modifying cloud processes and consequent rainfall distribution in the region.

CHAPTER 5

ROLE OF FINE MODE AEROSOL PARTICLES IN MODULATING CLOUD PROPERTIES

5.1 Introduction

One of the main challenges the world facing today is the rapid growth of population and the increased demand for water sources. Climate change and subsequent variation in hydrological cycle is a major global concern especially in a developing economy like India. Intergovernmental Panel for Climate Change (IPCC) has pointed out that atmospheric aerosols affect climate by altering the Earth's energy budget. The aerosol cycles are closely connected with the hydrological processes in the atmosphere due to a substantial interaction between aerosols and clouds. Clouds and precipitation play an important role in the formation, transformation, and removal of aerosols from the atmosphere; on the other hand, aerosols strongly affect the microphysical processes in clouds.

It is well known that aerosols have important climate effects. Among the three modes of aerosol particles, the accumulation mode or the fine mode particles are most relevant to aerosol's climate effect for these aerosols have the largest residence time and its ability to form cloud condensation nuclei (CCN) and to light absorption and scattering. They scatter or absorb incident solar radiation which is termed as aerosol direct effects. Aerosol particles can also indirectly affect climate through modifying cloud properties by acting as CCN. The initial sizes and concentrations of CCN determine the precipitation efficiency in clouds. These are termed as aerosol indirect effects. Aerosol indirect effects have the largest magnitude of all the aerosol effects but also have large uncertainty. This aspect of the cloud microphysics and its impacts on precipitaton is the major focus of this chapter.

5.1.1 Aerosol indirect effects

Clouds are an important regulator of the Earth's radiation budget. They have a large impact on the Earth's energy budget since they are highly reflective of solar radiation and strongly absorb long wave thermal radiation. Clouds play a major role in the hydrological cycle, which is coupled to the energy budget through the release of latent heat that results from condensation of water vapour or from evaporation. This, in turn, influences the atmospheric circulation on a variety of scales. By acting as CCN, aerosol particles, along with other meteorological conditions, determine cloud droplet number concentration. By changing cloud droplet number concentration, aerosols can affect cloud optical and physical properties, which will change short wave and long wave cloud radiative forcing and the hydrological cycle, further affecting atmospheric circulation. This is the aerosol radiative indirect effect.

Several aerosols indirect effects have been identified (Denman et al., 2007). For a given cloud liquid water content, increase in cloud droplet number concentration from anthropogenic aerosols will decrease droplet size, and will increase cloud optical depth and cloud albedo. This is called the *first aerosol indirect effect* (Ramaswamy et al., 2001) or the *Twomey effect* (Twomey, 1977) or the *cloud albedo effect* (Lohmann and Feichter, 2005). The *first indirect* or the *Twomey effect* says that in a polluted environment the intensification of hygroscopic aerosols (eg. sulphates, nitrates) will lead to an increase in available cloud condensation nuclei (CCN) for cloud formation. By acting as CCN, aerosols along with other meteorological conditions determine cloud droplet number concentration. Clouds with large amount of smaller droplets will have a higher albedo compared to a pristine environment (Twomey, 1977; Kaufman and Fraser. 1997). With the substantial increase in global mean burden of aerosol particles in the atmosphere from pre-industrial times to the present day, (Collins et al., 1994) Earth Radiation Budget Experiment (ERBE) indicate that a small change in macrophysical and microphysical properties in clouds have a significant effects on climate.

Increase in cloud droplet number concentration and cloud droplet size are hypothesized to reduce the precipitation efficiency and to increase the cloud water path, prolonging cloud lifetime. This is called the *second aerosol indirect effect* (Ramaswami et al., 2001) or the *Albrecht effect* (Albrecht, 1989), or the *cloud lifetime effect* (Lohmann and Feichter, 2005). Both the first and second aerosol indirect effects act to cool the Earth-atmosphere system by increasing the cloud optical depth and cloud cover, respectively. This reduces the net solar radiation at the top of the atmosphere as well as at the surface.

A decrease in cloud droplet size reduces the precipitation efficiency by delaying the onset of collision and coalescence in warm cloud thereby delaying the onset of rainfall. Martins et al. (2008) has suggested that biomass burning aerosols delay the onset of precipitation through slower droplet growth. The drag on updrafts produced by raindrops is reduced, allowing a greater number of smaller droplets to reach higher altitudes, causing additional release of latent heat when they freeze. This increases the stability of the atmosphere. Rosenfeld (1999) and Rosenfeld and Woodley (2000) using aircraft data together with satellite data suggested that in a polluted environment aerosols suppress precipitation by decreasing cloud droplet size. This hypothesis was later confirmed by a modelling study with a cloud resolving model by Khain et al. (2001). In short, in a polluted environment both the first and second aerosol indirect effects lead to a reduction in precipitation (Ramanathan et al., 2001).

Indo Gangetic Plain (IGP) with its unique valley type topography and rapid industrialisation has shown a sustained increase in aerosol burden during the last decade. In addition to regional aerosol loading accumulation of dust aerosols through long distance transport contribute to the concentration of absorbing aerosols in the Northern Indian region. The importance of potential effects of aerosol forcing on clouds and precipitation has been identified in recent years (Lau et al., 2006). Therefore, it is reasonable to analyse the effect of aerosols on the cloud properties and in the onset of precipitation.

5.2. Data description

Monthly mean MODIS (MODerate resolution Imaging Spectroradiometer) data onboard *Terra* and *Aqua* satellites are used to determine the cloud properties and aerosol properties over the chosen location. The data ranges from 2000 to 2010. Here the year 2010 is also considered to include two contrasting years 2009 and 2010 in which 2009 is a drought year where as 2010 a wet year. MODIS monthly data is available in 36 spectral bands from visible to thermal infrared (29 spectral bands with 1 km, 5 spectral bands with 500 m, and 2 spectral bands with 250 m, nadir pixel dimensions). The *Terra* and *Aqua* spacecrafts has an equator crossing time of 10:30 and 13:30 local time respectively. Due to its larger swath widths of MODIS and instrument-scanning angle of 110° a nearly global image is produced (Levy et al., 2003). This sensor measures the land aerosol characteristics using the algorithm based on 'dark target' approach (Kaufman and Sendra, 1988; Kaufman et al., 1997; Remer et al., 2006), therefore does not retrieve over bright surfaces such as snow, ice and deserts. Angstrom exponent, which is a measure of spectral dependence of the aerosol optical depth, is one of the several measures of particle size included in the MODIS product. Angstrom exponent over land is given by

$$\text{Angstrom exponent} = - \frac{\ln(\text{AOD}_{470} / \text{AOD}_{660})}{\ln(470 / 660)} \qquad \ldots(5.1)$$

Where, AOD_{470} and AOD_{660} are the aerosol optical depths at the wavelengths 470 nm and 660 nm respectively. The two wavelengths 470 nm and 660 nm represent the spectral range of AOD retrieval over land. Fine mode aerosol optical depth is another measure of particle size used in this study. It is the aerosol optical depth due to the presence of sub micron particles in the atmosphere and is sometimes referred as accumulation mode aerosol particles.

The aerosol properties are derived by the inversion of the MODIS observed reflectance using pre-computed radiative transfer look-up tables based on aerosol

models (Remer et al., 2005; Levy et al., 2007). The initial versions of the MODIS algorithms have been under continued development, and have recently received an improved aerosol determination, via processing to Collection 5 (C005) Level 3 products (Levy et al., 2007). The C005 Level 3 (spatial resolution of 1°×1°) MODIS products are obtained from Giovanni website (*http://giovanni.gsfc.nasa.gov/*). Through MODIS, simultaneous observations of aerosols in the cloud free and clouds in the cloudy regions are possible (*see http://modis-atmos.gsfc.nasa.gov/*). MODIS retrieves the column aerosol concentration (in cloud free, solar glint free) conditions that is represented as aerosol optical depth (AOD) and cloud properties like cloud optical depth, effective radius, liquid water path and cloud cover.

5.3. Results and discussions

5.3.1. Angstrom exponent and its relation to aerosol size

Angstrom exponent (AE) is a useful quantity to assess the particle size of atmospheric aerosols or clouds. Fig. 5.1 represents the time series variations between total AOD and AE for the years taken into consideration. It can be seen that lower values of AE exists during the southwest monsoon months with minimum during the month of July. By the withdrawal of maritime southwesterly monsoon winds, the AE starts to increase. A secondary minimum is observed during the month of October which is probably due to the transition of maritime winds to continental winds and also due to the near neutral conditions that exists during this reversal of wind patterns. Afterwards due to the prevailing continental wind system the AE values starts to increase indicating the dominance of fine mode aerosol particles in the atmosphere.

High aerosol loading can be found during the monsoon months (June-September) which peak in the month of July due to the influx of large quantities of coarse mode sea-salt aerosols from adjoining oceanic regions. During dry months (October to May) a comparatively lower aerosol optical depth (AOD) is

seen where the ambient air is laden mostly with fine mode aerosols (eg. dust, soot, organic aerosols) when the airmass is continental in nature. These seasonal variations in aerosols are compared with the Angstrom exponent. Large values of AE imply the presence of finer mode aerosols and vice versa. In short, during the monsoon season the total AOD comprises mostly of coarse mode aerosols while fine mode aerosols dominate in the airmass during the dry months.

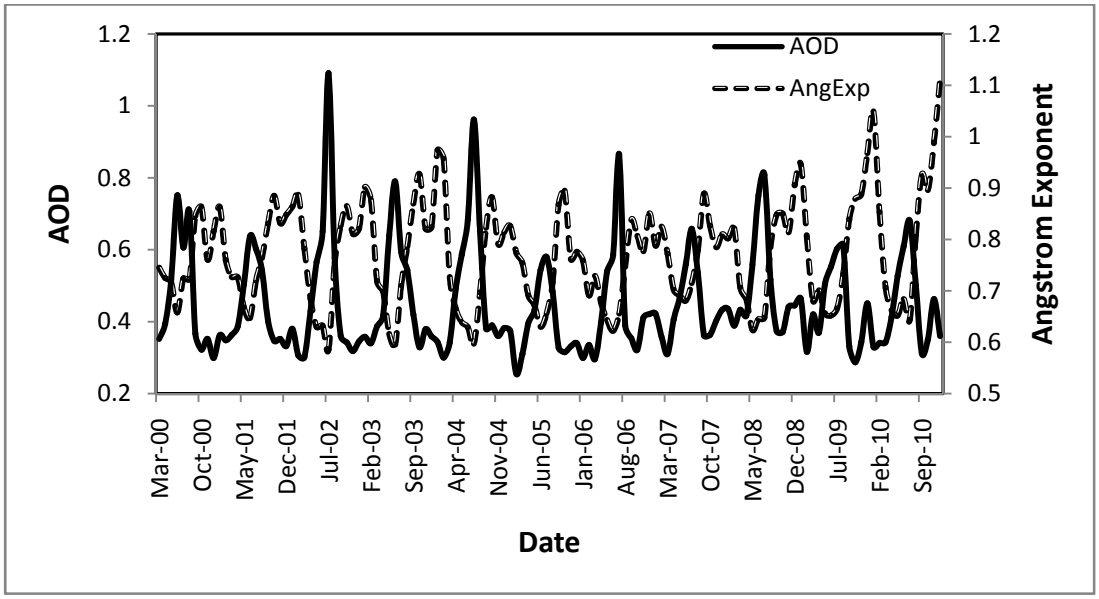

Fig. 5.1. Monthly mean time series between AOD (solid line) and angstrom exponent (broken line) for the years 2000 to 2010

As mentioned before, these fine mode aerosols have the longest life time in the troposphere and act as excellent cloud condensation nuclei (CCN) for the formation of clouds. In industrial cities the fine mode particles consisted largely of ammonium sulphate while coarse particles consisted of mixed nuclei containing a good deal of sulphuric acid or consisted of chlorides. The industrial aerosols generated from the gas to particle conversion of pollutions are a significant contributor of fine mode aerosol particles. The atmospheric aerosols contained in continental air mass are coated with a thin layer of these hygroscopic substances. In moist conditions, these *mixed nuclei* react to humidity changes becoming wholly soluble particles of equivalent size, but at humidities below 70% (like that existing during dry months) the solution coat shrinks until

the particle becomes almost completely solid. This favours the transformation of atmospheric aerosols to be hygroscopic. Therefore, in a polluted environment like that existing over the IGP, such an abundant supply of hygroscopic aerosols will act as CCN for cloud formation.

5.3.2. Aerosol Indirect Effect and its influence on precipitation

5.3.2.1. *First Aerosol Indirect Effect*

Fig 5.2 illustrates the time series analysis between monthly mean values of AOD of fine mode aerosols and cloud effective radius (CER). The top panel gives the time series between AOD (fine mode) and CER for the years 2000 to 2004 and the bottom panel that for the years between 2005 and 2010. The rectangular boxes in both the panels indicate the non-monsoon months (October to May). It can be seen from Fig 5.2 that during the non-monsoon months the AOD shows a higher value compared to that of monsoon months. Associated with this increase in aerosol loading, a decrease in CER is seen. This inverse relationship is more evident after 2002. Aerosol loading peaks in the month of January and thereafter it decreases to a minimum value during the monsoon season. An important factor which has to be noted is that for the years 2002, 2004 and 2009 a high AOD of 0.3 occurred in the months preceding the monsoon season. Consequently a decrease of CER to 11 microns is also noticed. The following monsoon season of all these years was a failure in this region. The drought conditions that prevailed in 2009 enabled the atmospheric aerosol loading in large quantities. A high value of 0.35 in the year 2010, which is the highest in the decade, indicates the high concentration of fine mode aerosols in these months. This resulted in the reduction of CER to 10 microns which is also the least value in the decade. The monsoon season that followed has a deficit of 24% in June rainfall. A decrease in rainfall persisted throughout the monsoon season (June – September) while rest of the country received more than normal rainfall.

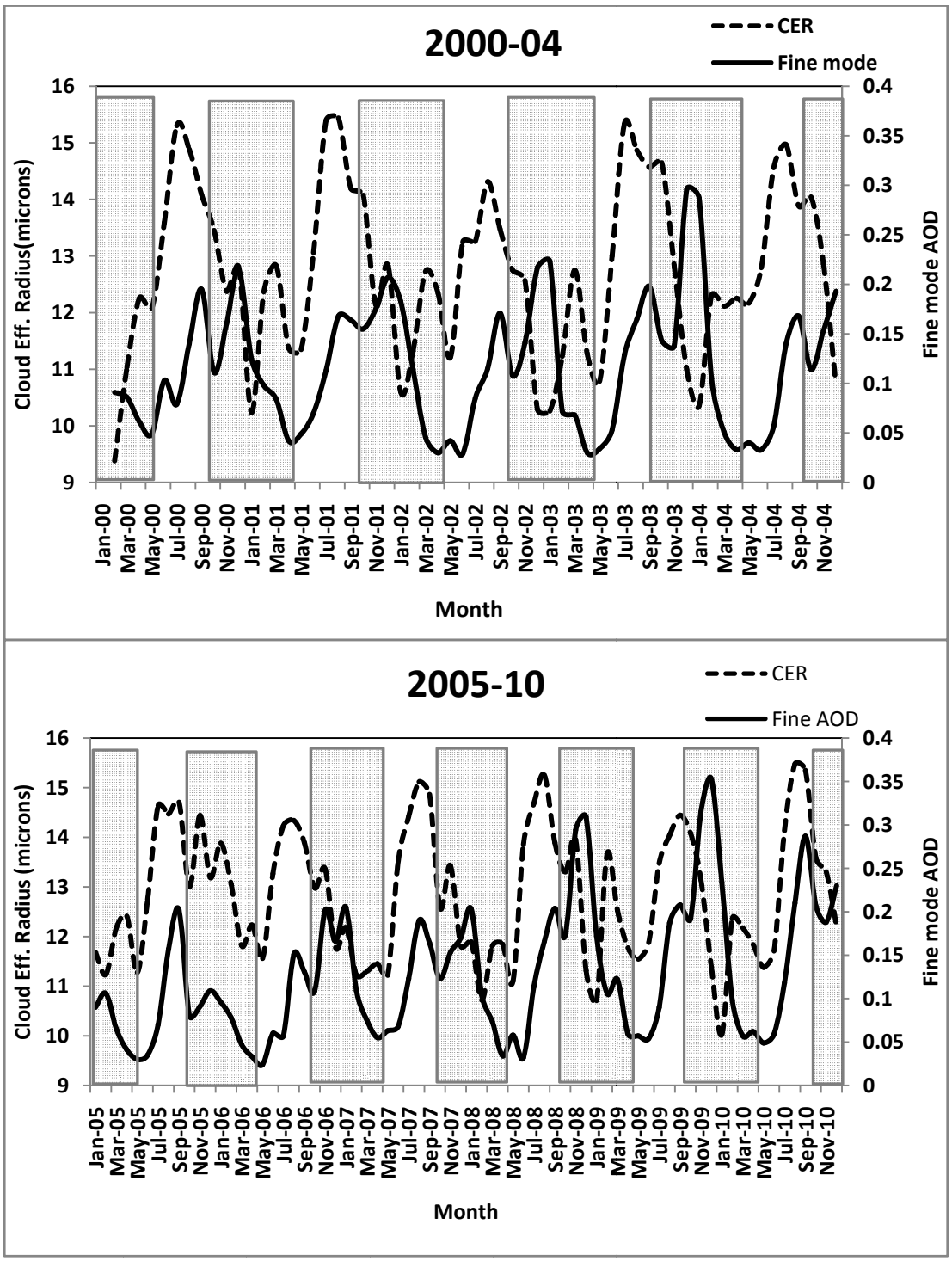

Fig. 5.2.Time series of monthly mean fine mode AOD and CER over the study region. The rectangular boxes indicate the dry months .

The years 2002, 2004, 2009 and 2010 attains significance due to El-Nino conditions that prevailed during the time. Dry season associated with El-Nino is favourable for the production and increases the life time of atmospheric aerosols. This explains the large AOD seen during the time. Moreover, as indicated by

Oceanic Nino Index (*see* Chapter 3, Table 3.1.), severe El-Nino conditions occurred in the non-monsoon months of 2010, which justifies the higher aerosol content in that period.

In the years 2001 to 2010 the CER during May was well below 12 microns. In all these years, even though onset of south west monsoon was either early or normal in southern peninsula, the progress and subsequent onset of monsoon got delayed over North India (*see* Table 5.1.). The normal date of onset over the region is 15th June. This delay in onset was so pronounced in North India that even after an early onset in southern peninsula, the advancement of monsoon towards North India got delayed by two to three weeks. In 2000 and 2004 when CER was above 12 microns, there was a rapid advancement of monsoon circulation towards North India.

Table 5.1. Monsoon onset dates over Kerala and IGP (www.imd.gov.in/section/nhac/dynamic/Monsoon_frame.htm)

Year	**Onset (Kerala)**	**Onset(IGP)**
2000	1-Jun	7-Jun
2001	26-May	17-Jun
2002	9-Jun	20-Jun
2003	13-Jun	20-Jun
2004	3-Jun	15-Jun
2005	7-Jun	23-Jun
2006	26-May	24-Jun
2007	28-May	18-Jun
2008	31-May	12-Jun
2009	23-May	28-Jun
2010	31-May	4-Jul

This signifies that the role of CER in the month of May in determining the progress of monsoon circulation and the onset of monsoon in the region. If second indirect effect is occurring then a decrease in CER should reduce the

precipitation efficiency and it can be postulated that the delay in the onset of monsoon rainfall during these years may be due to this effect.

Fig 5.3 represents the diagram indicating the latitudinal variation of CER. A significant reduction in CER can be observed when there is a dominance of atmospheric fine mode aerosols during the non-monsoon months. This depletion in CER is prominent in the study region compared to the surrounding areas as illustrated in the figure. This distinct characteristic is visible during almost all the years during the dry months.

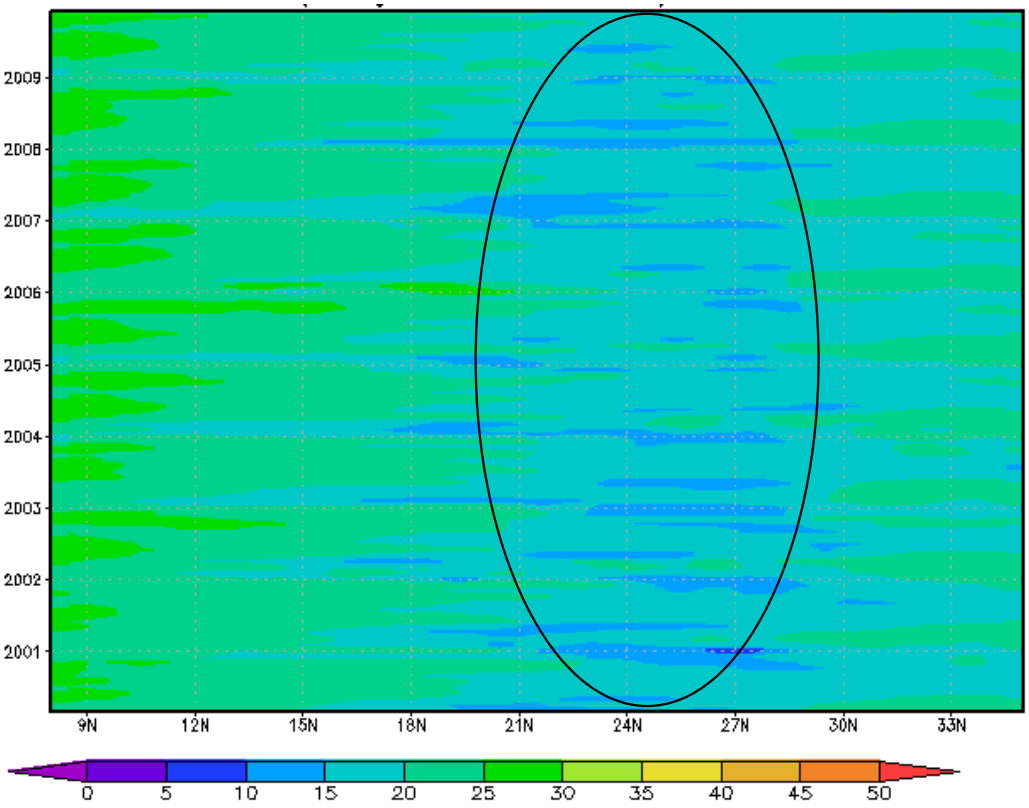

Fig 5.3. Diagram showing the latitudinal variation of CER There area in the ellipse indicates the study region (21^0 N – 29^0 N).

The presence of large quantity of fine mode aerosols contributed by both natural and anthropogenic source caused a decrease in the size of cloud droplets. The difference in aerosol concentration with season is primarily due to the humidity level that exists in the atmosphere and also the size and the nature of the aerosols

on which the water vapour condense. In most of the years this inverse relationship between fine mode aerosols and CER is more pronounced during the months between November and May. During this time the CER varies between 5 to 20 µm with a minimum value of 5 µm seen during the months between January and April.

The CER shifts to the higher values towards the onset of the monsoon season. Statistical analysis shows that during the dry month period, as the fine mode AOD increases from 0.04 to 0.3, the CER decreases by about 38%. These changes were attributed to an increase in hygroscopic aerosols. In the next section, we will examine how a decrease in droplet size has the additional effect of delaying the onset of collision and coalescence in warm clouds, reducing precipitation efficiency and increasing the lifespan and the areal coverage of the cloud.

5.3.1.2. *Second Aerosol Indirect Effect*

Precipitation efficiency in clouds can be identified by means of changes in cloud liquid water path (LWP) with respect to CER. Larger the LWP lesser will be precipitation efficiency (Reid and Hobbs, 1998; Schwartz et al., 2002). Several studies have shown that both LWP and CER change with varying aerosol concentrations (Minnis et al., 1992; Han et al., 1994). Fig 5.4 depicts the scatter plot between and LWP and CER for both non-monsoon months and monsoon months. It is seen that during non-monsoon a decrease in CER results in an increase in LWP. The scatter plot shows that they are anti-correlated with a correlation coefficient of 0.68. During non-monsoon months the clouds present over the region will be optically thinner which is evident from the less LWP values. The LWP values during this season range around 80 gm^{-2}.

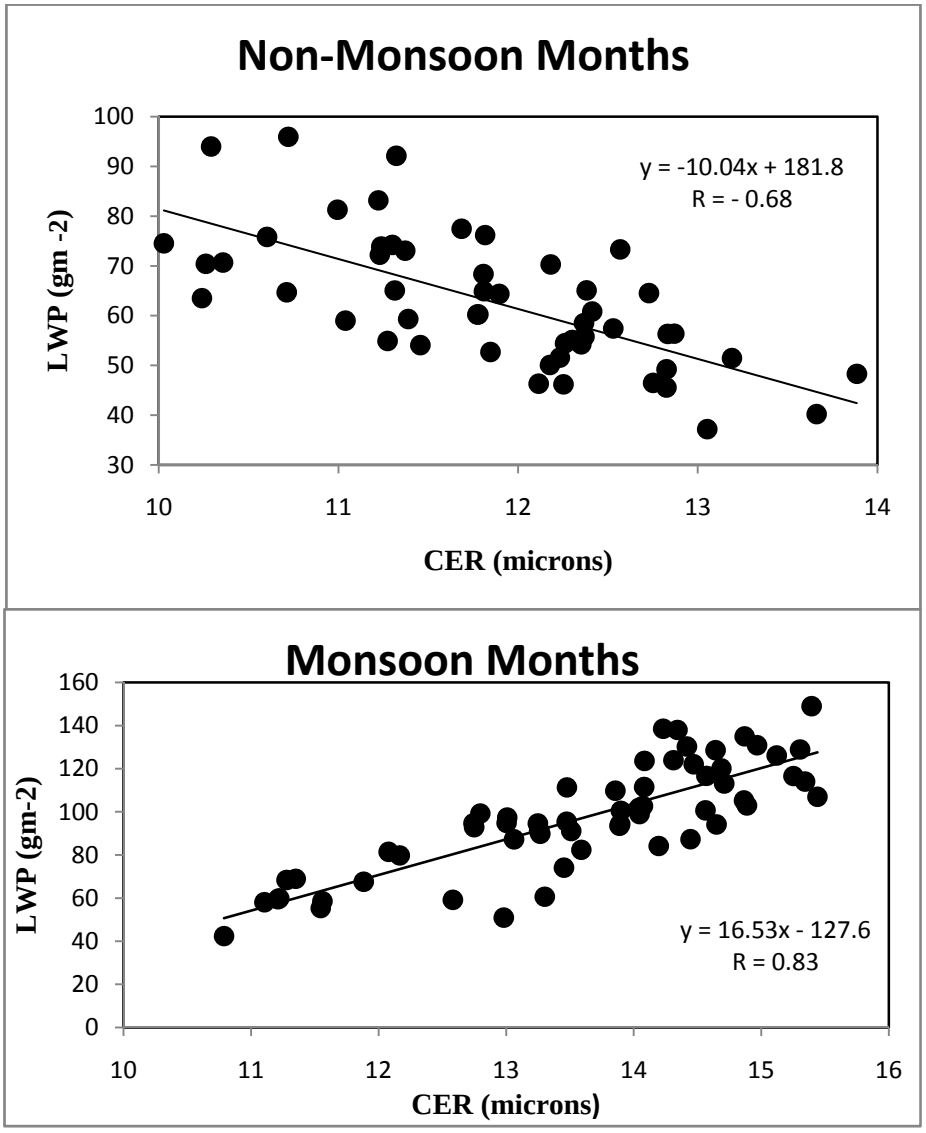

Fig. 5.4 Scatter diagram between LWP and CER for (a) non-monsoon months and (b) monsoon months

For a cloud to precipitate it is required to attain larger value of LWP so as to maintain its precipitation efficiency. When the CER decreases, the drag on the updrafts produced by raindrops gets reduced, allowing a greater number of smaller droplets to reach higher altitudes, causing additional latent heat when they freeze. Therefore the stability of the atmosphere at the lower levels gets increased further inhibiting the possibility of precipitation. Such a condition is more pronounced in a polluted environment such as in IGP. The water droplets that are unable to precipitate remain in the atmosphere, and accounts for the higher water content in clouds.

An increase in water loading in the clouds suggests a reduction in the precipitation efficiency. As a result, when the CER becomes very small (in the range of 10 to 11 microns) there is an appreciable rise in LWP to as high as 80 to more than 90 gm^{-2} . When the cloud drop size increases to 12 microns and above there is a depletion of LWP to below 60 gm^{-2} . Moreover, when size of the cloud droplet increases the water content in the clouds get depleted. In a polluted environment this reduction of LWP is attributed to the entrainment of dry air into clouds resulting in an evaporation of cloud droplets (Ackerman et al., 2004).

In the monsoon season a high positive correlation of 0.83 exists between CER and LWP. It can be reasoned that the positive correlation that exists between LWP and CER during the monsoon season is due to the dominant marine air-mass. In such a state the atmosphere will be predominantly composed of coarse mode aerosol particles. Therefore, as suggested by Rosenfeld et al. (2002), these coarse mode hygroscopic CCN override the precipitation suppression effect of the large number of fine mode aerosols originated from anthropogenic sources. At high concentrations, these large aerosol particles undergo collision and coagulation and may grow to precipitation size by collecting small cloud droplets. Coagulation process is more enhanced when there is fast relative particle motion such as that occurring in shearing or turbulent flows. These types of flows are more frequent in the monsoon season so that it induces increased coagulation rates between particles. Therefore, the coagulation of particles at higher concentrations rapidly reduces the number density of finer mode of aerosols while increasing the droplet size, which explains the higher CER during the monsoon season.

Availability of enormous amount of moisture is another important factor that has to be taken into account during the monsoon season. In this season, the relative humidity (RH) is very high as a result it gives an opportunity for the increase in water vapour condensed upon aerosol particles. Eventually, these particles begin to grow with increasing RH. This growth in particle diameter intensifies the

thickness of cloud mass which is explained by increasing values during the monsoon season. The water holding capacity of the cloud droplet intensifies with the buildup of the LWP and this explains the close association between LWP and CER. Presence of large number of smaller water droplets increases the spatial extend of the clouds. Moreover, as these water droplets become incapable of further growth by accretion process, the weight of the droplet never exceeds the buoyant force. As a result, these droplets cannot fall down in the form of rain. Therefore, the life span of clouds increases.

An increase in aerosol concentration and the resulting increase in cloud droplet number density are expected to increase the cloud optical depth (COD). As explained earlier a reduction in precipitation efficiency also acts to increase water loading, leading to an increase in cloud liquid water path (LWP) and a corresponding increase in cloud thickness, which is clearly illustrated in the scatter diagrams Fig. 5.5 (a) and 5.5(b). The figures shows the Cloud optical depth (COD) and liquid water path (LWP) drawn for the non-monsoon months and monsoon seasons respectively. During both the seasons, LWP shows a strong association with COD. As given in Fig 5.5(a) for the non-monsoon months, the COD values are quite large when the LWP ranges between 60 and 80 gm^{-2}.

When the LWP values are less than 40 gm^{-2} and greater than 80 gm^{-2}; the COD lies below the regression line. The correlation coefficient between COD and LWP during the dry months gives a value of 0.86, which is statistically significant at 99% level. During the monsoon season, the COD and LWP have a very tight association. The magnitudes of LWP and COD are relatively large and the correlation coefficient between these two parameters gives a value of 0.97 which is very highly significant at 99% level.

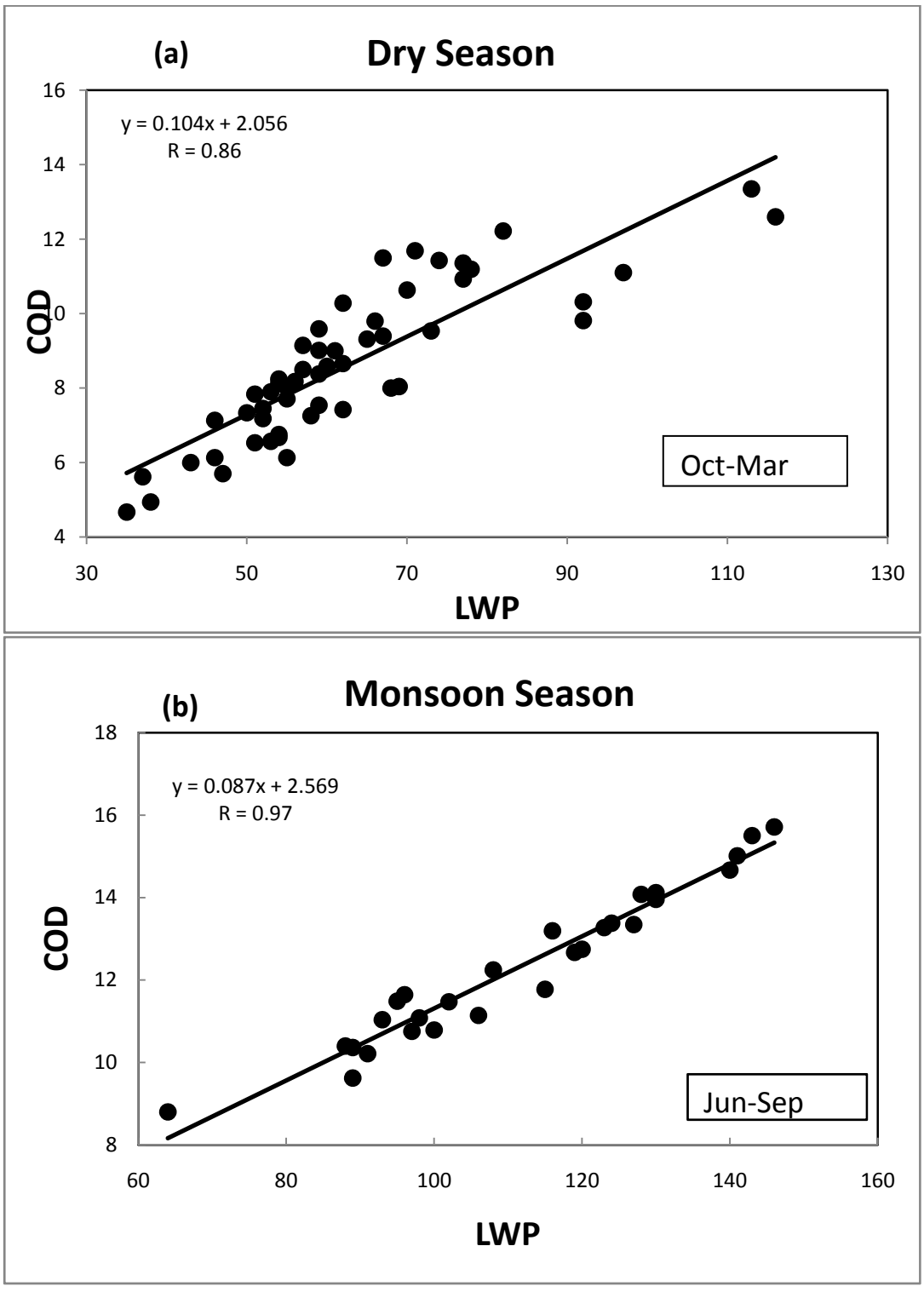

Fig. 5.5 Scatter plots between COD and LWP for (a) dry months and (b) monsoon months

It can be reasoned that the high correlation that exists between COD and LWP during the monsoon season is because during the monsoon season the dominant air-mass will be marine in nature. In such a condition the atmosphere will

predominantly be composed of giant sea-salt nuclei. These coarse hygroscopic sea-salt nuclei override the precipitation suppression effect of the large number of finite aerosols formed as a result of anthropogenic sources.

At high concentrations, these large aerosol particles undergo collision and coagulation and may grow to precipitation size by collecting small cloud droplets. It is the result of particles coming in contact due to *Brownian diffusion* or due to electrostatic force. Therefore, the coagulation of particles at higher concentrations rapidly reduces the number density of finer mode of aerosols while increasing the droplet size. Coagulation process is more enhanced when there is fast relative particle motion such as that occurring in shearing or turbulent flows. These types of flows are more frequent in the monsoon season so that it induces increased coagulation rates between particles.

During the monsoon season the RH is very high so that the nucleation of CCN begins rapidly consuming all of the water vapour in excess of saturation in a cooling (ascending) air parcel and subsequent growth of the particles begin with increasing RH. This growth in particle diameter intensifies the thickness of cloud mass which is explained by increasing trend during the monsoon season. The water holding capacity of the cloud droplet intensifies with the buildup of the COD and this explains the close association between COD and LWP as noted in the Fig 5.5(b). In short, during the monsoon season, an enhanced optical thickness in cloud leads to an increase in LWP in precipitating clouds. Therefore, as reported by Reid et al. (1998) and Scwartz et al. (2002) this increase in water loading in the clouds should lead to a reduction in the precipitation efficiency in the atmosphere.

Thus, the reduction in precipitation efficiency in warm clouds results in extending the lifespan and the areal coverage of the cloud which is also called the *second indirect effect* (Quaas et al. 2004). The combined result of both the first and second indirect effects is to cool the atmosphere (Lohmann and

Feichter, 2005). In the next section, the study aim to analyse if there is indeed a cooling effect due to the aerosol loading in the atmosphere.

5.3.3. Relation between Aerosols and Cloud Cover

Fig 5.6 shows a correlation between fine mode AOD and cloud cover in the non-monsoon months. A high positive correlation can be seen over the land regions than over ocean due to the prevalence of large amount of fine mode aerosol particles that constitutes the continental polluted air mass compared to a pristine airmass over the oceanic regions. Since our objective is to analyse the effect of continental region we focused our study on the aerosol effects on cloud microphysics over the study area. As illustrated in the Fig.5.6 a positive correlation between cloud cover and fine mode AOD occurs over locations in Pakistan, industrialised and urban locations in Punjab, New Delhi, Noida, Lucknow, Allahabad and Kanpur. These regions constitutes majority of the arable land in the country. This increases the propensity of crop waste burning which is the major source of organic aerosols that contribute to aerosol indirect effects.

All the above mentioned places lie in almost the same line and the aerosol concentration appears to be flowing as if through a valley towards the Bay of Bengal. The topography of IGP is such that those aerosols which reach North India by means of long distance transport as well as due to the local anthropogenic processes are funneled to the plains of Ganga towards the Bay of Bengal Sea. By the time it reaches oceanic region, these aerosols have acquired the regional meteorology of these places. It is evident from the figure that cloud micro-properties over the North India are more affected than the peninsular Indian region.

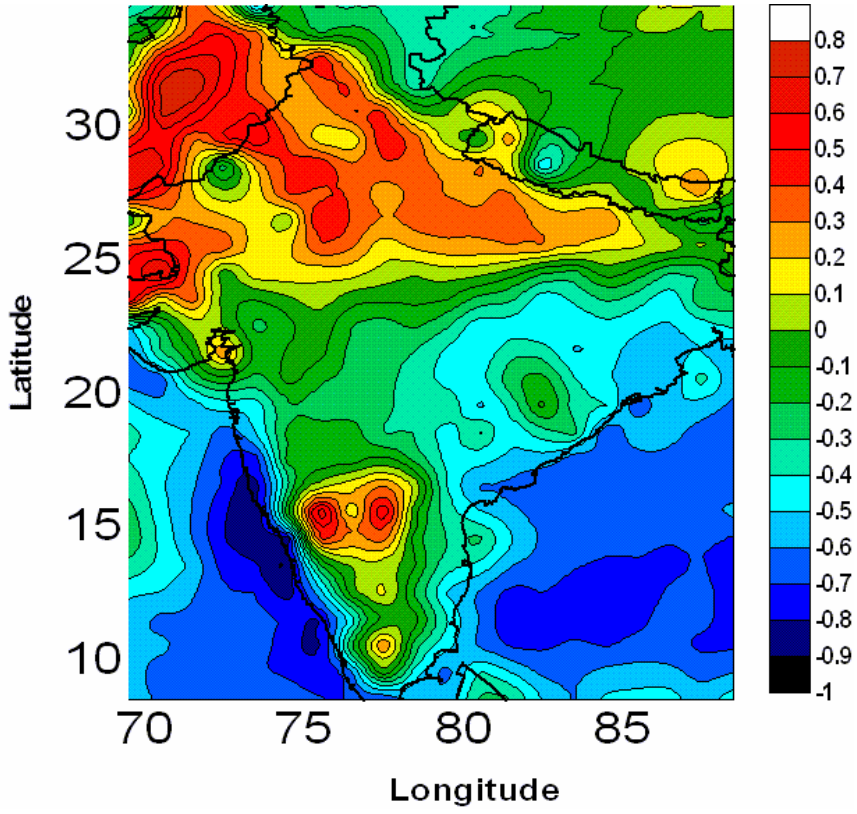

Fig. 5.6. Correlation between fine mode aerosols and cloud cover during the non-monsoon months for the years 2000 to 2010

The sustained aerosol loading that takes place during the non-monsoon months contributes to the cloud formation process in the region. Even though dust aerosols constitutes coarse mode particles, due to long distance transport the coarse particles will get settled easily, while the finer particle which has more life-time in the upper troposphere that continues its journey towards the IGP. During its passage through the atmosphere, these aerosols get internally mixed with sulphates that are hydrophilic. They act as excellent CCN for cloud liquid water droplets resulting in an increase in available CCN for cloud formation. Another possible reason is due to the enhanced biomass burning in dry season after the harvesting season. The precipitation efficiency gets affected by the presence of organic aerosols by delaying the onset of precipitation through slower droplet growth (Reid et al., 1999, Andreae et al., 2004, Mircea et al., 2005). In a polluted environment, this formation will reduce the precipitation efficiency that results in an increase in cloud life time.

In such a condition, the spatial area of clouds increases thereby increasing the cloud albedo and reflecting more solar radiation back into space. This reduction in solar radiation reaching the surface is balanced partially by a reduction in latent heat flux due to evaporation. Reduction in evaporation will have to be compensated by a reduction in rainfall and effectively spin down the hydrological cycle (Koren et al., 2004). Such a perturbation in the dry season, lead to a large regional cooling at the surface accompanied by a warming of the lower troposphere. Therefore the stability of the atmosphere at the lower levels gets increased further inhibiting the possibility of precipitation. These conditions are more pronounced in a polluted environment than in a pristine one. The suppression of rainfall induces a positive feedback mechanism. The drier conditions due to the suppressed rainfall are conducive to raising more dust and smoke from burning of the drier vegetation further enhancing their impacts.

The average life time of the clouds gets enhanced and therefore spatial coverage and optical thickness of the cloud gets proliferated which is evident from the high correlation that exists between AOD and cloud coverage over the urban and industrialised locations in North India that includes IGP. Therefore, the analysis reveals that pollution aerosols present at major urban areas and industrialised facilities like power plants causes a reduction in cloud drop size and suppressed precipitation. This further increases the areal extent and life time of clouds. Together these processes might affect the hydrological cycle and the dynamics of atmospheric circulation.

As the cloud life time increases, the spatial coverage and cloud thickness increases so that most of the solar radiation incident on it gets reflected back to space, thereby decreasing the amount of solar radiation reaching the surface of the Earth. As a result the Earth's surface gets cooled. Fig. 5.7 shows a linear fit between surface air temperature and fine mode aerosols.

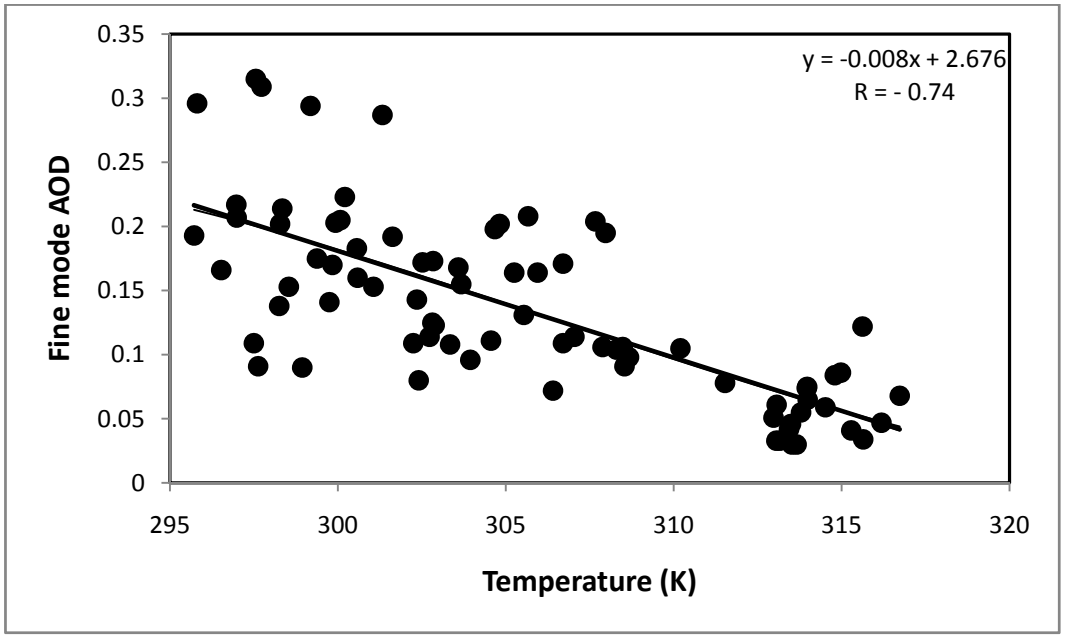

Fig. 5.7. Scatter plot between fine mode AOD and surface temperature indicating a negative relation. Increase of fine more aerosols reduces the surface air temperature.

The best fit gives an inverse relationship between fine mode AOD and temperature which suggests that as the AOD increases the surface temperature decreases. The correlation analysis shows that fine mode AOD and surface air temperature are negatively correlated by a factor of 0.74 which is significant at the 0.01 level of confidence. The *coefficient of determination*, r^2 which is 0.55 gives the proportion of the variance (fluctuation) of temperature for an increase in AOD. From the regression equation, 55% of the total variation in surface temperature can be explained by the linear relationship between fine mode AOD and the surface temperature. From these results, it is seen that the effect of fine mode aerosols on surface temperature is significant and its coefficient being negative indicates that greater the proportion of fine mode aerosols in the atmosphere, lower will be the surface temperature with every 1% increase in fine mode AOD result in a decrease of 0.02^0 K in surface air temperature.

Therefore, the analysis reveals that as the amount of fine mode aerosol increases in the atmosphere there is a fall in surface temperature. These findings are corroborating well with the *Twomey theory* and show that over the continental location, a buildup of fine mode aerosols leads to enhanced cloud droplet

concentrations of smaller size, which increases cloud optical depth and albedo, inducing a negative effect on surface air temperature.

5.4. Conclusions

During non-monsoon months there is indeed a decrease in CER with increase in aerosol concentration which is in accordance with well known *Twomey effect.* Fine mode aerosols which are present in large quantities during these months are responsible for the inverse relationship existing between these two parameters. This inverse relationship is more prominent in the non-monsoon months of the years 2002, 2004, 2009 and 2010 for which El-Nino conditions occurred. The pre-monsoon seasons of 2004, 2009 shows an abnormal rise in fine mode AOD to 0.3. A subsequent reduction in CER has caused more than 19% deficient rainfall in the following monsoon season.

It is seen that in the month of May, when the CER diminished below 12 microns, there is a delay in advancement and onset of monsoon over North India even after a normal or early onset over southern peninsula. However, in the same time when CER was above 12 microns, there is a rapid advancement of monsoon towards the region. Prior to the monsoon season, intense loading of aerosols has resulted in a diminution of CER to as low as 10 microns. Highest AOD in the last decade was recorded in the year 2010 resulting in a diminution of CER to its least value. Subsequently, there has been a deficiency of 24% in June rainfall alone and monsoon was a failure in the entire season over the region while rest of the country received above normal rainfall. These results signify that enhanced aerosol during the dry months and the resulting change in CER prior to the south west monsoon season has an impact on the monsoon circulation in the region.

Moreover LWP and CER exhibit an inverse correlation of 0.68 during non-monsoon months, while high positive correlation of 0.83 existed during monsoon months. Therefore, a change in cloud particle size has affected the precipitation efficiency in the clouds. These results show that *second indirect effect* indeed occurs and a decrease in CER affects the onset of precipitation in clouds. The

decreased precipitation efficiency has in fact increased the areal coverage and thickness of the clouds.

The cloud coverage due to the ambient fine mode aerosol accumulation was more in the industrialised and urban location over North India when compared to other parts of the country. The analysis reveals that due to an increase in fine mode aerosols cooling of the surface occurs. It suggests a decrease of 0.02^0 K in surface air temperature for every 1% increase in fine mode AOD. The cooling of the surface air temperature certainly affects the vertical temperature profile of the atmosphere. More studies are required to understand the changes in circulation patterns as well as on cloud formation due to aerosol induced cooling effects.

CHAPTER 6

TIME SERIES ANALYSIS AND FORECASTING USING THE STATISTICAL MODEL ARIMA

6.1. Introduction

A time series is a sequence of observations ordered in time. A basic assumption in the time series analysis or modeling is that some aspects of the past pattern will continue to remain in the future. The main advantage of the time series models is that they can be used more easily for forecasting purposes because historical sequences of observations on study variables are readily available. These successive observations are statistically dependent and time series modeling is concerned with techniques for the analysis of such dependencies. Thus in time series models the predictions of future values are considered to be based on pattern of past values of the variable under study. These properties of time series models are used to predict the future values of fine mode AOD and CER. Based on the analysis given in chapter 5 it can be seen that these two parameters exhibit a definite seasonal pattern and there exists a close association between these two parameters that exerts an indirect effect on climate in the region. In this context time series forecasting approach is useful in predicting future values of AOD and CER.

Several statistical models are used for time series analysis and forecasting. One of time series models which is popular and mostly used is Box-Jenkins Autoregressive Integrated Moving Average (ARIMA) model (Box et al., 1994). Based on Wei (2006), autoregressive (AR) model shows that there is a relation between a value in the present (Z_t) and values in the past (Z_{t-k}), added by random

value. Moving average (MA) model shows that there is a relation between a value in the present (Z_t) and residuals in the past (a_{t-k} with k = 1,2,…). ARIMA (p,d,q) model is a mixture of AR(p) and MA(q), with a non-stationery data pattern where p is the number of autoregressive terms, q the number of lagged forecast errors in the prediction equation and d differencing order.

6.2. Methodology

6.2.1. Description of Box-Jenkins ARIMA model

Monthly mean AOD and CER datasets covering the periods of 2000 to 2010 acquired from *Terra* and *Aqua* are used in the study. The Box-Jenkins ARIMA model was used to model the time series pattern to generate the forecasting trend. ARIMA as mentioned earlier is an acronym for Autoregressive Integrated Moving Average, with each term representing steps taken in the model construction until only random noise remains. The methodology consisting of a four-step iterative procedure was used in this study. The first step is the identification, where the historical data were used to identify an appropriate Box-Jenkins model. It is followed by estimation of the parameters of the tentatively identified model. After that, the diagnostic checking step must be executed to check the adequacy of the identified model in order to choose the best model. A better model should be identified if the model is inadequate. Finally, the best model is used to establish the time series forecasting value. The description on the model and the steps involved in selecting the model are given as follows.

Each term in ARIMA model describes the steps taken in the model construction. The first term represents an autoregressive (AR) part of model of the order p having the form of

$$Z_t = \rho_1 Z_{t-1} + \rho_2 Z_{t-2} + \cdots + \rho_p Z_{t-p} + \varepsilon_t \qquad \ldots(6.1)$$

Each AR term corresponds to the use of a lagged value of the residual in the forecasting equation for the unconditional residual. The term 'autoregressive' refers to the fact that this model expresses the current time series values z_t as a function of past time series values z_{t-1}, z_{t-2},...,z_{t-p}. The ρ_1, ρ_2,…., ρ_p are unknown parameters relating z_t to z_{t-1}, z_{t-2}, ...,z_{t-p}. A moving average forecasting model uses lagged values of the forecast error to improve the current forecast. A first-order moving average term uses the most recent forecast error; a second-order term uses the forecast error from the two most recent periods and so on.

The moving average term MA(q) term of the model can be represented as,

$$Z_t = \varepsilon_t - \theta_1\varepsilon_{t-1} - \theta_2\varepsilon_{t-2} - \ldots - \theta_q\varepsilon_{t-q} \qquad \ldots(6.2)$$

Where, $\varepsilon_{t-1},\varepsilon_{t-2},$ ……,ε_{t-p} are the past random shocks θ_1, θ_2 ……..θ_q are the unknown parameters relating z_t to $\varepsilon_{t-1},\varepsilon_{t-2},$ ……,ε_{t-p}.

The autoregressive and moving average specifications are combined together with integration(differencing) term to from an ARIMA model characterized by the notation ARIMA(p,d,q) where p, d and q denote orders of autoregression, differencing and moving average respectively. This model is a dependent time series is defined as a linear combination of its own past values and the past error values. Given a dependent time series Z_t: $1 \leq t \leq n$, mathematically the ARIMA model is written as

$$(1-B)^d Z_t = \mu + \frac{\theta(B)}{\phi(B)}\alpha_t \qquad \ldots(6.3)$$

Where *t* denotes the time indexes, μ is the mean, *B* the backshift operator; *i.e.*, $B\,Z_t = Z_{t-1}$. The terms $\phi(B)$ and $\theta(B)$ are the autoregressive and the moving average

operators respectively. They are represented as a polynomial in the back shift operator in which $\phi(B)$ and $\theta(B)$ can be shown as

$$\phi(B) = 1 - \phi_1 B - \cdots - \phi_p B^p \quad \ldots(6.4)$$

and

$$\theta(B) = 1 - \theta_1 B - \cdots - \theta_q B^q \quad \ldots(6.5)$$

Each parameter in the model is tested to determine whether it is zero (null hypothesis, H_o) or different from zero (alternative hypothesis, H_1). If the t >1.96, we can reject H_o: $\theta_1 = 0$ in favor of H_1: $\theta_1 \neq 0$ by setting α equal to 0.05.

6.2.2. Model Identification

The first consideration of the data that are used is to determine whether the time series data is stationary or non-stationary. A time series is said to be stationary if it has a constant mean and variance with its autocorrelation function (ACF) essentially constant through time. Autocorrelation function refers to the way the observations in a time series are related to each other and is measured by the simple correlation between current observation (z_t) and observation from *p* periods before the current one (z_{t-p}). The value of ACF ranges from -1 to +1. If the *n* values fluctuate with constant variation around a constant mean μ, it shows that the time series is stationary. The stationary time series value z_t, z_{t+1}, …, z_n can be determined through the behavior of the ACF. If the stationary condition is achieved, then the different subset of the time series sample will typically have means, variance and auto correlation functions that do not differ significantly.

If the data are not stationary, a differencing process should be performed until an obvious pattern such as a trend or seasonality in the data fades away. The first differences of a non-stationary time series value y_1, y_2,…y_n are described as $z_t = y_t - y_{t-1}$ where t = 2,…, n. If the differences of a time series are still not stationary, the second differences should be implemented. The second differences of time series value y_1,y_2, …y_n are $z_t = y_t - 2y_{t-1} + y_{t-2}$ for t = 3, 4, ..., n.

6.2.3. Model parameter estimation

The ACF and partial autocorrelation function (PACF) of the stationary data was examined to identify the autoregressive or moving average terms to be suggested. Partial autocorrelation function is used to measure the degree of association between z_t and z_{t-p} when the z effects at other time lags 1,2,3,…,p-1 are removed.

The ACF at lag *k*, denoted by ρ_k , is defined as

$$\rho_k = \frac{\gamma_k}{\gamma_0} \qquad \ldots(6.6)$$

Where γ_k is the covariance at lag *k* and γ_0 the variance.

Since both covariance and variance are measured in the same units, ρ_k is a unitless and lies between -1 and +1. An ACF with large spikes (spikes refers to lines at various lags in the plot with length equals to the magnitude of the autocorrelations) at initial lags that decays to zero or a PACF with a large spike at the first and possibly at the second lag indicates an autoregressive process. An ACF with a large spike at the first and possibly at the second lag and a PACF with large spikes at initial lags that decay to zero indicate a moving average process. If both the ACF and PACF exhibiting large spikes that gradually die out, this indicates both autoregressive and moving averages processes.

6.2.4. Seasonal ARIMA model (SARIMA):

Seasonality is defined as a pattern that repeats itself over fixed interval of time. In general, seasonality can be found by identifying a large autocorrelation coefficient or large partial autocorrelation coefficient at a seasonal lag. Often, autocorrelation at multiples of the seasonal lag will also be significant, such as at lag 24 or even lag 36. The seasonal differencing is the difference between an observation and the corresponding observation from the previous year. It used to obtain the stationary seasonal time series data, $z_t' = z_t - z_{t-s}$. The seasonally differenced series, z_t, is the change between observations separated by s time periods, where *s* is the number of seasons. For monthly data, *s* = 12, for quarterly data, *s* = 4 and so on. For the seasonal model, the minimum Akaike Information Criterion (AIC) and Schwarz Bayesian Criterion (SBC) were considered to select the ARIMA model (Akaike, 1974). The AIC is a combination of two conflicting factors: the mean square error and the number of estimated parameters of a model. Generally, the model with smallest value of AIC and SBC is chosen as the best model.

The seasonal ARIMA or ARIMA (p,d,q) (P,D,Q)s model is defined by

$$\Phi_p(B^s)\varphi_p(B)\,\nabla^d\,\nabla^D Z_t = \Theta_Q(B^s)\,\theta_q(B)\,\varepsilon_t \qquad \ldots(6.7)$$

Where,

$\Phi_p(B^s) = 1 - \Phi_1 B^s - \Phi_2 B^s - \ldots\ldots - \Phi_p B^{sp}$; $\Theta_Q(B^s) = 1 - \Theta_1 B^s - \ldots\ldots\ldots - \Theta_Q B^{sQ}$

$\varphi_p(B) = 1 - \varphi_1 B - \ldots\ldots - \varphi_p B^p$; $\theta_q(B) = 1 - \theta_1 B - \ldots\ldots\ldots - \theta_q B^q$

B is the backshift operator (*i.e.*, $Bz_t = z_{t-1}$, $B^2 y_t = z_{t-2}$ and so on), *s* the seasonal lag and ε_t a sequence of independent normal error variables with mean 0 and variance σ^2. Φ

and φ are the seasonal and non-seasonal autoregressive parameters respectively. Θ and θ are the seasonal and non-seasonal moving average parameters respectively. The orders of non-seasonal auto regression and moving average parameters are given by p and q respectively whereas P and Q are that of the seasonal and auto regression and moving average parameters respectively. Also d and D denote non- seasonal and seasonal differences respectively.

6.2.5. Diagnostic Stage

Once the parameters are statistically estimated, before forecasting the series, it is necessary to check the adequacy of the tentatively identified model. The model is declared adequate if the residuals cannot improve the forecast any more. In other words, the residuals are random. To check the overall model adequacy, the following diagnostics are done.

6.2.5.1 Plot of residual ACF

Once the appropriate ARIMA model is fitted, one can examine the goodness of fit by means of plotting the ACF of residuals of the fitted model. If most of the sample autocorrelation coefficients of the residual are within the limits $\pm \frac{1.96}{\sqrt{N}}$, where N is the number of observations upon which the model is based then residuals are white noise indicating that the model is a good fit.

6.2.5.2. Box- Pierce or Ljung-Box tests

After tentative model has been fitted to the data, the overall model adequacy is checked by analysis of residuals. The Box-Pierce statistic (a function of autocorrelations of residuals) is employed to check the randomness of residuals which follows the Chi-square distribution and is expressed as:

$$Q = n \Sigma r^2(j) \quad ...(6.8)$$

Where *n* is the number of observations in the series, *r (j)* the estimated autocorrelation at lag *j*. Q follows Chi-square with *(k-m)* degrees of freedom where *k* is the maximum lag considered, *m* the number of parameters estimated in the model. A modified Q statistic is the Ljung-box statistic which is given by

$$Q = n(n+2) \sum \frac{r^2(j)}{(n-j)} \quad \ldots(6.9)$$

If the chosen model fits well, then residuals should be uncorrelated, insignificant and Q should be small. Apart from these two conditions, low Akaike Information Criteria (AIC)/ Bayesian Information Criteria (BIC)/ Schwarz-Bayesian Information Criteria (SBIC) indicate that the selected model has a good fit.

6.2.5.3. Forecasting

Once the model adequacy is established the series in question shall be forecasted for specified period. It is always good to keep track on the forecast errors and depending on the magnitude of errors, the model can be re-evaluated. The forecast thus obtained is provided at an upper and lower confidence interval of 95%. Any forecasted values within this confidence limit are satisfactory. Finally, the accuracy of the model is checked with the mean square error (MS) to compare fits of different ARIMA models. A lower MS value corresponds to a better fitting model.

6.3. Results and Discussion

6.3.1. ARIMA model forecasting for AOD

A seasonal autoregressive integrated moving average (ARIMA) model has been selected to predict the future values of fine mode AOD. The monthly mean fine mode AOD data from February 2000 to December 2010 obtained from MODIS is used in the present analysis. The data consist of 131 observations with no missing values. The seasonality of the observed data series is clearly evident from the plot of ACF and PACF (Fig. 6.1(a) and 6.1(b)) respectively. The first step in identification of an appropriate ARIMA model is by examining the patterns in the ACF and PACF plots.

In Fig 6.1(a), the seasonal autocorrelation relationships are shown prominently. Strong correlation appears at lags 6, 12 and so on. It is readily seen that AOD series provides an ACF that is slowly declining sinusoidal wave. At the non-seasonal levels, the ACF has significant spikes at lag 1 and 2 and cuts off after that. Therefore the series is considered as non-stationary. Since the series is non-stationary, the next step is to transform it to a stationary series by taking 12 month differencing of data to remove seasonal influence.

In Fig 6.1(b), it is seen that the PACF has significant spike at lag 1 and tails off after lag 1. At the seasonal level, the ACF and PACF have significant spikes at lag 12 and 13 and cuts off after that. Hence the orders of non-seasonal auto regression and moving average parameters denoted by p and q are 1 and 2 respectively whereas order of the seasonal and auto regression and moving average parameters P and Q are 2 and 2 respectively. Also the seasonal difference D is equal to 1.

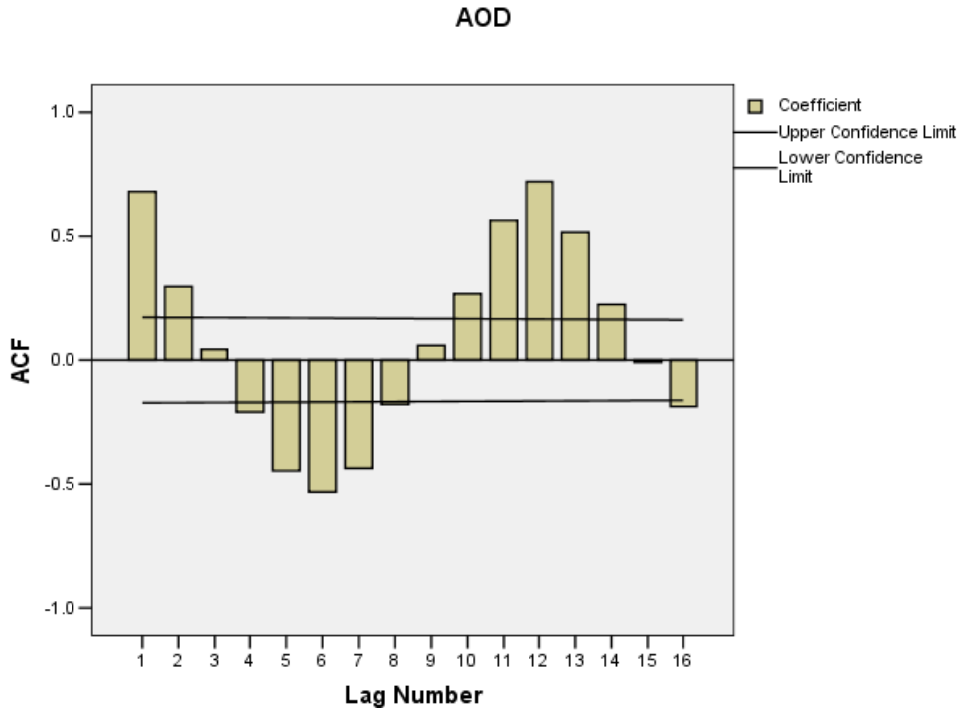

Fig. 6.1(a) Autocorrelation function (ACF) for AOD

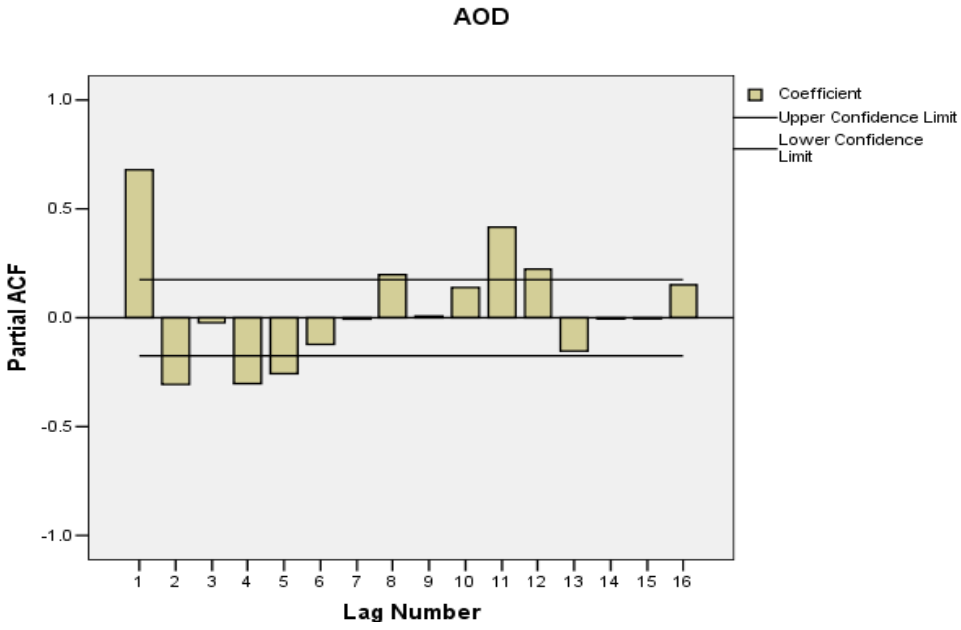

Fig. 6.1(b) Partial Autocorrelation function (PACF) for AOD

The parameters for the ARIMA(1,0,2)x$(2,1,2)_{12}$ are estimated using the *SPSS* statistical package. The maximum likelihood estimates of the parameters are given in Table 6.1. The coefficients of estimates are highly significant at 99% confidence level. If the model fits well, the standardized residuals from this model should be white noise.

Table 6.1. Parameter Estimates for the ARIMA(1,0,2)x$(2,1,2)_{12}$

Parameter	Estimate	Std. Error	t
AR(1)	1.00	0.005	183.60**
MA(1)	0.40	0.085	4.68**
MA(2)	0.46	0.084	5.51**
SAR(1)	0.73	0.081	9.00**
SAR(2)	-0.55	0.080	-7.2**
SMA(1)	1.64	0.045	32.8**
SMA(2)	-0.70	0.045	-15.62**

** Significance at 1% level

The model for forecasting AOD using ARIMA (1, 0, 2) x $(2, 1, 2)_{12}$ can be written as

$$(1 - B^{12})Z_t = \frac{(1-\theta_1 B-\theta_2 B^2)(1-\Theta_{12}B^{12}-\Theta_{24}B^{24})}{(1-\varphi_1 B)(1-\emptyset_{12}B^{12}-\emptyset_{24}B^{24})}\epsilon_t \quad \ldots (6.10)$$

The Fig 6.2 shows the estimated autocorrelations between the residuals at various lags using ARIMA (1, 0, 2) x $(2, 1, 2)_{12}$. The lag *k* autocorrelation coefficient measures the correlation between the residuals at time t and time *t-k*. Also shown are 95% probability limits around 0. If the probability limits at a particular lag do not contain the estimated coefficient, there is a statistically significant correlation at that lag at the

95% confidence level. In this case, none of the 24 autocorrelations coefficients are statistically significant, implying that the time series may well be completely random (white noise). If the series is white noise, then it follows Box-Pierce statistic (Q-statistic) whose approximate distribution is Chi-square and the selected forecast model has a good fit.

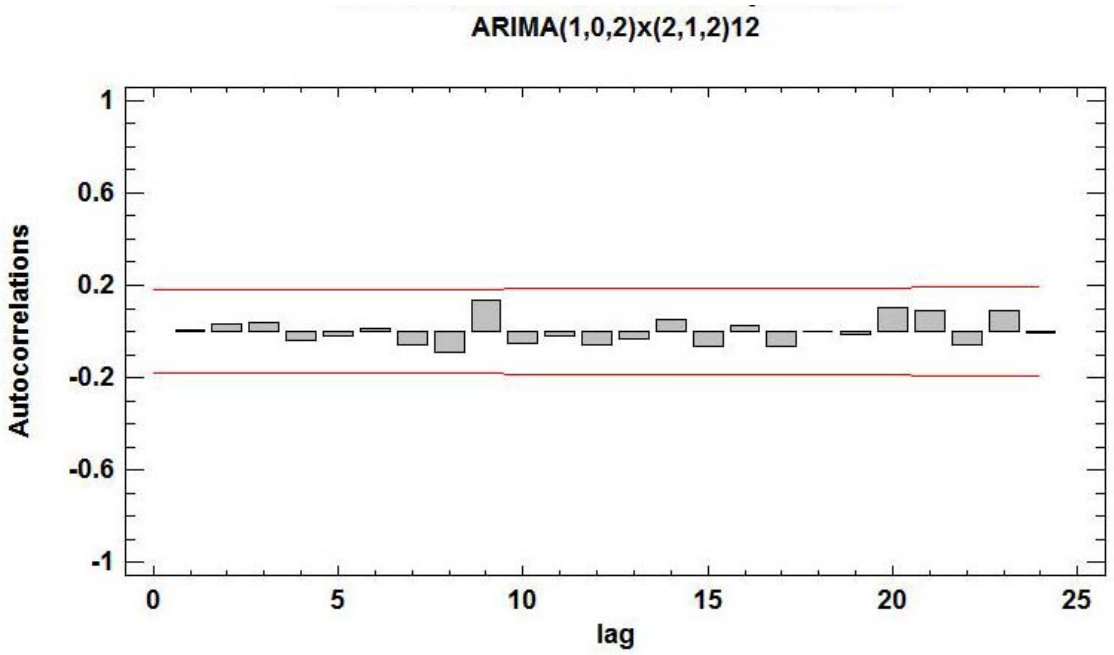

Fig.6.2 Estimated autocorrelation function between residuals for fine mode AOD at various lags. The ACF indicates that time series follows white noise model.

The Fig 6.3 shows the estimated partial autocorrelations between the residuals at various lags. The lag *k* partial autocorrelation coefficient measures the correlation between the residuals at time *t* and time *t+k* having accounted for the correlations at all lower lags. It can be used to judge the order of autoregressive model needed to fit the data. Also shown are 95% probability limits around 0. If the probability limits at a particular lag do not contain the estimated coefficient, there is a statistically significant correlation at that lag at the 95% confidence level. In this case, none of the 24 partial autocorrelations coefficients is statistically significant at the 95% confidence level.

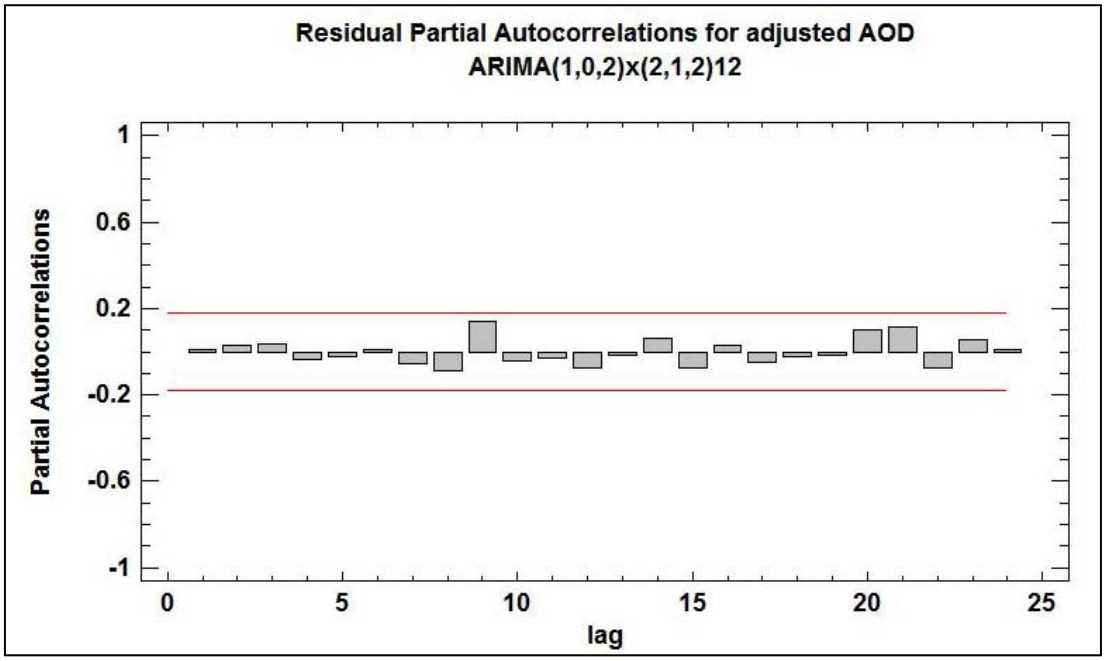

Fig.6.3 Estimated partial autocorrelation between residuals for fine mode AOD at various lags. The residuals are within the probability limits

Other statistics illustrated in Table 6.2 are (1) The root mean squared error (RMSE); (2) the mean absolute error (MAE); (3) the mean absolute percentage error (MAPE); (4) the mean error (ME) (5) the mean percentage error (MPE)

Table 6.2. ARIMA forecast summary

Statistic	**Estimation Period**
RMSE	0.031
MAE	0.022
MAPE	21.847
ME	0.002
MPE	-4.00

Each of the statistics is based on the one-ahead forecast errors, which are the differences between the data value at time *t* and the forecast of that value made at time *t-1*. The first three statistics measure the magnitude of the errors. A better model will give a smaller value. The last two statistics measure bias. A better model will give a value close to 0.

6.3.1.1. Model Comparison

The following gives the models used for comparison and the estimates based on RMSE, MAE, MAPE, ME, MPE, Akaike Information Criterion (AIC), SBIC and HQC. The Table 6.3 compares the estimation parameters of fitting different models to the data. The model with the lowest value of the Akaike Information Criterion (AIC) is model I, which has been used to generate the forecasts.

6.3.1.2. Models

(A) Random walk
(B) Random walk with drift = 0.00014
(C) Constant mean = 0.12
(D) Linear trend = 0.11 + 0.00024 t
(E) Simple moving average of 2 terms
(F) Simple exponential smoothing with alpha = 0.2
(G) Brown's linear exp. smoothing with alpha = 0.1
(H) Holt's linear exp. smoothing with alpha = 0.2 and beta = 0
(I) ARIMA(1,0,2)x(2,1,2)12
(J) ARIMA(1,0,0)x(2,1,2)12
(K) ARIMA(1,0,1)x(2,1,2)12
(L) ARIMA(2,0,2)x(2,1,2)12
(M) ARIMA(2,0,0)x(2,1,2)12

Table 6.3. Comparison of estimation parameters of different models fitted to the data

Model	RMSE	MAE	MAPE	ME	MPE	AIC	HQC	SBIC
(A)	0.0371	0.0262	24.201	-0.00046	-4.52	-6.41	-6.31	-6.17
(B)	0.0373	0.0262	24.207	-0.00059	-4.64	-6.39	-6.28	-6.13
(C)	0.0401	0.0263	24.300	-0.00068	-8.38	-6.24	-6.14	-5.98
(D)	0.0377	0.0246	23.184	-0.00096	-7.89	-6.35	-6.23	-6.06
(E)	0.0369	0.0257	22.463	-0.00102	-4.90	-6.41	-6.30	-6.14
(F)	0.0341	0.0241	21.317	-0.00049	-5.36	-6.57	-6.46	-6.30
(G)	0.0352	0.0249	21.884	-0.00141	-5.83	-6.50	-6.40	-6.24
(H)	0.0342	0.0243	21.219	0.00139	-3.53	-6.54	-6.43	-6.26
(I)	0.0306	0.0222	21.846	0.00177	-4.00	-6.86	-6.80	-6.71
(J)	0.0312	0.0224	21.546	0.00190	-4.24	-6.85	-6.81	-6.74
(K)	0.0312	0.0225	21.708	0.00207	-4.11	-6.83	-6.78	-6.70
(L)	0.0308	0.0224	21.663	0.00271	-2.84	-6.83	-6.76	-6.65
(M)	0.0314	0.0226	21.767	0.00180	-4.41	-6.82	-6.77	-6.69

The Table 6.4 shows the forecasted values for AOD. During the period where actual data is available, it also displays the predicted values from the fitted model and the residuals (data-forecast). For time periods beyond the end of the series, it shows 95% prediction limits for the forecasts. These limits show where the true data value at a selected future time is likely to be with 95% confidence, assuming the fitted model is appropriate for the data. A graph plotted using the values given in table are shown in Fig. 6.4. The figure shows the actual and fitted values for AOD using the ARIMA(1,0,2)x$(2,1,2)_{12}$ model. The figure also depicts the forecasts and 95% forecast limits for a lead time of 12 months for the AOD series.

Table. 6.4 Forecast for AOD

Month	Forecast	Lower 95.0% Limit	Upper 95.0% Limit
Jan-11	0.22	0.16	0.28
Feb-11	0.14	0.06	0.21
Mar-11	0.08	0.01	0.15
Apr-11	0.08	0.01	0.15
May-11	0.07	-0.001	0.15
Jun-11	0.1	0.02	0.17
Jul-11	0.13	0.05	0.21
Aug-11	0.19	0.11	0.26
Sep-11	0.23	0.15	0.31
Oct-11	0.14	0.07	0.22
Nov-11	0.12	0.04	0.19
Dec-11	0.18	0.1	0.26

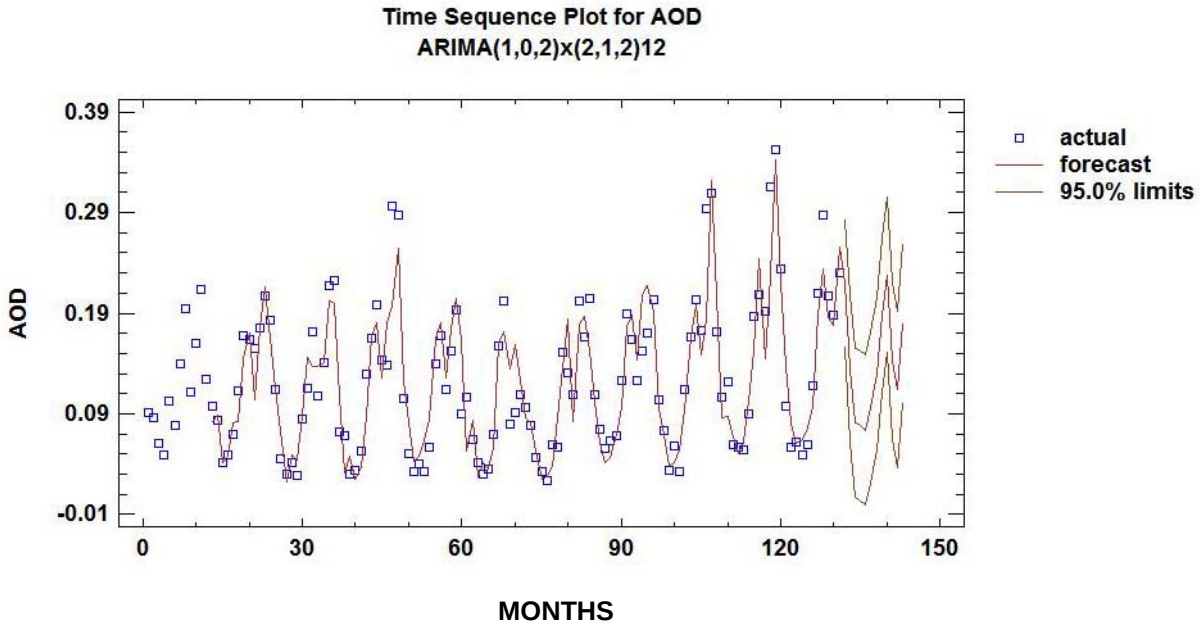

Fig. 6.4. Time series plot showing the actual and model output values. The forecast values till December 2011 is shown at 95% confidence level.

The Fig 6.4 shows that the forecasts mimic the periodicity in the data quite well, and the forecast limits give the precision of the forecasts. The actual values it up to December 2010. The forecasts are made further for 12 months i.e. till December 2011 at 95% confidence level. The forecasted value shows a peak AOD value of about 0.22 and thereafter it decreases.

6.3.2. ARIMA model forecasting for CER

The procedure to determine forecast future values of CER are as follows. The observed datasets cover 131 time periods with no missing values. From the plots of ACF and PACF in Fig 6.5(a) and 6.5(b) clearly shows the seasonality of the data. As a first step towards model identification it is required to do differencing to make the series stationary.

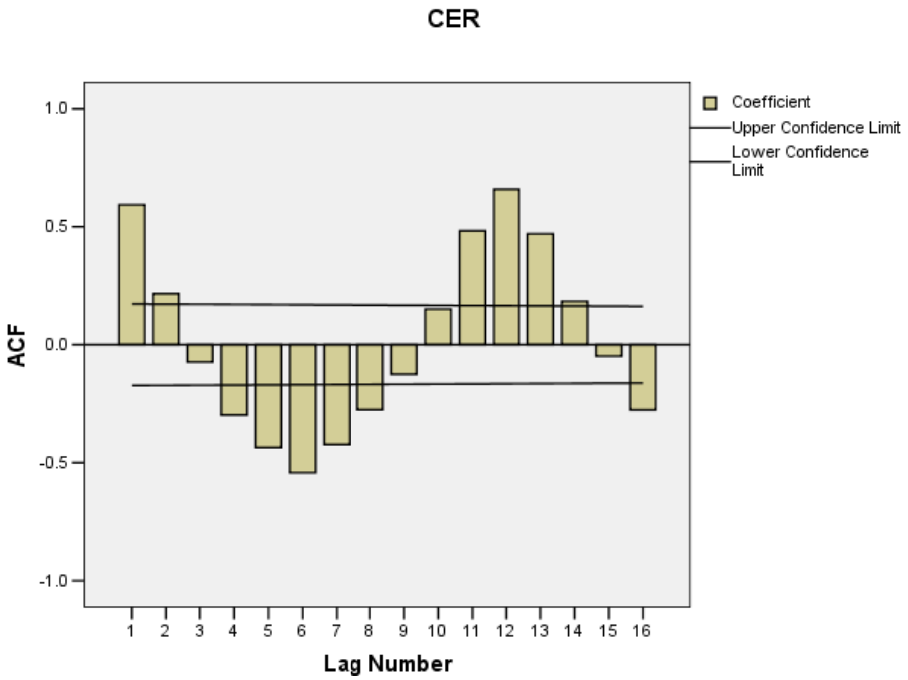

Fig. 6.5(a) Autocorrelation function (ACF) for CER

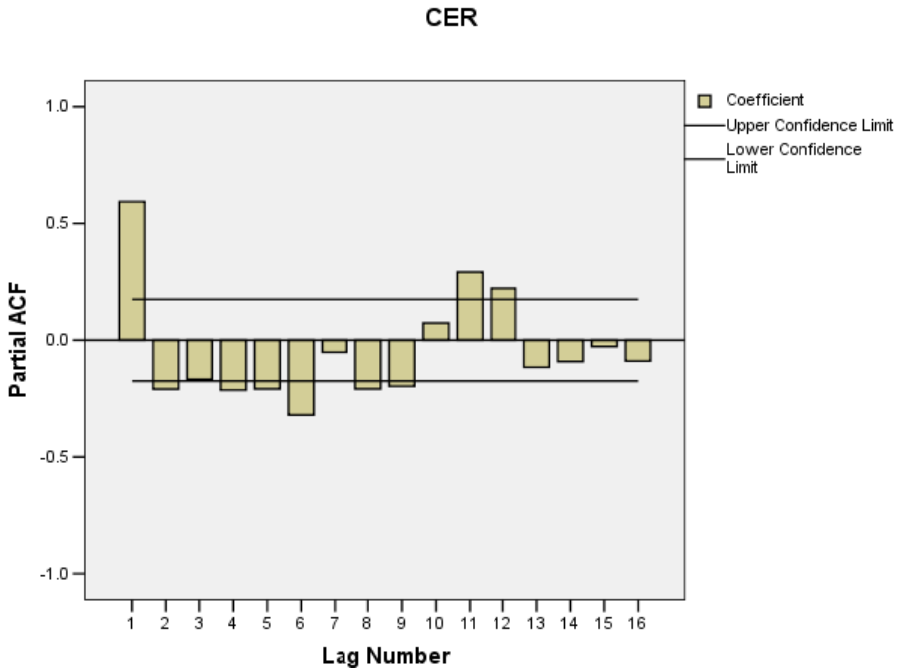

Fig. 6.5(a) Partial Autocorrelation function (PACF) for CER

A seasonal autoregressive integrated moving average (ARIMA) model has been selected. This model assumes that the best forecast for future data is given by a parametric model relating the most recent data value to previous data values and previous noise. Each value of CER has been adjusted in the following way before the model was fit.

The Table 6.5 summarizes the statistical significance of the terms in the forecasting model. Terms with P-values less than 0.05 are statistically significantly different from zero at the 95% confidence level. The P-value for the AR(1) term is greater than or equal to 0.05, so it is not statistically significant. It is therefore required for reducing the order of the AR term to 0. The P-value for the MA(2) term is greater than or equal to 0.05, so it is not statistically significant. The order of the MA term is reduced to 1. The P-value for the SAR(1) term is less than 0.05, so it is significantly different from 0. The P-value for the SMA(2) term is less than 0.05, so it is significantly different from 0. The estimated standard deviation of the input white

noise equals 0.78. With this criterion the forecast model selected is ARIMA(1,1,2)x(1,1,2)12 with number of forecasts generated is 12. The estimated white noise variance is 0.61 with 112 degrees of freedom and the estimated white noise standard deviation is 0.78. The Table 6.5 summarizes the performance of the currently selected model in fitting the historical data. It displays: (1) the root mean squared error (RMSE); (2) the mean absolute error (MAE); (3) the mean absolute percentage error (MAPE); (4) the mean error (ME); (5) the mean percentage error (MPE).

Table 6.5. ARIMA model Summary for CER

Statistic	**Estimation Period**
RMSE	0.69
MAE	0.51
MAPE	4.1
ME	-0.12
MPE	-1.14

The Table 6.6 displays the statistics which is based on the one-ahead forecast errors, which are the differences between the data value at time *t* and the forecast of that value made at time *t-1*.

Table 6.6. Parameter Estimates for CER ARIMA(1,1,2)x(1,1,2)$_{12}$

Parameter	**Estimate**	**Std. Error**	**t**	**P-value**
AR(1)	0.36	0.44	0.82	**0.41**
MA(1)	1.06	0.46	2.29	0.02
MA(2)	-0.13	0.42	-0.32	0.75
SAR(1)	-0.82	0.08	-10.57	0.00
SMA(1)	-0.18	0.06	-2.97	0.00
SMA(2)	0.85	0.04	20.95	0.00

The first three statistics in the above Table 6.6 measures the magnitude of the errors. In this case, ARIMA (1,1,2) X (1,1,2) is the model selected . The model for forecasting CER using ARIMA (1, 1, 2) x (1, 1, 2)$_{12}$ can be written as

$$(1-B)(1-B^{12})Z_t = \frac{(1-\theta_1 B-\theta_2 B^2)(1-\Theta_{12}B^{12}-\Theta_{24}B^{24})}{(1-\varphi_1 B)(1-\emptyset_{12}B^{12})}\,\varepsilon_t \qquad \ldots(6.11)$$

6.3.2.1. Model Comparison

The following Table 6.7 gives the models used for comparison and the estimates based on RMSE, MAE, MAPE, ME, MPE, Akaike Information Criterion (AIC), SBIC and HQC. The Table 6.9 compares the estimation parameters of fitting different models to the data. The model with the lowest value of the Akaike Information Criterion (AIC) is model I, which has been used to generate the forecasts.

6.3.2.2. Models

(A) Random walk

(B) Random walk with drift = 0.025

(C) Constant mean = 12.78

(D) Linear trend = 12.7 + 0.00129 t

(E) Simple moving average of 2 terms

(F) Simple exponential smoothing with alpha = 0.016

(G) Brown's linear exp. smoothing with alpha = 0.02

(H) Holt's linear exp. smoothing with alpha = 0.18 and beta = 0.02

(I) ARIMA(1,1,2)x(1,1,2)$_{12}$

(J) ARIMA(1,1,1)x(2,0,2)$_{12}$

(K) ARIMA(0,1,1)x(2,1,2)$_{12}$

(L) ARIMA(1,0,0)x(0,1,1)$_{12}$

(M) ARIMA(0,0,1)x(0,1,1)$_{12}$

Table 6.7. Comparison of estimation parameters of different models fitted

Model	RMSE	MAE	MAPE	ME	MPE	AIC	HQC	SBIC
(A)	0.93	0.72	5.7	0.02	-0.04	0.03	0.13	0.27
(B)	0.94	0.71	5.69	-0.002	-0.24	0.06	0.16	0.32
(C)	0.75	0.56	4.49	0.003	-0.35	-0.38	-0.28	-0.12
(D)	0.76	0.56	4.50	0.003	-0.34	-0.36	-0.25	-0.08
(E)	0.86	0.66	5.22	0.023	-0.07	-0.12	-0.02	0.14
(F)	0.76	0.56	4.52	-0.006	-0.41	-0.37	-0.26	-0.10
(G)	0.77	0.58	4.60	0.069	0.17	-0.33	-0.22	-0.07
(H)	0.8	0.60	4.82	-0.058	-0.79	-0.25	-0.14	0.03
(I)	0.69	0.51	4.1	-0.115	-1.14	-0.66	-0.61	-0.53
(J)	0.7	0.5	4.0	0.003	-0.222	-0.63	-0.58	-0.5
(K)	0.71	0.57	4.44	-0.035	-0.534	-0.62	-0.58	-0.5
(L)	0.73	0.55	4.34	0.031	-0.009	-0.60	-0.58	-0.56
(M)	0.73	0.55	4.32	0.031	-0.013	-0.60	-0.58	-0.55

The Fig 6.6 shows the estimated autocorrelations between the residuals at various lags. The lag *k* autocorrelation coefficient measures the correlation between the residuals at time *t* and time *t-k*. Also shown are 95% probability limits around 0. If the probability limits at a particular lag do not contain the estimated coefficient, there is a statistically significant correlation at that lag at the 95% confidence level. In this case, none of the 24 autocorrelations coefficients are statistically significant, implying that the time series will be completely random (white noise). Fig 6.4 shows the autocorrelations drawn using the above table.

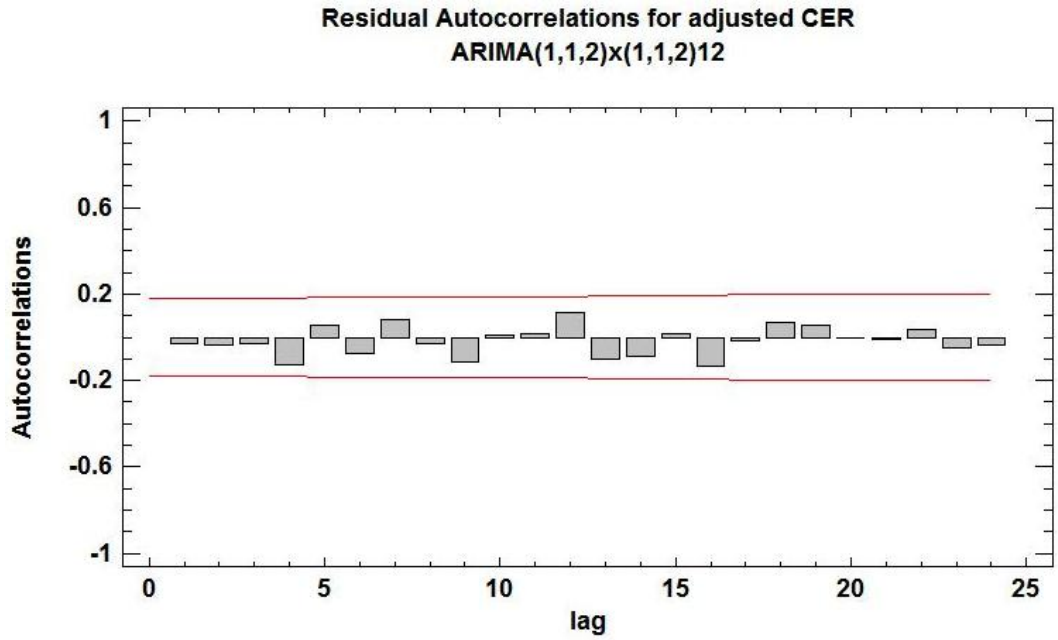

Fig.6.6. Estimated autocorrelation between residuals for CER at various lags. The ACF indicates that time series follows white noise.

The Fig 6.7 shows the estimated partial autocorrelations between the residuals at various lags. The lag *k* partial autocorrelation coefficient measures the correlation between the residuals at time *t* and time *t+k* having accounted for the correlations at all lower lags. It can be used to judge the order of autoregressive model needed to fit the data. Also shown are 95% probability limits around 0. If the probability limits at a particular lag do not contain the estimated coefficient, there is a statistically significant correlation at that lag at the 95% confidence level. In this case, none of the 24 partial autocorrelations coefficients is statistically significant at the 95% confidence level.

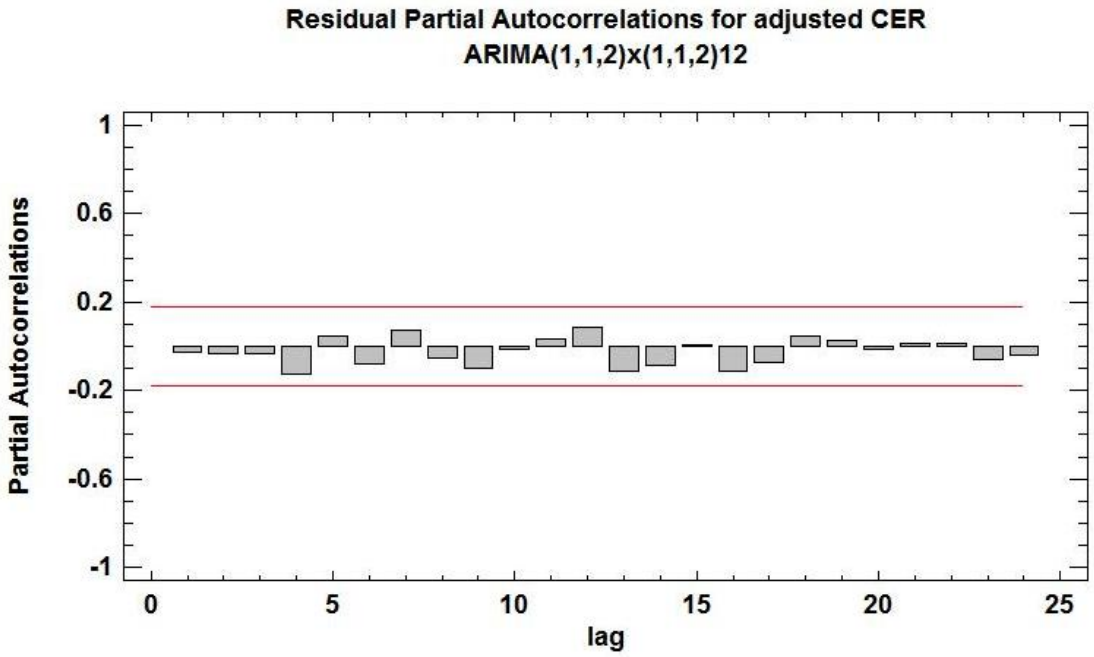

Fig.6.7. Estimated partial autocorrelation between residuals for CER at various lags. The residuals are within the probability limits

The Table 6.8 shows the forecasted values for CER. During the period where actual data is available, it also displays the predicted values from the fitted model and the residuals (data-forecast). For time periods beyond the end of the series, it shows 95% prediction limits for the forecasts. These limits show where the true data value at a selected future time is likely to be with 95% confidence, assuming the fitted model is appropriate for the data. The Fig 6.8 shows the graph plotted using the forecasted values given in Table 6.12. The predicted values for January 2011 show that CER decreases to a value of 11.3 microns and increases thereafter. But, in the month of May, 2011 the CER diminishes to 11.7, after which it again increases in the month of June.

Table 6.8. Forecast Table for CER given by ARIMA(1,1,2) x $(1,1,2)_{12}$

Month	Forecast	Lower 95.0% Limit	Upper 95.0% Limit
Jan-11	11.2886	9.73861	12.8387
Feb-11	12.0968	10.4794	13.7142
Mar-11	12.2296	10.5883	13.8709
Apr-11	12.2467	10.5916	13.9018
May-11	11.7354	10.0694	13.4013
Jun-11	12.9892	11.3133	14.665
Jul-11	14.4643	12.7789	16.1497
Aug-11	15.1203	13.4256	16.815
Sep-11	14.6328	12.9289	16.3368
Oct-11	13.6305	11.9174	15.3436
Nov-11	13.4399	11.7176	15.1621
Dec-11	11.908	10.1767	13.6394

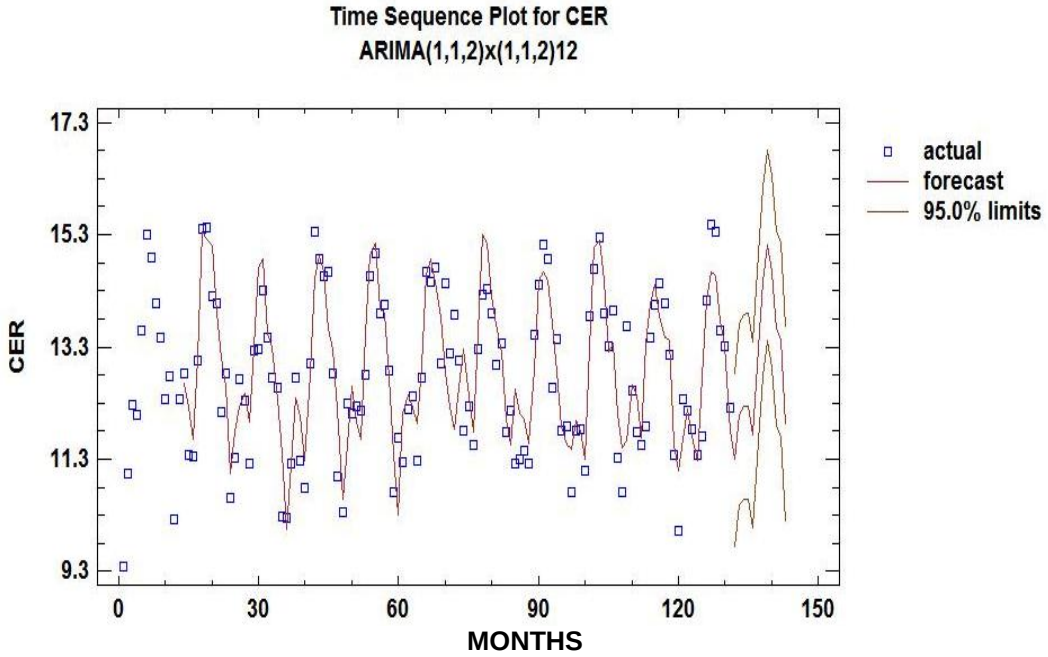

Fig. 6.8. Time series plot showing the actual and model output values for CER. The forecast values till December 2011 is shown at 95% confidence level.

6.4. Conclusions

Based on the features of data, the classes of seasonal ARIMA models were considered to fit the data. Since the series showed clear seasonal variations, seasonal differencing was done to make it stationary. The autocorrelation function and the partial autocorrelation function of the transformed series are estimated and the significant lags were used for finding out the order of the model. The residual analysis and *Akaike* information criterion were compared to evaluate the goodness-of-fit of the model. Forecasting of AOD was done using the model which had the least value of AIC was ARIMA (1,0,2) x (2,1,2). To predict the future values of CER, the ARIMA (1,1,2) x $(1,1,2)_{12}$ had the least value of AIC. This model was selected to forecasting CER.

The forecast accuracy for each model was evaluated via mean absolute percentage error. The values thus obtained are found to have a reasonably well goodness of fit with the observed CER and AOD datasets. The forecasts are also carried out based on the selected model. The forecast values show a decrease of AOD in May 2011 to 0.08 from a peak value of 0.22 in January. A corresponding decrease in CER to 11.3 microns was observed in January which gradually increases to about 12 microns as the season progress and a sudden decrease of 11.74 is shown in the month of May 2011 after which an abrupt increase occurs in the month of June. The value of CER which is approximately 12 microns in the month of May indicates that there could be a rapid advancement of south west monsoon towards the north Indian region in the year 2011.The model and the observed data obtained till March 2011 shows an analogous pattern which justifies the predictability and accuracy of the selected model.

CHAPTER 7
SUMMARY AND FUTURE SCOPE OF STUDY

7.1. Summary

The variation in aerosol composition and distribution depends on a complex combination involving primary and secondary sources, transport, dispersion and removal processes. It is widely acknowledged that the presence of aerosols in the atmosphere is essential to the initial formation of clouds. However, the overall influence of aerosols on cloud droplet growth, spatial distribution of clouds and delaying the onset of precipitation is highly uncertain. This uncertainty arises due to the lack of understanding of cloud processes. The main objective of this doctoral thesis is to suggest how variations in distribution of aerosols indirectly affect the cloud properties which translate to affecting onset of precipitation.

This study addresses the growing concern about the significant changes in the climate and weather patterns due to the aerosol loading that have taken place in the Indo Gangetic Plain (IGP) which comprises most of the northern Indian region (69^0 E – 89^0 E; 22^0 N – 29^0 N). This chosen study region comprises of major industrial cities in India (New Delhi, Kanpur, Allahabad, Jamshedpur and Kolkata). The IGP has a major source of coal; therefore most of the industries including numerous thermal power plants that run on coal are located around this region. They inject copious amount of aerosols into the atmosphere. Moreover, northern and central parts of India are one of the most thickly populated areas in the world and have the most intensely farmed areas. Rapid increase in population and urbanization has resulted in an abrupt increase in aerosol concentrations in recent years. Burning of agricultural wastes after each harvest season causes a large quantity of biomass aerosols in the dry season. In addition to these anthropogenic sources, the transport

of dust aerosols from arid locations is prevalent during the dry months which increase the aerosol loading in the atmosphere. The topography and weather in the region is ideal for the piling up of these aerosols.

The region is bounded by the Himalayas in the north, Thar Desert in the west, the Vindhyan range in the south and Brahmaputra ridge in the east. During the non-monsoon months (October to May) the weather in the location is dry with very little rainfall. Surface winds are weak during most of the time in this dry season. These geographical characteristics of the region enable the buildup of aerosols, increasing their surface concentration. This complex combination of aerosol transport and anthropogenic factors mixed with the contribution from the natural sources, particularly in the pre-monsoon and post-monsoon seasons modify the optical properties of the atmospheric aerosols at this region as a result of which it influences the meteorological parameters in the location. Such a situation will severely affect the region which depends upon southwest monsoon as a major source of water. Therefore, any change in weather which disturbs the normal hydrological pattern is alarming in the socio-economic point of view. The present doctoral thesis focuses to understand the variation in transport and distribution of aerosols in the region and to determine the interaction of these aerosols with meteorological parameters and cloud properties.

Analysis shows that transport of aerosols is more during the pre-monsoon season than in post-monsoon season for all the years taken into consideration. Aerosols reach India as a result of long distance transport by means of prevailing winds at 700 hPa (~ 3km). These aerosols get deposited in the longitudinal belt ranging from 70^0 E to 89^0 E. The piling up of aerosols increases the surface concentration as indicated by higher values in Aerosol Index (AI) during pre-monsoon season. The following monsoon season washes out the aerosols present in the atmosphere so that AI will be lower during the monsoon season. During post monsoon season, the prevailing westerlies are not stronger as in the case of pre-monsoon. Therefore, the aerosol

concentration is lower during post-monsoon than in pre-monsoon. Weakening and strengthening of zonal winds has an influence in the concentration of aerosols in the region. During the El-Nino years the Indian subcontinent shows an enhancement of aerosol concentration. The prevailing zonal winds and the subsidence of upper level winds are very intense during those years due to which the aerosol concentration becomes higher. In La-Nina years the situation reverses. The weakening of zonal winds at 700 hPa level decreases the amount of aerosols transported towards the Indian region. Moreover, the subsiding air mass from upper levels is of lesser magnitude. This results in a low aerosol loading over the north Indian locations during La-Nina conditions. The composite of AI during El-Nino years shows that higher aerosol concentrations over most parts of India, while La-Nina years are characterized by less than normal AI values.

Further analysis indicates a biennial variability in aerosol optical depth (AOD) in the region. The time series of monthly mean AOD over the Indian region shows that this biennial variability is associated with the positive and negative phases of quasi biennial oscillation (QBO) in stratospheric zonal winds. Detailed analysis reveals that QBO modulates the tropical tropopause layer by which the tropopause undergoes an oscillation in tropopause characteristics (height, pressure and temperature). The warming (cooling) of the troposphere during the positive (negative) phase of QBO enables intense convection thereby resulting in an increase (decrease) in concentration of atmospheric aerosols. The QBO, which is predominantly a stratospheric phenomenon, induces changes in the tropospheric characteristics that in turn modify the distribution of tropospheric constituents including concentrations of atmospheric aerosols.

So far it is seen that there exists a seasonal variation as well as a biennial variation in aerosol concentration in the region. Since the primary objective is to understand the aerosol indirect effects on cloud properties, a study is done in that direction. An analysis on the influence of aerosols on cloud shows that there is indeed a

modification in cloud micro physics due to an increase in aerosol concentration over industrial locations in North India. This in turn affects the net solar radiation reaching the surface. It is seen that during the non-monsoon months there is an increase in fine mode aerosols, whereas during the monsoon season coarse mode aerosol dominates. High Angstrom exponent (AE) during the non-monsoon months and low AE during the monsoon months signify these characteristics. Presence of large amount of finer mode aerosols decreases the cloud effective radius (CER) during the dry months. It is seen that aerosol indirect effect is evident during non-monsoon months in the region. While during the monsoon season they are in phase, probably due to the presence of coarse mode sea-salt aerosols. For the dry months, the association of fine mode aerosols and CER are in accordance with the well known *Twomey* and cloud life time effects. The aerosol indirect effect is more prominent during El-Nino years than in other years. An excessive aerosol loading induced a sharp increase in AOD of 0.35 in the year 2010 which is the highest value of the last decade. The following monsoon was a failure in the region even though rest of the country got an excess rainfall. It is seen that for the years that has high pre-monsoon AOD is followed by a monsoon failure. Moreover, whenever the CER decreases below a threshold value in the month of May, there is a delay in the progression of monsoon over north India. In the non-monsoon months, the decrease in CER is by about 38% when fine mode AOD increases from 0.04 to 0.3. But, such characteristics are not observed during the monsoon season due to the prevalence of marine airmass and the influx of large quantity of moisture from the surrounding oceanic regions.

Based on the features of time series data of CER and AOD, the classes of Seasonal ARIMA (autoregressive integrated moving average) models are considered to predict the future values of these two parameters. Forecasting methods applying the ARIMA time series method has a good fit to these datasets. Since the series showed clear seasonal variations, seasonal differencing is done to make it stationary. The

autocorrelation function and the partial autocorrelation function of the transformed series are estimated and the significant lags are used for finding out the order of the model. The residual analysis, *Akaike* information criterion and *Bayesian* information criterion are compared to evaluate the goodness-of-fit of the model. The forecast accuracy for each model is evaluated via mean absolute percentage error (MAPE). The empirical values thus obtained are found to have a reasonably well goodness of fit with the observed values. Correlations between CER and AOD at various lags are computed and the results indicate an inverse relationship between the two series. Forecasts are also carried out based on the selected model. The forecast values show a decrease of AOD in May 2011 to 0.08 from a peak value of 0.22 in January. A corresponding decrease in CER to 11.3 microns is observed in January which gradually increases to about 12 microns as the season progress and a sudden decrease of 11.74 is shown in the month of May 2011 after which a sudden increase occurs in the month of June.

The present study highlights the role of aerosols transported from distant locations getting accumulated in the region due to favourable topographical and meteorological conditions. This study advances knowledge on aerosol-cloud relationship which is still less understood facets in atmospheric science. An attempt has been made to investigate the interaction of aerosols cloud properties which in turn has an impact on the top of the atmosphere albedo as well as on the surface temperature. The study suggests that increase in aerosols in the region has an impact on the precipitation efficiency, though clear causal effect of aerosols on precipitation as well as on the monsoon circulation is still uncertain.

7.2. Future Scope

The present doctorial study analyses the aerosol indirect effect over the North Indian region and IGP. It will be interesting to know how the aerosol effects will be over peninsular Indian region which has an entirely different topography and weather

patterns compared to IGP. The vast coastline and the proximity to ocean will have a different aerosol characteristics and effect in the region. A comparative study in this direction will throw light upon how a difference in aerosol type and source induces changes in the cloud parameters over the region.

Further study is needed to understand the changes in atmospheric circulations as a result of changes in cloud cover and thickness due to aerosol indirect effects. The reduction in surface temperature and variations in latent heat released due to condensation of water vapour may have an impact on atmospheric circulations. A detailed study is required to comprehend if the piling up of the aerosols in the pre-monsoon has any effect on the advancement of south west monsoon towards the regions.

REFERENCES

Ackerman, A. S., Kirkpatrick, M. P., Stevens, D. E., and Toon,O. B., 2004. The impact of humidity above stratiform clouds on indirect climate forcing, Nature, 432, 1014–1017.

Ackerman, A.S., Toon,O.B., Stevens, D.E., Heymsfield, A.J., Ramanathan, V., Welton, E.J., 2000. Reduction of tropical cloudiness by soot, *Science*, 288, 1042-1047.

Ackerman, A. S., Strabala, K.I., Menzel,W.P., Frey, R.A.,. Moeller, C.C., and Gumley L.E., 1998. Discriminating clear sky from clouds with MODIS, *J. Geophys. Res*., 103, 32 139 – 32 140.

Akaike, H., 1974. A New Look at the Statistical Model Identification, *IEEE Transaction on Automatic Control*, AC-19, 716-723.

Albrecht, B., 1989. Aerosols, Cloud Microphysics, and Fractional Cloudiness, Science, 245, 1227–1230.

Aloysius, M., Mohan, M., Parameswaran, K., George, S.K., and Nair, P.R., 2008. Aerosol transport over the Gangetic basin during ISRO-GBP Land Campaign-II, *Ann. Geophys*., 26, 431- 440.

Amiridis V., Balis, D., Kazadzis, S., Giannakaki, E., Papayannis, A., and Zerefos, C.,2005. Four years aerosol observations with a Raman lidar at Thessaloniki, Greece, in the framework of European Aerosol Research Lidar Network (EARLINET). *J. Geophys.Res.*, *110*, D21203, doi:10.1029/2005JD006190.

Andrae, M.O., 1983. Soot Carbon and excess potassium long-range transport of combustion derived aerosols. *Science*, 220, 1148-1151.

Andreae, M.O., et al., Long range transport of soot carbon in the marine atmosphere, *Sci. Total Environ.*, 36, 73-80, 1984.

Andreae, M.O., Browell, E.V.,. Garstang, M., Gregory, G.L., Harriss, R.C., Hill, G.F., Jacob, D.J., Pereira, M.C., Sachse, G.W., Setzer, A.W., Dias, P.L.S., Talbot, R.W., Torres, A.L., and Wofsy, S.C., 2004. Biomass-burning emissions and associated haze layers over Amazonia. *J. Geophys. Res*., 93, 1509-1527,

Angell J.K, Korshover J. 1964. Quasi-biennial variations in temperature, total ozone and tropopause height. *Journal of Atmospheric Science* 21:479–492.

Ardanuy, P.E., Kyle L., and Hoyt D.,1992. Global relationships among the earth's radiation budget, cloudiness, volcanic aerosols and surface temperatures. J. clim, 5, 1120-1139.

Artaxo, P., Fernandes, E.T., Martins, J.V., Yamasoe, M.A., Hobbs, P.V., Maenhaut, W., Longo, K.M., and Castanho, A., 1998.Large-scale aerosol source apportionment in Amazonia. *J. Geophys. Res*., 103, 31837-31847.

Aumann H.H, Chahine M.T, Gautier C, Goldberg M.D, Kalnay E, McMillan L.M, Revercomb H, Rosenkranz P.W, Smith W.L, Staelin D.H, Strow L.L, Susskind J. 2003. AIRS/AMSU/HSB on the Aqua Mission: Design, Science Objectives, Data Products, and Processing Systems. *IEEE Transactions on Geoscience and Remote Sensing* 41: 253-264.

Babu, S. S., and Krishna Moorthy, K., 2002. Aerosol black carbon over a tropical coastal station in India, *Geophys. Res. Lett.*, 29.

Baldwin, M. P., and Coauthors, 2001. The Quasi-Biennial Oscillation. *Rev. Geophys.*, 39, 179-229.

Bates, T.S., Huebert, B.J., Gras, J.L., Griffiths, F.B., and Durkee, P.A., 1998. International Global Atmospheric Chemistry (IGAC) project´s first aerosol experiment (ACE1): Overview, *J. Geophys. Res*., 103, 16297-16318,

Beegum,N.S., Krishna Moorthy K., Suresh Babu S., Ramakrishna Reddy R., Rama Gopal K, Nazeer Ahmed Y. 2009. Quasi-biennial oscillations in spectral aerosol optical depth. *Atmos. Sci. Lett.* 10: 279-284.

Bengtsson, L., Kanamitsu, M., K°allberg, P., and Uppala, S., 1982. FGGE 4-dimensional data assimilation at ECMWF. *Bull. Am. Meteorol. Soc*., 63:29–43.

Betzer, P.R., Carder, K.L., Duce, R.A., Merrill, J.T., Tindale, N.W., Uematsu, M., Costello, D., Young, R., Feely, R.A., Breland, J.A., Bernstein, R., Greco, T., 1988. A pulse of Asian dust to the central North Pacific: long-range transport of giant mineral aerosols, *Nature* ,336, 568-571.

Bigg, E.K., Gras, J.L., and Evans, C., 1984. Origin of Aitken particles in remote marine region of the southern hemisphere, *J. Atmos. Chem*., 1, 203-214.

Blanchet, J.P., Heintzenberg, J., and Winkler, P., 1986. *Beitr.Phys.Atmos*. 59,359.

Box, G.E.P., Jenkins, G.M., and Reinsel, G.C., 1994. Time series analysis – Forecasting and control. 3rd ed. Prentice Hall, Englewood Cliffs, NJ, USA

Browell, E. V., Ismail, S. and Grant W. B., 1998. Differential absorption lidar (DIAL) measurements from air and space, Appl. Phys. B 67, 399-410.

Cachier, H., Liousse, C., Buat-Menard, P., and Gaudichet, A., 1995. Particulate content of savanna fire emissions. *J. Atmos. Chem*., 22, 123-148.

Carder, K. L., Steward, R. G., Betzer, P. R., Johnson, D. L., and Prospero, J. M., 1986. Dynamics and composition of particles from an aeolian input event to the Sargasso Sea, *J. Geophys. Res.*, D91, 1055–1066.

Charlson, Lovelock, J.S., Andreae, M.O., Warren, S.G., 1987. Oceanic Phytoplankton, Atmospheric Sulfur, Cloud albedo and Climate, *Nature*, 326, 655-661.

Charlson, R.J., Schwartz, S.E., Heles, J.M., Cess, R.D., Coakley Jr., J.A., Hansen, J.E., and Hoffman, D.J., 1992. Climate Forcing by Anthropogenic Aerosols, *Science*, 255, 423-430.

Charlson, R.J., Langner, J., Rodhe, H., Leovt, C.B., and Warren, S.G., 1991. Perturbation of the Northern Hemispheric Radiative balance by Backscattering from Anthropogenic Sulphate Aerosols, *Tellus*, 43AB, 152-163

Chen, L.W.A., B.G. Doodridge, R.R. Dickerson, J.C. Chow, P.K. Mueller, J. Quinn, and W.A. Butler, seasonal variations in elemental carbon aerosols, carbon monoxide and sulphur dioxide: Implications for sources, *Geophys. Res. Lett.*, 28, 1711-1714, 2001.

Chu, D. A., Kaufman, Y. J., Remer, L. A., and Holben, B. N., 1998. Remote sensing of smoke from MODIS airborne simulator during the SCAR-B experiment, *J. Geophys. Res.*, 103(D24), 31,979–31,987, doi:10.1029/98JD01148.

Chu, D. A., Kaufman, Y.J., Ichoku, C., Remer, L.A., Tanre, D., and Holben, B.N., 2002. Validation of MODIS aerosol optical depth retrieval over land, *Geophys. Res. Lett*., 29(12), 10.1029/2001GL013205.

Chu, D.A., Kaufman, Y.J., Zibordi, G., Chern, J.D., Mao, J., Li, C., and Holben, B.N., 2003. Global monitoring of air pollution over land from EOS-Terra MODIS. *J. Geophys. Res.*, 108(D21), 4661, doi:10.1029/2002JD003179.

Chung, C. E., Ramanathan, V., 2004. Aerosol loading over the Indian Ocean and its possible impact on regional climate. *Ind. J. Mar. Sci.* 33(1), 40–55

Clarke, A.D., 1993. Atmospheric Nuclei in the Pacific Mid Troposphere: Their Nature, concentration and Evolution, *J. Geophys. Res*, 98, 20633-20647.

Collimore C.C, Martin D.W, Hitchman M.H, Huesmann A., Waliser D.E., 2003. On the Relationship between the QBO and Tropical Deep Convection. *Journal of Climatology*, 16: 2552–2568.

Collins, W. D., Conant, W. C., Ramanathan, V., 1994. Earth radiation budget, clouds, and climate sensitivity, in: The Chemistry of the Atmosphere: Its Impact on Global Change, edited by: J. G. Calvert, Blackwell Scientific Publishers, Oxford, UK, 207–215.

Cordero E.C., Kawa S.R., Schoeberl M.R.. 1997. An analysis of tropical transport: Influence of the quasi-biennial oscillation. *J. Geophys. Res.*, 102: 16,453-16,462.

Cotton, W. R. and Anthes, R. A. 1989. *Storm and Cloud. Dynamics*. International Geophysics Series Volume 44. New York.

Covert, D. S., Kapustin, V.N., Bates, T. S., and Quinn, P. K., 1996. Physical properties of marine boundary layer aerosol particles of the mid-Pacific in relation to sources and meteorological transport. *J. Geophys. Res*., 101, 6919-6930.

Crutzen,P.J., and M.O.Andreae, Biomass burning in the tropics: Impact on atmospheric chemistry and biochemical cycles, *Science*, 250, 1669-1678,1990.

Crutzen,P.J., Galbally, I., and Bruhl, C.,1984. Atmospheric effects from post nuclear fires, *Clim. Change*, 6, 323-364

d'Almeida A.G., Koepke, P., Shettle, P.E.,1991. *Atmospheric Aerosols, Global climatology and Radiative Characteristics*, A.Deepak Publishing, Hampton, Virginia USA,

Dave, J. V., 1978. Effect of aerosols on the estimation of total ozone in an atmospheric column from the measurement of its ultraviolet radiance. *J. Atmos. Sci*., 35, 899-911.

Dawson, A.G. and O'Hare, G. 2000. Ocean-atmosphere circulation and global climate: The El Nino southern oscillation. *Geogr.*, 85, 193–208

de Graaf M, Stammes P, Torres O and Koelemeijer , 2005. Absorbing aerosol index: sensitivity analysis, application to GOME and comparison with TOMS. J *Geophys Res*;110:D01201

Deepshikha, S., Satheesh,S. K., Srinivasan, J., 2006. Dust aerosols over India and adjacent continents retrieved using METEOSAT infrared radiance Part II: quantification of wind dependence and estimation of radiative forcing. *Ann. Geophys.* 24, 63–79.

Denman, K. L., G. Brasseur, A. Chidthaisong, P. Ciais, P.M. Cox, R.E. Dickinson, D.Hauglustaine, C. Heinze, E. Holland, D. Jacob, U. Lohmann, S Ramachandran, P.L.da Silva Dias, S.C. Wofsy and X. Zhang, 2007. Couplings between changes in the climate system and biogeochemistry, in: Climate change 2007: The physical science basis.Contribution of working group I to the fourth assessment

report of the intergovernmental panel on climate change, edited by: Solomon, S., D. Qin, M.Manning, Z. Chen, M. Marquis, K.B. Averyt, M.Tignor and H.L. Miller, Cambridge University Press, Cambridge, United Kingdom and New York, NY, USA.

Deuze´, J.L., Bre´on, F.M., Devaux, C., Goloub, Herman, M., Lafrance, B., Maignan, F., Marchand, A., Nadal, F., Perry, G., and Tanre´, D., 2001. Remote sensing of aerosols over land surfaces from POLDER-ADEOS-1 polarized measurements. *J. Geophys. Res.*, 106(D5), 4913–4926.

Dey, S., Tripathi, S. N., Singh, R. P., Holben, B. N., 2004. Influence of dust storms on the aerosol optical properties over the Indo-Gangetic plains. J. Geophys. Res. 109, D20211

Diaz, H.F. and Kiladis, G.N. 1992. Atmospheric teleconnections associated with the extreme phase of southern oscillation, in H.F. Diaz and V. Margraf (Eds.), *El Nino-Historical and Paleoclimatic Aspects of the Southern Oscillation*, Cambridge University Press, Cambridge, UK, pp. 7-29.

Draxler, R.R. and Hess, G.D., 1998. An Overview of the Hysplit_4 Modeling System for Trajectories, Dispersion, and Deposition, Aust. Met. Mag., 47, 295-308.

Duce R.A., 1995. Sources, distributions, and fluxes of mineral aerosols and their relationship to climate, in *Dahlem workshop on aerosol forcing of climate*, edited by R.J Charlson and J. Heitzenberg, pp – 43 – 72, John Wiley, New York, 1995.

Dunkerton T.J. 1997. The role of gravity waves in the quasi biennial oscillation. *Journal of Geophysical Research* 102: 26,053–26,076.

Durkee, P.A., Pfeil, F., Frost, E., and Shema, R., 1991. Global analysis of aerosol particle characteristics, *Atmos. Environ.*, 25A, 2457--2471,.

Finkele, K., Hacker, J .M., Kraus, H., Roland, A.D., Scott, B., 1995. A complex sea-breeze circulation cell derived from aircraft observations, *Boundary-Layer Meterol*., 73,299-317.

Fitzgerald, J.W., 1991. Marine aerosols: A review, *Atmos. Environ*., 25A,533-545.

Gao, B.C., Kaufman, Y. J., Tanre´, D., and Li, R.R.. 2002. Distinguishing tropospheric aerosols from thin cirrus clouds for improved aerosol retrievals using the ratio of 1.38-µm and 1.24-µm channels, *Geophys. Res. Lett.*, 29(18), 1890, doi:10.1029/2002GL015475.

Gautam, R., Hsu, N. C., Lau, K.M., Tsay, S.C., and Kafatos, M., 2009. Enhanced pre-monsoon warming over the Himalayan-Gangetic region from 1979 to 2007, *Geophys. Res. Lett*., 36, L07704, doi:10.1029/2009GL037641.

Gray W.M., Scheaffer J.D., Knaff J.A.,1992. Influence of the stratospheric QBO on ENSO variability. *Journal of Meteorological Society of Japan* 70: 975–995.

Griggs, M. 1975. Measurements of atmospheric aerosol optical thickness over water using ERTS-1 data, *J. Air Pollut. Control Assoc*., 25, 625 – 626, 1975.

Gupta,A.,.Singh, K.K.,.Baxla, A.K, Singh, J.V., and Ranjeet Singh, 2004. Monsoon-2004 Progress, Performance, Prediction & Agrometeorological Advisories, *www.ncmrwf.gov.in/monsoon_2004.pdf,*

Guttikunda, S. K., Carmichael, G. R., Calori, G., Eck, C., Woo, J.H., 2003. The contribution of megacities to regional sulfur pollution in Asia. *Atmos. Environ*. 37, 11– 22.

Habib, G., Venkataraman. C.,, Chiapello, I., Ramachadran, S and Boucher O.,,Reddy, M.S., 2006. Seasonal and interannual variability in absorbing aerosols over India derived from TOMS: relationship to regional meteorology and emissions. *Atmos Environ*;40:1909–21.

Hamonou, E., Chazette, P., Balis, D., Dulac, F., Schneider, X., Galani, E., Ancellet, G., and Papayannis, A. 1999. Characterization of the vertical structure of Saharan dust export to the Mediterranean basin. *J. Geophys. Res*., *104*, 22 275–22 270.

Han, Q., Rossow, W. B., and Lacis, A. A., 1994. Near-global survey of effective droplet radii in liquid water clouds using ISCCP data. *J. Climate,* 7, 465–497.

Hansen, J., M.Sato and R.Ruedy, I Tegen, Climate forcings in the industrial era, Proc. Natl. Acd. Sci. 12753-12758, 1998

Hansen, J., M.Sato and R.Ruedy, Radiative forcing and climate response, *J.Geophys.Res*., 102, 6831-6864, 1997a

Hansen, J., Mki. Sato, A. Lacis, and R. Ruedy, The missing climate forcing. *Phil.Trans. Royal Soc. London*. B 352, 231-240 1997b.

Hansen, J.E., M. Sato and R. Ruedy, Radiative forcing and climate response. *J. Geophys. Res*., 102, 6831-6864 , 1997c.

Harrison, S. P., Kohfeld, K. E., Roelandt, C., and Claquin T.,2001. The role of dust in climate changes today, at the Last Glacial Maximum and in the future. *Earth Sci. Rev*., 54,43–80.

Havers, N., Burba, P., Lambert, J. and Klockow, D., 1998. Spectroscopic characterization of humic-like substances in airborne particulate matter. *J. Atmos. Chem*., 29, 45-54.

Haywood, J., and Boucher O.,2000. Estimates of the direct and indirect radiative forcing due to tropospheric aerosols. *Rev.Geophys*., *38*, 513–543.

Haywood,J.M., and Shine K.P., 1995. The effect of anthropogenic sulphate and soot aerosol on the clear sky planetary radiation budget. *Geophys. Res. Lett*., 22, 603-606.

Haywood,J.M., Ramaswamy, V.,.Soden, B.J., 1999. Tropospheric aerosol climate forcings in clear sky satellite observations over the oceans, *Science*, 283, 1299-1303,

Herman, J. R., Bhartia, P. K., Torres, O., Hsu, C., Seftor, C., and Celarier E., 1997. Global distribution of UV-absorbing aerosols from Nimbus-7/TOMS data, *J. Geophys. Res*., *102*,16,911– 16,922,

Hess, M., Koepke, P., and Schult, I., 1998. Optical properties of aerosols and clouds. *Bull. Amer. Meteor. Soc.* 79, 831-44.

Hitchman M.H., McKay M., Trepte C.R.,1994. A climatology of stratospheric aerosol. *Journal of Geophysical Research 99*: 20,689 –20,700.

Holben, B.N., Eck, T.F., Fraser, R.S., 1991. Temporal and spatial variability of aerosol optical depth in the Sahel region in relation to vegetation remote sensing, *Int. J. Remote Sens. Environ.,* 12, 1147-1163.

Holben, B.N., Eck, T.F., Slutsker, I., Tanré, D., Buis, J.P., Setzer, A., Vermote, E., Reagan, J.A., Kaufman, Y.J., Nakajima, T., Lavenu, F., Jankowiak, I., and Smirnov, A., 1998. AERONET - A federated instrument network and data archive for aerosol characterisation, *Rem. Sens. Environ*., 66, 1-16.

Holton J.R., Lindzen R.S., 1972. An updated theory for the quasi-biennial cycle of the tropical stratosphere. *Journal of Atmospheric Science* 29: 1076-1080.

Hoppel, W.A. et al., Aerosol size distribution and optical properties found in the marine boundary layer over the Atlantic ocean, *J.Geophys. Res*., 95, 3659-3686,1990

Huesmann A.S, Hitchman M.H., 2001. The stratospheric quasibiennial oscillation in the NCEP reanalyses: Climatological structures. *Journal of Geophysical Research* 106(D11): 11,859– 11,874, doi:10.1029/2001JD900031.

Husar, R. B., Prospero, J. M., and Stowe, L. L., 1997.Characterization of tropospheric aerosols over the oceans with the NOAA advanced very high resolution radiometer optical thickness operational product. *J. Geophys. Res., 102*, 16,889–16,909.

IPCC 1994. Radiative forcing of Climate, report to IPCC from the scientific assessment group, Cambridge Uni. Press, New York..

IPCC 1996. In: Houghton, J.T., Meira Filho, L.G., Callander, B.A., Harris, N., Kattenberg, A., Maskell, K., (Eds.), *Climate Change 1995: The Science of Climate Change*, Cambridge University Press, Cambridge, UK.

IPCC, 2007. Climate Change 2007: The Physical Science Basis. Contribution of Working Group I to the Fourth Assessment Report of the *Intergovernmental Panel on Climate Change* [Solomon, S., Qin, D., Manning, M., Marquis, M., Averyt, K.M.B., Tignor, M., Miller, H.L., and Chen, Z. (eds.)]. Cambridge, UK: Cambridge University Press.

Israelevich, P., Ganor, E., Levin, Z., and Joseph, J.,2003. Annual variations of physical properties of desert dust. *J. Geophys. Res., 18*, D13, 4381, doi:10.1029/ 2002JD003163.

Jethva, H., Satheesh, S. K., and Srinivasan J., 2005. Seasonal variability of aerosols over the Indo-Gangetic basin, *J. Geophys. Res.*, 110, D21204, doi:10.1029/2005 JD005938.

Jethva, H., Satheesh, S. K., and Srinivasan, J., 2007. Assessment of second generation MODIS aerosol retrieval (Collection 005) at Kanpur, India, *Geophys. Res. Lett.*, 34, L19802, doi:10.1029/2007GL029647.

Junge, C.E., 1963. Air Chemistry and Radioactivity. Academic Press, New York.

Kalnay, E., M. Kanamitsu, R. Kistler, W. Collins, et al. 1996. The NCEP/NCAR Reanalysis 40-year Project, *Bull. Am. Meteorol. Soc*., *77*, 437–471.

Kane RP. 1992. Relationship between QBOs of stratospheric winds, ENSO variability and other atmospheric parameters. *Int. Jour. of Clim.* 12: 435–447.

Kaufman, Y.J., Boucher, O., Tanre, D., Chin, M., Remer, L.A., Takemura,T., 2005. Aerosol anthropogenic component estimated from satellite data. *Geophys. Res. Lett*. 32, L17804.

Kaufman, Y., Tanre´,D. and Boucher, O. 2002a. A satellite view of aerosols in the climate system, *Nature,* 419, doi:10.1038/nature01091.

Kaufman, Y.J., N. Gobron, B. Pinty, J.L. Widlowski and M.M. Verstraete, 2002b. Relationship between surface reflectance in the visible and mid-IR used in MODIS aerosol algorithm – theory, *Geophys.Res. Lett*., 29(18), art. no.-2116.

Kaufman, Y.J., D. Tanre, O. Dubovik, A. Karnieli, and L.A. Remer 2001. Absorption of sunlight by dust as inferred from satellite and ground-based remote sensing, *Geophys. Res. Lett., 28*, 1479-1483.

Kaufman,Y.J., Karnieli, A., Tanre, D.,2000. Detection of dust over deserts using satellites data in the solar wavelengths, *IEEE Trans. Geosci. Remote Sensing*, 38, 525-531, Part 2.

Kaufman, Y.J., Tanre´, D., Remer, L.A., Vermote, E.F., Chu, A., and Holben, B.N., 1997a. Operational remote sensing of tropospheric aerosol over land from EOS moderate resolution imaging spectroradiometer. *J. Geophys. Res.*, 102(D14), 17,051–17,067.

Kaufman, Y. J., Fraser, R. S., 1997b. The effect of smoke particles on clouds and climate forcing. *Science* 277, 1636–1639.

Kaufman, Y.J., D. Tanre, H.R. Gordon, T. Nakajima, J. Lenoble, R. Frouin, H. Grassl, B.M. Herman, M.D. King, and P.M. Teillet 1997c. Passive remote sensing of tropospheric aerosol and atmospheric correction for the aerosol effect, *J. Geophys. Res*., 102, 16 815 – 16 830.

Kaufman, Y. J., Sendra, C., 1988. Algorithm for atmospheric corrections of visible and near IR satellite imagery. *Int. J. Remote Sens*. 9, 1357–1381

Khain, A. P., Rosenfeld, D., and Pokrovsky, A. , 2001. Simulating convective clouds with sustained super cooled liquid water down to −37.5_C using a spectral microphysics model, *Geophys. Res. Lett.*, 28, 3887–3890

Khain, A. P., Rosenfeld, D., Pokrovsky, A., 2005. Aerosol impact on the dynamics and microphysics of convective clouds. Q. J. Roy. Meteorol. Soc. 131, 2639–2663

Kiehl, J.T., and Briegleb, B.P., 1993. The relative roles of sulfate aerosols and greenhouse gases in climate forcing, *Science, 260*, 311,

King, M.D., Kaufman, Y.J., Menzel, W.P., and Tanre, D., 1992. Remote sensing of cloud, aerosol, and water vapour properties from the Moderate Resolution Imaging Spectrometer (MODIS*), IEEE Trans. Geosci. Remote Sens*., 30. 2-27.

King, M.D., Kaufman, Y.J., Tanre´, D., and Nakajima, T. 1999. Remote sensing of Tropospheric Aerosols from Space: Past, Present, and Future, *Bull. Am. Meteorol. Soc.*, 80, 2229 – 2259.

Kistler, R., Kalnay, E., Collins, W., Saha, S., White, G., Woollen, J., Chelliah, M., Ebisuzaki, W., Kanamitsu, M., Kousky, V., Huug van den Dool, Jenne, R. and Fiorino, M., 2001. The NCEP-NCAR reanalysis: Monthly means CD-ROM and documentation, *Bull. Am. Meteorol. Soc*., 82, 247– 267.

Kohler, Ines, Martin Dameris, Ingmar Ackermann and Heinz Hass, Contribution of road traffic emissions to the atmospheric black carbon burden in the mid-1990s, *J. Geophys. Res*.,106, No. D16, 17,997-18,014, 2001

Koren I, Kaufman, Y.J., Rosenfeld, D., Remer L.A., Rudich Y., 2005. Aerosol invigoration and restructuring of Atlantic convective clouds. *Geophys. Res. Lett.* 32(14): L14828.

Koren, I., Kaufman, Y. J., Remer, L. A., and Martins, J. V., 2004. Measurements of the effect of smoke aerosol on inhibition of cloud formation, *Science*, 303, 1342–1345.

Krishnamurthy T. N., Jha, B., Prosperpo, J., Jayaraman, A., and Ramanathan,V., 1998. Aerosol and pollutant transport and their impact on radiative forcing over the tropical Indian Ocean during the January–February 1996 pre-INDOEX cruise *Tellus*,

Kubilay, N., Oguz, T., Kocak, M., and Torres, O.,2005. Ground based assessment of Total Ozone Mapping Spectrometer (TOMS) data for dust transport over the northeastern Mediterranean. *Global Biogeochemical Cycles*, 19, GB1012, doi:10.1029/2004GB002370.

Lau, K. M., Kim, M. K., and Kim K. M., 2006. Asian monsoon anomalies induced by aerosol direct effects, *Clim. Dyn.*, 26, 855– 864, doi:10.1007/s00382-006-0114-z.

Léon J.F., Legrand M., 2003. Mineral dust sources in the surroundings of the north Indian Ocean. *Geophys. Res. Lett.* 30(6),1309 -1313.

Levy R.C, Remer L, Mattoo S, Vermote E, Kaufman Y.J., 2007. Second-generation algorithm for retrieving aerosol properties over land from MODIS spectral reflectance. *Journal of Geophysical Research* 112: (D13), pp. 13,211.

Levy, R. C., Remer, L. A., Tanre´, D., Kaufman, Y. J., Ichoku, C., Holben, B. N., Livingston, J. M., Russell, P.B., Maring, H., 2003. Evaluation of the Moderate-Resolution Imaging Spectroradiometer (MODIS) retrievals of dust aerosol over the ocean during PRIDE. *J. Geophys. Res.* 108(D19), 8594

Li F., Ginoux, P., and Ramaswamy, V.,2008. Distribution, transport, and deposition of mineral dust in the Southern Ocean and Antarctica: Contribution of major sources. *J. Geophys. Res*., 113, D10207, doi:10.1029/2007JD009190.

Li, R.R., L. Remer, Kaufman, Y.J., Mattoo, S., Gao, B. C., and Vermote, E.,2005. Snow and ice mask for the MODIS aerosol products. *IEEE Geo. and Rem.Sens. Lett*., 2(3), 306–310.

Liao, H. Seinfeld, J. H., 1998. Effect of clouds on direct aerosol radiative forcing of climate. *J. Geophys. Res.* 103, 3781–3788.

Liepert, B. G., 2002. Observed reductions of surface solar radiation at sites in the United States and worldwide from 1961 to 1990. *Geophys. Res. Lett.* 29,1421- 1424.

Lindberg, J.D., Douglass, R.E., and Garvey, D.M., *Appl. Opt*.32,6077,1993

Lindzen R.S, Holton J.R. 1968. A theory of the quasi biennial oscillation. *Journal of Atmos. Sci.* 25: 1095-1107.

Liousse, C., Penner, J.E., Chuang, C., Walton, J.J., Eddleman, H., and Cachier, H., 1996. A global three-dimensional model study of carbonaceous aerosols. *J. Geophys. Res.* 101, 19411-19432.

Lohmann, U., Feichter, J., 2005. Global indirect aerosol effects: a review. *Atmos. Chem. Phys.* 5, 715–737.

Mahowald, N., Baker, A., Bergametti, G., Brooks, N., Duce, R. Jickells, T., Kubilay, N., Prospero, J., Tegen, I., 2005. Atmospheric global dust cycle and iron inputs to the ocean, *Global Biogeochem. Cycles, 19*, GB4025,10.1029/2004GB002402

Martins, J. A., M. A. F. Silva Dias, and F. L. T. Gonçalves 2009, Impact of biomass burning aerosols on precipitation in the Amazon: A modeling case study, *J. Geophys. Res.*, 114, D02207, doi:10.1029/2007JD009587.

Martins, J. V., Tanre, D., Remer, L.A., Kaufman, Y., Mattoo, S., and Levy, R., 2002. MODIS Cloud screening for remote sensing of aerosols over oceans using spatial variability, *Geophys. Res. Lett.*, 29(12), 8009, doi:10.1029/2001GL013252.

Martonchik, J.V., Diner, D.J., Kahn, R.A., Ackerman, T.P., Verstraete, M.M., Pinty, B., and Gordon, H.R.,1998: Techniques fot the retrieval of aerosol properties over land and ocean using multiangle imaging. *IEEE Trans. Geosci. Remote Sens.*, 36, 1212–1227.

McCartney, E.J., 1976, Optics of the Atmosphere, John Wiley & Sons, New York.

McCormick, M.P., Hamill, P., Pepin, P.J., Chu, W.P., Swissler, T.J., and McMaster, L.R., 1979. Satellite studies of the Stratospheric aerosol, *Bull. American Meteorol. Soc.*, 60(9), 1038–1046.

McPeters R.D. Bhartia P.K., Krueger A.J., Hermand J.R., Schlesinger B.M., Wellemeyer C.G., Seftor C.J., Jaross G., Taylor S.L., Swissler T., Torres O., Labow G., Byerly W. and Cebula, R., 1996. Nimbus-7 Total Ozone Mapping Spectrometer (TOMS) User's Guide, NASA Reference Publication 1996. National Aeronautics and Space Administration.

Mekler, Y., Quenzel H., Ohring G., and Marcus I., 1977. Relative atmospheric aerosol content from ERS observations. *J. Geophys. Res.,* 82, 967–972.

Middleton, N. J., Goudie, A. S., Wells, G. L., 1986. *The frequency and source areas of dust storms, in Aeolian Geomorphology*. Allen and Unwin, New York, 237–259

Minnis, P., Heck, P. W., Young, D. F., Fairall, C.W., and Snider, J. B., 1992. Stratocumulus cloud properties derived from simultaneous satellite and island-based instrumentation during FIRE. *J. Appl Meteor.*, 31, 317–339.

Mircea, M., Facchini, M. C., Decesari1, S., Cavalli, F, Emblico, L., Fuzzi, S., Vestin, A. Rissler, J., Swietlicki, E., Frank, G., Andreae, M. O., Maenhaut, W., Rudich, Y., Artaxo, P., 2005. Importance of the organic aerosol fraction for modeling aerosol hygroscopic growth and activation: a case study in the Amazon Basin. *Atmos. Chem. Phys.* 5, 3111–3126.

Mohanakumar K. 2008. Stratosphere troposphere interactions. *Springer*, New York

Moorthy, K.K., and A. Saha, Aerosol study during INDOEX: Observation of enhanced aerosol availability over the mid Arabian sea during the northern winter, *J. Atmos. Sol. Terr. Phys.*, 62, 65-72, 2000.

Moorthy, K.K., Auromeet Saha, B.S.N. Prasad , K Niranjan, D. Jhurry and Preetha.S.Pillai, Aerosol Optical Depths over peninsular India and adjoining oceans during the INDOEX campaigns: Spatial, temporal and spectral Characteristics, *J.Geophys. Res*,106, 28,539-28,554, 2001

Moorthy, K.K., Babu, S.S., Satheesh, S.K., 2003. Aerosol Spectral Optical Depths over Bay of Bengal: Role of Transport, *Geophys.Res.Lett.*,330, 1249-1253.

Moorthy, K.K., Babu, S.S., Satheesh, S.K., Srinivasan, J., and Dutt, C.B.S., 2007. Dust absorption over the "Great Indian Desert" inferred using ground-based and satellite remote sensing. *J. Geophys. Res., 112*.

Moorthy, K.K., Satheesh, S.K., 2000. Characteristics of aerosols over a remote island, Minicoy in the Arabian Sea, Optical properties and retrieved size characteristics, *Quarterly J. Royal Met. Soc*., 126, 81-109 ,

Moulin, C., Lambert, C . E., Dayan, U ., Masson, M.V ., Ramonet, M ., Bousquet , P .,Legrand, M., Balkanski , Y . J., Guellel, W ., Marticorena B., Bergametti, G., and Dula ,F., 1998. Satellite climatology of African dust transport in the Mediterranean atmosphere. *J. Geophys. Res., 103*, 13,137-13,144.

Murayama, T., Sugimoto, N., Uno, I., Kinoshita, K., Aoki, K., Hagiwara, N., Liu, Z., Matsui, I., Sakai, T., Shibata, T., Arao, K., Sohn, B.-J., Won, J.-G., Yoon, S.-C.,

Li, T., Zhou, J., Hu, H.,Abo, M., Iokibe, K., Koga, R., Iwasaka, Y. , 2001. Ground-based network observation of Asian dust events of April 1998 in East Asia. *J. Geophys. Res*., *106*, 18 345–13 360.

Murphy, D.M., Thomson, D.S., and Mahoney, T.M.J., 1998. In situ measurements of organics, meteoritic material, mercury, and other elements in aerosols at 5 to 19 kilometres, *Science*, 282, 1664-1669

Nair, V. S., Krishna moorthy, K., Denny P. Alappattu. Kunhikrishnan, P. K., Susan George, Prabha R. Nair, Suresh Babu, S., Abish, B., Satheesh, S. K., Sachchidanand Tripathi, Niranjan, K., Madhavan, B. L., Srikant, V., Dutt, C. B. S., Badarinath, K. V. S. , Ramakrishna Reddy, R., 2007. Wintertime aerosol characteristics over the Indo-Gangetic Plain (IGP): Impacts of local boundary layer processes and long-range transport. J. Geophys. Res.112, D13205.

O'Sullivan D, Dunkerton T.J., 1997. The influence of the quasi-biennial oscillation on global constituent distributions, *Journal of Geophysical Research* 102: 21,731–21,743.

Opik, E.J., 1958. Physics of Meteor Flight in the atmosphere., Wiley (Interscience), New York,

Orgen, 1982. Deposition of particulate elemental carbon from the atmosphere. In particulate carbon: atmospheric life cycle edited by G.T.Wolff and R.L. Klimisch, pp, 379-391, Plenum Press, New York,

Parrish, D. F., and. Derber, J. C., 1992. The National Meteorological Center's spectral statistical interpolation analysis system. Mon. Wea. Rev., 120, 1747–1763.

Pease P.P., Tchakerian V.P., Tindale, N.W., 1998. Aerosols over the Arabian Sea: geochemistry and source areas for aeolian desert dust. J. Arid Environ. 39,477–96.

Penner, J. E., Dong, X., Chen, Y., 2004. Observational evidence of a change in radiative forcing due to the indirect aerosol effect. Nature, 427, 231–234.

Penner, J., et al., 2001. Aerosols: Their direct and indirect effects, in Climate .Change 2001: The Scientific Basis, Contribution of Working Group I to the Third Assessment Report of the Intergovernmental Panel on Climate Change, edited by J. T. Houghton et al., pp. 289– 348, Cambridge Univ. Press, New York.

Penner, J.E., C.C. Chuang and K. Grant Climate change and radiative forcing by anthropogenic aerosols: A review of research during the last five years. Submitted 1999.

Penner, J.E., C.C. Chuang and K. Grant, Climate forcing by carbonaceous and sulphate aerosols, Clim. Dyn., 14, 839-851, 1998.

Penner, J.E., Ghan, S.J., Walton, J.J., 1991. The role of biomass burning in the budget and cycle of carbonaceous soot aerosols and their climate impact. In: Levine,J.S.(Ed.), Global Biomass Burning: Atmospheric, Climatic, and Biospheric Implications. MIT Press, Cambridge, MA, pp. 387- 393

Penner, J.E., Zhang, S.Y., Chin, M., Cjauang, C.C., Feichter, J., Feng, Y., Geogdzhagev, I.V., Ginoux, P., Jerzog, M., Higurashi, A., Koch, D., Land, C., Lohmann, U., Mishchenko, M., Nakajima, T., Pitari, G., Soden, B., Tegen, I., Stowe, L., 2002. A comparison of Model and Satellite derived aerosol optical depth and reflectivity, *J. Atmos. Sci.* 59, 3-10,

Philander, G.S. 1990. *El Nino, La Nina and the Southern Oscillation*, Academic Press, New York, NY, USA.

Platnick, S, King, MD, Ackerman, SA, Menzel, WP, Baum, BA, Riedi, JC, Frey, RA (2003). The MODIS cloud products: Algorithms and examples from Terra. *IEEE Trans. on Geosci. AND Remote Sensing*

Plumb RA, Bell R.C. 1982. A model of the quasi-biennial oscillation on an equatorial beta-plane. *Quarterly Journal of Royal Meteorological Society* 108: 335–352.

Plumb, R.A., 1996. A “tropical pipe” model of stratospheric transport, *J. Geophys. Res.*, 101, 3957-3972.

Prospero, J. M. and Carlson, T. , 1972. Saharan air outbreaks over the tropical North Atlantic, Pure Appl. Geophys., 119, 678–691.

Prospero, J. M.,1999. Long-term measurements of the transport of African mineral dust to the south eastern United States: Implications for regional air quality. *J. Geophys. Res., 104*, 15,917–15,927.

Prospero, J., Ginoux, P., Torres, O., Nicholson, S., and Gill, T.,2002. Environmental characterization of global sources of atmospheric soil dust identified with the Nimbus 7 Total Ozone Mapping Spectrometer (TOMS) Absorbing Aerosol product, *Rev. Of Geophys.,40,* 1.1002. doi:10.1029/2000RG000095.

Prospero,J.M., Charlson, R.J., Mohnen, B., Jaenicke,R., Delany, A.C. Mayers, J., Zoller, W.,and Rahn,K., 1983. The atmospheric aerosol system- An overview, *Rev. Geophys.Space. Phys.*, 21,1607-1629.

Pruppacher, H.R., Klett, J.D., 1978. Microphysics of clouds and precipitation, Riedal Publishing Co., USA, 193-195,

Quaas, J., Boucher, O., Br´eon, F.M., 2004. Aerosol indirect effects in POLDER satellite data and the Laboratoire de M´et´eorologie Dynamique-Zoom (LMDZ) general circulation model. J. Geophys. Res. 109, D08205.

Quinn, P.K., Asher, W.E., and Charlson, R.J.,1992. Equilibrium of the marine multiphase ammonia system, *J. Atmos. Chem.*, 14, 11—30.

Ramanathan, V., Crutzen, P. J., Lelieveld, J., Mitra, A. P., Althausen, D., Anderson, J., Andreae, M. O., Cantrell, W., Cass, G. R., Chung, C. E., Clarke, A. D., Coakley, J. A., Collins, W. D., Conant, W. C., Dulac, F., Heintzenberg, J., Heymsfield, A. J., Holben, B., Howell, S., Hudson, J., Jayaraman, A., Kiehl, J. T., Krishnamurti, T. N., Lubin, D., Macfarquhar, G., Novakov, T., Ogren, J. A., Podgorny, I. A., Prather, K., Priestley, K., Prospero, J. M., Quinn, P. K., Rajeev, K., Rasch, P., Rupert, S., Sadourny, R., Satheesh, S. K., Shaw, G. E., Sheridan, P., Valero, F. P. J., 2001. Indian Ocean Experiment: An integrated analysis of the climate forcing and effects of the great Indo-Asian haze. J. Geophys. Res. 106(D22), 28, 378-28,398.

Ramaswamy, V., Boucher, O., Haigh, J., Hauglustaine, D., Haywood, J., Myhre, G., Nakajima, T., Shi, G. Y., and Solomon,S., 2001. Radiative Forcing of Climate Change, in: Climate Change 2001: The Scientific Basis. Contribution of working group I to the Third Assessment Report of the Intergovernmental Panel on Climate Change, edited by: J. T. Houghton, Y. Ding, D. J. Griggs, M. Noguer, P. J. van der Linden, X. Dai, K. Maskell, and C. A. Johnson, pp. 349–416, Cambridge Univ. Press, New York.

Randel W.J, Wu F, Gaffen D.J. 2000. Interannual variability of the tropical tropopause derived from radiosonde data and NCEP reanalysis. *Journal of Geophysical Research* 105(D12): 15,509–15,523. DOI: 10.1029/2000JD900155.

Reddy, M.S., and C. Venkataraman, Atmospheric Optical and Radiative Effects of Anthropogenic Aerosols from India, *Atmospheric Environment*, 34, 4511-4523, 2000.

Reddy,M.S., and C. Venkataraman, 1999. Direct radiative forcing from anthropogenic carbonaceous aerosols over India, *Current Science*, 76, 1005-1011.

Reid G.C, and Gage K.S.1985. Interannual variations in the height of the tropical tropopause. *J. Geophys. Res*. 90: 5629-5635.

Reid, J.S., Hobbs, P.V., 1998. Physical and optical properties of young smoke from individual biomass fires in Brazil. *J. Geophys. Res*. 103, 32,013-32,030

Reid, J.S., Thomas F. Eck, Sundar A. Christopher, Peter V. Hobbs, Brent Holben,1999. Use of the Ångstrom exponent to estimate the variability of optical and physical

properties of aging smoke particles in Brazil. *J. Geophys. Res.* 104(D22), 27,473-27,489

Reist.P.C., 1984. Introduction to Aerosol Science, Mc Millan Publishing company.

Remer, L. A., Tanre´, D., Kaufman, Y. J., Levy, R. C., and Mattoo, S., 2006. Algorithm for remote sensing of tropospheric aerosol from MODIS: Collection 005, Algorithm Theoretical Basis Document, NASA Goddard Space Flight Cent., Greenbelt, Md. (Available at *http://modis-atmos. gsfc.nasa. gov/reference _atbd.php*).

Remer, L.A., and Y.J. Kaufman, Dynamic aerosol model: Urban/industrial aerosol, *J. Geophys. Res*., 103, 13859-13871, 1998

Remer, L.A., Y.J. Kaufman, D. Tanre, S. Mattoo, D.A. Chu, J.V. Martins, R.R. Li, C. Ichoku, R.C. Levy, R.G. Kleidman, T.F. Eck, E. Vermote, and B.N. Holben 2005. The MODIS aerosol algorithm, products and validation, *J. Atmos. Sci*., 62, 947 – 973.

Ribera P, Pen˜a-Ortiz C, An˜el J.A, Gimeno L, de la Torre L, Gallego D. 2008. Quasi-biennial modulation of the Northern Hemisphere tropopause height and temperature. *Journal of Geophysical Research* 113: D00B02. DOI:10.1029/2007JD009765.

Rivera-Carpio, C.A., Corrigan, C.E., Novakov, T., Penner, J.E., Rogers, C.F., and Chow, J.C., 1996. Derivation of contributions of sulphate and carbonaceous aerosols to cloud condensation nuclei from mass size distributions. *J. Geophys. Res. Atmos*., 101, 19483-19493

Rosenfeld, D. 1999. TRMM observed first direct evidence of smoke from forest fires inhibiting rainfall, *Geophys. Res. Lett*., 26, 3105– 3108.

Rosenfeld, D. and Woodley, W. L., 2000. Deep convective clouds with sustained supercooled liquid water down to −37.5_C, *Nature*, 405, 440–442,

Rosenfeld, D., 2000. Suppression of rain and snow by urban and industrial air pollution. *Science, 287*, 1793–1796.

Rosenfeld, D., Kaufman, Y. J., Koren, I., 2006. Switching cloud cover and dynamical regimes from open to closed Benard cells in response to the suppression of precipitation by aerosols. Atmos.Chem. Phys. 6, 2503–2511.

Rosenfeld, D., Lahav, R., Khain, A., and Pinsky, M. 2002. The role of sea spray in cleansing air pollution over ocean via cloud processes, Science, 297, 1667–1670,

Ross, J.I., Hobbs, P.V., and Holben, B., 1998. Radiative characteristics of regional hazes dominated by smoke from biomass burning in Brazil: Closure test and direct radiative forcing, *J. Geophys. Res*., 103, 31925-31941,

Russel et al., 1994. Aerosol production and growth in marine boundary layer, *J. Geophys. Res.* 99, 20989-21003,

Russell, P.B., P.V. Hobbs, and L.L. Stowe, 1999. Aerosol properties and radiative effects in the United States East Coast haze plume: An overview of Tropospheric Aerosol Radiative Forcing Observational Experiment (TARFOX), *J. Geophys. Res*., 104, 2213-2222.

Saha A, and Moorthy K.K., 2005. Interannual variations of aerosol optical depth over coastal India: Relation to synoptic meteorology. *Journal of Applied Meteorology* 44: 1066–1077.

Salby M, Callaghan P. 2004. Interannual changes of the stratospheric circulation: Influence on the tropics and Southern Hemisphere. *Journal of Climatology* 17: 952– 964

Salomonson, V.V., Barnes, W.L., Maymon, P.W., Montgomery, H.E., Ostrow, H.,1989. MODIS: Advanced facility instrument for studies of the Earth. *IEEE Transactions on Geoscience and Remote Sensing* 27, 145 – 153

Santer B.D, Wigley T.M.L., Mears C., 2005. Amplification of Surface Temperature Trends and Variability in the Tropical Atmosphere. *Science 309*: 1551–1556. DOI:10.1126/science.1114867.

Satheesh, S. K. and Ramanathan, V., 2000. Large differences in tropical aerosol forcing at the top of the atmosphere and Earth's surface. *Nature* 405, 60–63

Satheesh, S.K. and Srinivasan, J., 2002. Enhanced aerosol loading over Arabian Sea during the pre-monsoon season: Natural or anthropogenic? Geophys. Res. Lett., 29, 1029-1033

Saxena, P. and L.M. Hildemann, Water soluble organics in atmospheric particles: A critical review of the literature and application of thermodynamics to identify candidate compounds. *J. Atmos. Chem*., 24, 57-109, 1996

Saxena, P., L.M. Hildemann, McMurry, P.H., and Seinfeld, J.H., 1995. Organics alter hygroscopic behavior of atmospheric particles. *J. Geophys. Res. Atmos*., 100, 18755-18770,

Schnell, R. C. and Vali, G., 1976. Biogenic ice nuclei: Part I. Terrestrial and marine sources. *J. Atmos. Sci*., 33, 1554-1564.

Schwartz, S.E., Harshvardhan, Benkovitz, C.M., 2002. Influence of anthropogenic aerosol on cloud optical depth and albedo shown by satellite measurements and chemical transport modeling. Proc. Natl. Acad. Sci. USA, 99, 1784-1789.

Sempéré, R. and Kawamura, K., 1996. Low molecular weight dicarboxylic acids and related polar compounds in the remote marine rain samples collected from western Pacific. *Atmos. Environ*., 30, 1609-1619.

Sharma, M., Kiran, Y.N.V.M., Shandilya, K. K., 2003. Investigations into formation of atmospheric sulfate under high PM10 concentration. Atmos. Environ. 37, 2005–2013.

Sikka, D. R., 1997. Desert climate and its dynamics. Curr. Sci. 72(1), 35 – 46.

Slingo, A., Ackerman, T. P., Allan, R. P., Kassianov, E. I., McFarlane, S. A., Robinson, G. J.,Barnard, J. C., Miller, M. A., Harries, J. E., Russell, J. E., and Dewitte, S 2006. Observations of the impact of a major Saharan dust storm on the atmospheric radiation balance, *Geophys. Res. Lett.*, 33, L24817, doi:10.1029/2006GL027869.

Smirnov, A., Villevalde, Y., O'Neill, N. T., Royer, A., and Tarussov, A 1995. Aerosol optical depth over the oceans: Analysis in terms of synoptic air mass types, *J. Geophys. Res*., 16, 639–650, 24513

Sokolik, I. N., Winker, D. M., Bergametti, G., Gillette, D. A., Carmichael, G., Kaufman, Y., Gomes, L., Schuetz, L., and Penner, J. E., 2001. Introduction to special section: Outstanding problems in quantifying the radiative impacts of mineral dust. *J.Geophys. Res*., *106*, 18,015– 18,028.

Tanre, D., Kaufman, Y.J., Herman, M. and Mattoo, S., 1997. Remote sensing of aerosol properties over oceans using the MODIS/EOS spectral radiances, *J. Geophys. Res*., 102, 16,971 – 16,988.

Tegen, I. and Fung, I., 1995. Contribution to the atmospheric mineral aerosol load from land surface modification, *J Geophys. Res.*, 100, 18,707-18,726.

Tegen, I., Lacis, A. A., and Fung, I., 1996. The influence on climate forcing of mineral aerosols from disturbed soils, Nature, 380, 419–422.

Tegen, I., and Lacis, A.A., 1996. Modeling of particle size distribution and its influence on the radiative properties of mineral dust aerosol, *J. Geophys. Res.*, 101, 19237-19244.

ten Brink, H. M., Veefkind, J. P., Waijers-Ijpelaan, A., and van der Hage, J. C. 1996. Aerosol light-scattering in the Netherlands, *Atmos. Environ*., 30, 4251-4261 ,

Thampi, B. V., Sunilkumar, S. V., and Parameswaran, K.,2009. Lidar studies of particulates in the UTLS region at a tropical station over the Indian subcontinent, *J. Geophys. Res.*, 114, D08204, doi:10.1029/2008JD010556

Torres, O., Bhartia, P.K., Herman, J.R., Ahmad, Z., and Gleason, J., 1998. Derivation of aerosol properties from satellite measurements of backscattered ultraviolet radiation. Theoretical basis. *J. Geophys. Res.*, 103, 17,099–17,110.

Torres, O., Bhartia, P.K., Herman, J.R., Sinyuk, A., Ginoux, P., and Holben, B., 2002a: A long term record of aerosol optical depth from TOMS observations and comparison to AERONET measurements, *J.Atm. Sci.*, 59, 398–413.

Torres, O., Decae, R., Veefkind, J.P., and de Leeuw, G., 2002b: OMI aerosol retrieval algorithm. In: P. Stammes and R. Noordhoek (eds.), OMI Algorithm Theoretical Basis Document, Vol. III: *Clouds,Aerosols and Surface UV Irradiance,* ATBD-OMI-03,46–71.

Trenberth,K.E., 1997. The definition of El-Nino. *Bull. Amer. Met. Soc.*, 78, 2771-2777.

Trepte C.R, Hitchman M.H.1992. Tropical stratospheric circulation deduced from satellite aerosol data, *Nature* 355: 626–628.

Trepte C.R., 1993. Tracer transport in the lower stratosphere, *Ph.D. dissertation*, University of Wisconsin—Madison, 169 pp.

Tripathi, S. N., Tare, V., Chinnam, N., Srivastava, A.K., Dey, S.et al. 2006. Measurements of atmospheric parameters during Indian Space Research Organization Geosphere Biosphere Programme Land Campaign II at a typical location in the Ganga basin: 1. Physical and optical properties, *J. Geophys. Res*., 111, D23209, doi:10.1029/2006JD007278.

Twomey, S., 1977. The influence of pollution on the shortwave albedo of clouds. J. Atmos. Sci. 34, 1149- 1152.

Twomey, S., Piepgrass, M., and Wolfe, T.L., 1984. An assessment of the impact of pollution on global cloud albedo. *Tellus*, 36B, 356-366,

Twomey, S., 1974. Pollution and the planetary albedo, *Atmos. Environ.*, 8, 1251-1256.

Twomey, S., 1991. Aerosols, clouds and radiation, *Atmos. Environ*., 25(A). 2435-2442.

Tyson et al., 1996. An air transport climatology for subtropical Southern Africa, *Int. J. Climatology*, 16,256-291.

Uematsu,M., *et al*., Transport of mineral Aerosol from Asia over the north Pacific Ocean, *J. Geophys. Res*., 88, 5343-5352,1983

Uno, I.S., Wakamatsur, M., Susuki, T., Ogawa, Y., Three dimensional behaviour of photochemical pollutants covering the Tokyo metropolitan area, *Atmos*. *Environ.* 18, 751-761. 1984.

Uppala, S. M., K°allberg, P. W., Simmons, A. J. , Andrae, U., V. da Costa Bechtold, M. Fiorino J. K. Gibson, J. Haseler A. Hernandez G. A. Kelly X. Li K. Onogi, S. Saarinen, N. Sokka, R. P. Allan, E. Andersson, K. Arpe, M. A. Balmaseda, A. C. M. Beljaars L. van de Berg J. Bidlot N. Bormann S. Caires F. Chevallier A. Dethof M. Dragosavac M. Fisher M. Fuentes S. Hagemann E. H´olm B. J. Hoskins L. Isaksen P. A. E. M. Janssen,R. Jenne, A. P. McNally J.-F. Mahfouf, J.-J. Morcrette N. A. Rayner R. W. Saunders P. Simon, A. Sterl K. E. Trenberth A. Untch D., Vasiljevic P., Viterbo J. Woollen, 2005. The ERA-40 re-analysis, *Quart. J. R. Meteorol. Soc*., 131, 2961–3012.

Veefkind, J.P., de Leeuw, G., and Durkee, P.A., 1998. Retrieval of aerosol optical depth over land using two-angle view satellite radiometry during TARFOX. *Geophys. Res. Lett.*, 25(16), 3135–3138.

Vignati, E., de Leeuw, G., Berkowicz, R., 2001. Modeling coastal aerosol transport and effects of surf-produced aerosols on processes in the marine atmospheric boundary layer, *J. Geophys. Res*., 106, 20225-20238,

Wallace, J.V., Hobbs, P.V., 2006. *Atmospheric Science –An introductory survey*, Academic press , New York

Washington R., Todd M., Middleton N.J., Goudie A.S., 2003. Dust-storm source areas determined by the Total Ozone Monitoring Spectrometer and surface observations. Annals of the Association of American Geographers 93(2), 297–313

Wei, W.W.S., 2006. Time Series Analysis, Univariate and Multvariate Methods, 2nd Edition, Boston: Pearson Addison Wesley

Whitby, K.T., 1978. The physical characteristics of sulfur aerosols, *Atmos. Environ*., 12, 135-159.

Wolf, G.T., Particulate elemental carbon in the atmosphere, *Journal of the Air Pollution Control Association*, 31, 935-939, 1981.

Xue, Y. and Shukla, J. 1997. *Model simulation of the influence of global SST anomalies on the Sahel rainfall*, COLA Preprint 41,Centre for Ocean, Land, Atmosphere Studies, Calverton, Maryland.

List of Publications

1. B. Abish and K. Mohanakumar, Biennial Variability in Aerosol Optical Depth Associated with QBO Modulated Tropical Tropopause, Atmospheric Science Letters (Under Review)

2. B. Abish and K. Mohanakumar, Role of Fine Mode Aerosol Particles in Modulating Regional Cloud Properties over Industrial Locations in North India, Annales Geophysicae (Under Review)

3. B. Abish and K. Mohanakumar, Variability in aerosol concentrations associated with El-Nino and La-Nina phases over the Indian subcontinent, Journal of Geophysical Research (Under Review)